HOLLOW STRUCTURAL SECTIONS

SUBJECTED TO INELASTIC STRAIN REVERSALS

HOLLOW STRUCTURAL SECTIONS
SUBJECTED TO INELASTIC STRAIN REVERSALS

by

Maguid Nashid, B.Sc.

A Thesis

Submitted to the School of Graduate Studies

in Partial Fulfilment of the Requirements

for the Degree

Master of Engineering

McMaster University

May, 1974

MASTER OF ENGINEERING
(Civil Engineering)

McMASTER UNIVERSITY
Hamilton, Ontario

TITLE: Hollow Structural Sections Subjected to Inelastic Strain Reversals

AUTHOR: Maguid Nashid, B.Sc. (Cairo University)

SUPERVISOR: Dr. Robert M. Korol

NUMBER OF PAGES: ix, 127

ABSTRACT

A research project is presented to assess the capabilities of Square Hollow Structural Sections for seismic design. This assessment is based mainly on the energy dissipation and ductility measures. An attempt is made to establish a preliminary guideline of the maximum slenderness ratio that qualify the aforementioned sections for conservative seismic design.

An experimental programme on seven different sections was performed to evaluate the loss in flexural capacity due to inelastic cyclic loads, and to construct the load-deflection and moment-curvature hysteresis loops.

A comparison is made between the flange slenderness requirements of both HSS and wide flange rolled sections capable of resisting the same level of inelastic strain reversals for the same number of cycles.

ACKNOWLEDGMENTS

I wish to express my deepest gratitude to Dr. R. M. Korol and Dr. W. K. Tso for their advice and patience during the course of this thesis work. Also, I would like to thank the staff of technicians of the Applied Dynamics Laboratory (A.D.L.) who helped in carrying out the experimental work.

This investigation was made possible through the financial assistance of Dr. Korol's research fund. Test specimens were fabricated and donated by the Steel Company of Canada, to whom I extend my sincere thanks.

TABLE OF CONTENTS

LIST OF FIGURES

LIST OF TABLES

CHAPTER I

INTRODUCTION

I.1 The Earthquake Problem

The Alaska Earthquake of March 27, 1964[1], was the strongest eqrthquake ever recorded on the North American Continent. Loss of life, although large, was not nearly as great as that resulting from a number of other earthquakes, for example, nearly 16,000 persons lost their lives in the earthquake in northeastern Iran on August 31, 1968. Property damage from the Alaska Earthquake, however, was extensive -- of the order of $300 million. The extent of physical suffering and mental anguish of the survivors cannot be estimated, but the enormity of it is an encouragement to man to improve his ability to locate developments and to design and build structures more resistant to earthquakes and other natural disasters.

The Alaska earthquake created a wide interest in earthquake engineering among many practicing engineers, with an increasing number expressing a desire to learn more about the cause of earthquakes and measures to be taken to lessen the loss of life and decrease property damage in the future.

Thus, the earthquake-resistance design requirements of the National Building Code of Canada 1970 provide minimum standards to

safeguard the public against major structural failure and consequent loss of life. Structures designed in conformity with its provisions should be able to resist minor earthquakes without damage and resist major catastrophic earthquakes without collapse. (Collapse is defined as that state when egress of the occupants from the building has been rendered impossible because of failure of the primary structure.)

Ideally the designer of an earthquake-resistant frame structure should be aware of the response of that structure to ground motion to which it would be subjected to during its lifetime. This response is not possible to determine. The nature of the ground motion encountered in earthquakes and the type of structures the engineer has to design make the problem a difficult one. In spite of these difficulties, much can be learned about structural behaviour in earthquakes by analyzing the response-spectrum from data obtained from previous strong earthquakes, thus providing the designer with a valuable tool to assist him in the design process. The general shape of the velocity response spectrum of an earthquake motion can also provide significant information about the expected inelastic response of a multistory structure.

A previous study of this branch of structural engineering brings us to the conclusion that we should design members and connections that can resist repeated and reversed loads.

Similar type provisions are necessary in the design of off-shore structures subjected to pounding by the seas and to some extent in the design of structures required to resist blast loadings. It is also an accepted design philosophy to allow inelastic deformations in steel

frames. This approach has developed mainly because of economic considerations, as a structure capable of resisting a severe earthquake in an elasti manner would be extremely uneconomical. The extent of the allowable inelastic deformations is a very difficult problem for nondeterministic type loadings. For a strong motion earthquake, some reasonable drift limitations are often imposed, and the design is conducted on this basis. Also, pending further research, there is great reluctance on the part of designers to allow inelastic cyclic action in the columns of building frames.

As a result, dissipation of energy from earthquake motions occurs through predetermined inelastic deformations restricted to the girders; hence it is important to investigate their behaviour where plastic hinges might occur. These hinges tend to form at the ends of girders and at or near the connections.

The hysteretic characteristics and fatigue properties of steel sections have been studied extensively. These studies were mainly directed to serve the designers of machine elements in which a huge number of cycles under fairly uniform conditions are commonly encountered.

Therefore, within the last ten years or so the need was apparent to study "low cycle fatigue endurance" of structural members, and to extend the applications to structural design. It is also necessary to study the feasibility of predicting the low cycle fatigue behaviour of rolled or fabricated members at large strains on the basis of results obtained from cyclic twisting, bending, or tension-compression experiments with coupons.

The anticipated behaviour so determined is not simple because of numerous factors involved in the actual beam-to-column connections. One of these factors is the type of connection, whether it is bolted or welded, and the technique used. The associated problems arising due to stress concentration in certain regions can also be serious.

Another major problem is that caused by the slenderness of structural components involved in design. The application of large compressive forces results in significant inelastic strains. Consequently, local buckling is often a problem and is first noticed in the compression flanges at a certain stage of loading. The greater the slenderness ratio of the flanges, and the larger the levels of strain imposed, the fewer the number of cycles needed to form local buckling. High values of inelastic strain continue to accumulate in regions of local buckling once initiated. The endurance of the member afterwards becomes completely dependent on the strength of a deteriorating buckling region.

Despite the great importance of the foregoing discussion, only a limited amount of experimental evidence exists for structural steel members and connections subjected to cyclically repeated loads.

1.2 Literature Review

In February, 1965 Bertero and Popov[2] conducted an experimental study on small rolled structural steel cantilever beams subjected to cyclic reversed loading. The maximum strain at the clamped end was carefully controlled and varied between ± 1.0 and ± 2.50 per cent. All of the beams tested were 4 by 4 M 13.0, cut from a long beam that was rolled from ASTM A7 steel and the average yield stress was 41 ksi. The cantilever had an effective length of 35 inches.

The actual loads were applied by means of a double acting hydraulic cylinder. In the set of eleven experiments examined the strains at the clamped edge were used to control the machine cycles.

When the maximum controlling cyclic strain was set at 1.0%, fracture of the beam occurred after 650 cycles. The fatigue life of the beams rapidly decreased as the controlling strain was increased. For the specimen tested under a controlling strain of 2.5%, fracture occurred during the 16th cycle. This drastic drop of fatigue endurance is caused by the early development of local buckling in the beam flanges.

The initiation of local buckling was determined from visual inspection, analysis of deflection records, and principally, from the record of strains obtained from electrical resistance wire gauges placed along the flanges.

Local buckling was detected after 70 cycles, at 1.0% controlling strain. As the controlling strain was increased, local buckling was

observed after far less number of cycles. For the controlling strain values greater than 2%, local buckling was observed during or just after the first cycle.

For such a section, compressive stresses caused severe flange distortion, which was unsymmetrical with respect to the vertical plane through the longitudinal axis of the beam. Torsional displacements of the section were induced and local reductions in the flexural stiffness of the member occurred which was aggravated with increasing number of cycles. These severe distortions of the flanges caused inelastic strains of a much greater value than those of the controlling strains at the beam's clamped edge.

Furthermore, wrinkles were observed to form in the flanges, at the position of local buckling. These enlarged with an increasing number of cycles, resulting in cracks that caused complete failure. It was important to notice that no cracks were detected at the clamped section, suggesting that if local buckling had been prevented, beams could have resisted many more cycles for the same controlled strain values.

The experiments done on the steel material itself, by Benham and Ford[3], at a level of cycling strain of $\pm$ 2.43%, proved that the number of cycles needed to cause complete failure was about 400. This fact demonstrates the important role of local buckling.

The initiation of local buckling can be explained on the basis of the effect of both residual stresses and initial imperfections. Bertero and Popov, however, tended to explain the rapid flexural loss in beam capacity on the basis of the induced inelastic curvature of the

flanges. In fact, most of this curvature remains during unloading, and a kink was observed even under zero load. During successive loading cycles, the compressive and tensile forces acting on the slightly kinked flanges of the beam, tended to establish a force component that acts perpendicularly to the flange and increase the distortion. If the induced stresses are sufficiently large, this distortion becomes plastic. As the process continues, the wrinkle of the flange becomes larger with increased cycling.

None of the eleven test specimens experienced local buckling during the first half of the first loading cycle, even in experiments with 2.5% control strain. The ratio of the flange width b, to the average flange thickness, t, of the tested members was 10.5. If premature local buckling of the flange is to be avoided for the static loading case, it is recommended by ASCE manual of 1971[4] that the ratio b/t must not exceed 17. This ratio should be reduced for purposes of cyclic and dynamic loading.

Popov and Pinkney[5], in November 1968, carried out a detailed experimental program on twenty-four structural steel connections. The beam size selected for this series of experiments was 8 WF 20. These sections were about one-third the size of sections commonly used in actual construction. They did not require special fabrication provisions. The ratio of flange width to thickness is about 20, which is close to the ratio used in actual floor beams in high-rise construction. The beam was attached as a cantilever to a short column stub.

All columns were made of 8WF48 sections. Those sections behaved satisfactorily in that they insured relative rigidity. Thus the rotation at the support was minimum, and the stresses in the column remained elastic in agreement with common practice.

The length of the cantilever was 66.0 inches which is the scaled-down half-span length of a representative prototype. The application of a concentrated load at the end of the cantilever was intended to simulate the distribution of bending moment produced in a typical beam by a lateral load on a structure. In order not to complicate the study, gravity loads were neglected, and cyclic loads were equal in magnitude, and opposite in sense.

Five different connection types were investigated. In three of them the beam was connected to the flange of the column. In the other two, the beam was connected indirectly to the flange of the column. The connection details were all commonly used in practice.

Some of the connections were welded and the others were bolted. All of them behaved satisfactorily throughout the cyclic test. However, some of the bolted connections experienced some slippage in spite of using high tensile bolts ASTM A-325, in addition to the thorough sonic inspection used to check the various parts of connections. That slippage resulted in a considerable distortion in the load-deflection hysteresis loops.

A wide variety of loading programs were used. They ranged between large loads causing fracture after a few cycles, and moderate loads through which specimens survived for a large number of cycles.

Most of the tests had cycling programs of an increasing strain or deflection amplitudes. Each amplitude was applied for a certain arbitrary number of cycles. Some specimens were subjected to constant load levels for the whole test.

The smallest number of cycles recorded was 18, at an incremental strain control which reached 2% at fracture. Cracks in the top and bottom plates of the connection were reported. The largest number of cycles was 120 due to 100 cycles at 0.5% strain followed by 20 cycles at 1.5% strain control. Failure was mainly due to flange buckling.

Comments on the Results

1. Tested connections proved to be highly dependable, as hysteresis loops were greatly reproducible during tests. The areas enclosed by these loops represented the energy dissipated through the loading programme.
2. Beam sections, size 8WF20, were capable of resisting the severe effects of cyclic testing without premature failure. On the other hand, local buckling of the compression flange was a major reason of complete failure of connections as expected.
3. Statistical prediction of the fatigue characteristics and expected life is impossible by means of rational analysis. This is mainly because of the numerous factors involved in design and lack of uniformity. The various failure patterns of connections emphasized the previous conclusion.

The most recent series of tests by Popov and Bertero were published in June, 1973[6]. In that investigation full size members 18WF50 and 24WF76 were utilized. Seven specimens were tested representing two types of connections. The first type is all welded, and the second one had bolted web and welded flanges. In all cases, the flanges of the beams were welded to the flanges of the column. The total length of the cantilever was chosen to be 8.00 feet. This length could be interpreted as one-half a short span of the prototype, or one-fifth a long span.

The b/t ratios of the two types of sections W18X50 and W24X76 were in the order of 20. Sections were made of A 36 steel. The yield stresses for the W18X50 and W24X76 beams were 45 ksi and 36 ksi, respectively. On that basis the b/t ratios are higher than those recommended by the ASCE manual[4] for the same yield stresses.

Most of the specimens exhibited superior ductile behaviour. In some of the specimens the webs participated considerably in resisting the loads, while in some other specimens the beam web next to column stubs were not severely strained. Kinks were also observed in some of the compression flanges near the connection. There were unfortunately no definite justifications for these wide differences in behaviour.

The cyclic load was applied in an arbitrary but increasing quasi-static manner. First, a beam was subjected to three to five complete cycles at a calculated maximum nominal stress of 24 ksi, at the column face. That stress corresponded to the practical working conditions. Then the stresses were raised to 45 ksi or 36 ksi according to each specimen's yield stress. Two cycles of loading were applied for each

level of selected values of deflection afterwards. Four levels of peak values were chosen, and if failure did not occur, additional upward and downward excursions were used to cause failure. Strain values were not used to control the previous series of tests, probably due to the difficulties encountered in having a dependable response of strain gauge reading throughout such severe cyclic tests.

The results of these tests were in close agreement with the previous results obtained by the authors. The following conclusions were drawn:

1. Both the all-welded, and the bolted web and welded flange connections, developed strengths higher than those predicted by the simple plastic theory due to strain-hardening of steel.
2. The flanges proved to be effective in fully developing the plastic moment capacity while transferring shear. That was observed for connections without web attachment.
3. Although high tensile bolts were used, the bolted connections experienced slippage under severe cyclic loads. Thus special attention should be paid to these connections.
4. Hysteresis loops were remarkably stable and similar for loadings of the same intensity.
5. It was believed that a skew-symmetric bilinear moment-curvature curve for cyclic loading is adequate in seismic analysis.

1.3 Current Work

As stated earlier, the capability of structural members to absorb energy through inelastic load excursions, is of a major importance in the design of earthquake resistant structures. However, cold-formed hollw structural sections have received very little attention in plastic methods of analysis and design in general. The residual stresses caused by forming are considerable when compared to those caused by cooling at standard hot-rolled shapes. However, hollow sections have the advantage of higher shape factors than for the conventional shapes and the advantage of high ductile properties which are essential for earthquake design. Therefore, the behaviour of HSS subjected to high inelastic strain reversals is the main purpose of this investigation.

The present study involves a wide range of sections, having various width-thickness ratios covering the following classifications according to the requirements of rotation capacity and yielding:

(a) Plastic Design Sections -- Sections which are capable of satisfying the minimum rotation requirement and the development and maintenance of the fully plastic moment.

(b) Allowable Stress Design Sections

(i) Compact Sections -- Sections which are capable of attaining the com-

puted plastic moment without necessarily satisfying the minimum rotation requirement.

(ii) Non-Compact Sections -- Sections which are capable of attaining the computed yield moment, defined as that moment in which yielding of the outermost fibre is attained.

(c) Reduced Stress Sections -- Sections which buckle locally before they reach the computed yield moment.

It is within the aspects of this study to establish some guidelines concerning the appropriate width-thickness ratios for sections that are capable of undergoing large strain reversals without premature local buckling or great deterioration in moment capacity. Stress relieved sections are also studied in comparison with cold formed sections in an attempt to assess the effects of residual stresses of the latter on the section's general behaviour.

The present study is confined to the investigation of the virgin properties of square hollow steel sections under the conditions of cyclic loading. The adequacy of connections for such loading was not investigated. The reason is mainly because a welded joint between members of HSS has not yet been fully analysed. The connection forms a complex three-dimensional intersecting shell structure, in which the walls are loaded by both membrane and local bending stress resultants. In addition, the residual stresses mentioned earlier, further complicate

the problem. Therefore, the existing classical methods are not sufficient to furnish a complete static stress analysis of the problem. The questions of determining the joint modulus, the stresses, and the deformations in these connections, are still being studied for a sound theoretical analysis.

CHAPTER II

DESIGN MEASURES

2.1 Hysteresis Diagrams

The load deflection hysteresis diagrams for a specimen contain a considerable amount of information about its performance. It provides a continuous record of the relationship between load and deflection (or moment and curvature), and it also makes it possible to determine the energy input to the specimen through integration of the work done by the external load.

Experimental work has shown that these load-deflection (or moment-curvature) relationships are not elasto-plastic curves. The actual load displacement curve has an elastic branch followed by a transition curve that leads to a plastic branch[7]. When the displacement is reversed, the transition becomes more gradual due to Bauschinger's effect. The non-linear load-deflection relationship is reasonably described by Ramberg and Osgood[8], and adapted by Jennings[9] and Kaldjian[10] as follows:

$$\frac{\Delta}{\Delta p} = \frac{P}{P_p}\left[1 + \alpha \left(\frac{P}{P_p}\right)^{r-1}\right] \qquad 2.1$$

where Δ is the deflection, Δp is the elastic deflection corresponding to the plastic load P_p, P is the load, and α and r are the Ramberg-Osgood parameters where r is a positive odd integer. This relation is represented graphically for various values of r, in Figure 2.1. It also concludes as limiting cases the elastic (r = 1) and the elastoplastic (r = ∞) relations. Masing[11] suggested that the hysteresis curve is identical in shape to equation 2.1 but enlarged by a factor of two. Thus the hysteresis curve is generated by equation 2.2:

$$\frac{\Delta-\Delta_i}{2\Delta p} = \frac{P-P_i}{2P_p}\left[1 + \alpha\left(\frac{P-P_i}{2P_p}\right)^{r-1}\right] \qquad 2.2$$

The point (Δ_i, P_i) is chosen as the point of last load reversal. These relationships are illustrated in Figure 2.2. The method of least squares can be utilized to fit equation 2.2 to the experimental results. If P_p and Δp are chosen to be fixed values for a certain case, the variables α and r would be changed according to the fitting process. As the elastic slope described by P_p and Δp is determined, a variable β is introduced in order to allow for any deviation in the slope of the unloading curve. Thus, a more general form of equation 2.2 is written as:

$$\frac{\Delta-\Delta_i}{2\Delta p} = \frac{1}{\beta}\,\frac{P-P_i}{2P_p}\left[1 + \alpha\left(\frac{P-P_i}{2P_p}\right)^{r-1}\right] \qquad 2.3$$

where β is such that $\beta(P_p/\Delta p)$ is the slope of the unloading curve. An example of least squares fitting of equation 2.2 to an experimental load-

deflection hysteresis curve is shown in Figure 2.3.

The exponent r is a measure of the sharpness of curvature of the load-deflection curve; it also appears to be independent of the number of excursions and the plastic deflection as long as premature local buckling, and subsequent fracture of the specimen, does not occur.

The parameter α is also found to be sensitive to changes in the peak load levels. However, the shape of the curve is slightly affected by small changes in α.

The slope factor β is a measure of the stiffness of a specimen. The value of β remains close to unity as long as local buckling is not existent. Once local buckling is initiated the value of β decreases continuously with an increasing number of cycles.

The fact that the stress-strain relationship (the skeleton curve) and both the ascending and descending branches of the hysteresis loop are described by the same general equation 2.3 has several computational advantages. Moreover, the previous equation is capable of handling cases of structures which do not have an ideal steady-state response under the effect of sinusoidal excitation.

The principal disadvantage of equation 2.3 is that an explicit expression for the force in terms of the displacement is not possible, which is inconvenient in the presentation and interpretation of the results. The following procedure could be utilized to overcome the previous difficulty: Assume

$$x = \frac{\Delta - \Delta_i}{2\Delta p} \qquad 2.4a$$

and

$$y = \frac{P-P_i}{2P_p} \qquad 2.4b$$

Equation 2.3 could be rewritten as:

$$x = \frac{1}{\beta} y + \frac{\alpha}{\beta} y^r \qquad 2.5$$

when it is desired to have the value of y, given x, iterative solutions must be used, because there is no explicit solution to the r^{th} degree polynomial of equation 2.5.

The iterative method developed by Newton and Raphson[12] is utilized herein to produce the following formula for the $n + 1^{st}$ iteration for y:

$$y_{n+1} = \frac{\frac{\alpha}{\beta}(r-1)\, y_n^r + x}{\frac{1}{\beta}(1 + \alpha r y_n^{r-1})} \qquad 2.6$$

Specifying r as a positive odd integer greater than one, r-1 would always be an even integer and the dominator will be finite causing definite convergence. The convergence is very fast as the error in each iteration tends to be the square of the previous error. Thus, slide rule work is sufficient to solve the problem within two or three iterations using a well chosen first value. Using digital computers, rapid convergence is obtained if the first chosen values y_o has an absolute value larger than that of the final solution and has the same sign as x.

2.2 Moment-Curvature Relationship

In order to develop a moment-curvature relationship for HSS under conditions of inelastic strain reversals, the Ramberg-Osgood type of equations is going to be utilized in the same fashion of equation 2.1 for load-deflection relationship.

The following assumptions are deemed necessary to accomplish our purpose:

1. Beams are prismatic and straight, and the cross-section is symmetrical about the plane of bending.
2. Planes normal to the axis of the beam remain plain after bending, which means that the strains vary linearly from the neutral axis.
3. The material properties in both tension and compression are identical; hence the Ramberg-Osgood relationship is applicable to the individual fibres in the two cases.

Thus, the required equation is:

$$\frac{\varepsilon}{\varepsilon y} = \frac{\sigma}{\sigma y}\left[1 + \alpha \left(\frac{\sigma}{\sigma y}\right)^{r-1}\right] \qquad 2.7$$

where ε is the strain, σ is the stress, εy is the yield strain, σy is the yield stress and α and r are the Ramberg-Osgood stress-strain parameters.

Assuming the maximum stress and strain values in the extreme fibres to be σ_{max} and ε_{max} respectively, for a certain bending moment, M at a section along the beam, the stress at any point y from the neutral axis (Figure 2.4) will be expressed as:

$$\sigma = \sigma_{max} - \sigma_x \qquad 2.8$$

where σ_x is the difference between the stress at the extreme fibre and the stress at point y. The corresponding expression for strain at point y becomes:

$$\frac{\varepsilon}{\varepsilon y} = \frac{\sigma_{max} - \sigma_x}{\sigma y} \left[1 + \alpha \left(\frac{\sigma_{max} - \sigma_x}{\sigma y} \right)^{r-1}\right] \qquad 2.9$$

The differential element of force dF and moment dM for the square hollow section of depth B and thickness t, shown in Figure 2.4, are:

$$dF = [2t\ (B-y-t)]d\ \sigma_x \qquad 2.10$$

The stress center $\bar{y}$, for the previous differential element is:

$$\bar{y} = \frac{\frac{t}{2}(B-2t)(B-t) + \frac{t}{4}(B-2y)(B+2y)}{2t\ (B-y-t)} \qquad 2.11$$

Thus the differential element of moment is:

$$dM = \overleftrightarrow{y}dF = \left[\frac{t}{2}(B-2t)(B-t) + \frac{t}{4}(B-2y)(B+2y) \right] d\sigma x \qquad 2.12$$

also from the geometry of Figure 2.4:

$$y = \frac{B}{2\varepsilon_{max}} \varepsilon \qquad 2.13$$

Substituting equations 2.9 and 2.13 into equations 2.10 and 2.12 gives:

$$dF = Bt \left\{ 2\left(1 - \frac{t}{B}\right) - \frac{1}{\mu} \left[\frac{\sigma_{max} - \sigma_x}{\sigma y} + \alpha \left(\frac{\sigma_{max} - \sigma_x}{\sigma y} \right)^r \right] \right\} d\sigma_x \qquad 2.14$$

and

$$dM = \frac{B^2 t}{4} \left\{ \left(3 - 6\frac{t}{B} + 4\frac{t^2}{B^2}\right) - \frac{1}{\mu^2} \left[\frac{\sigma_{max} - \sigma_x}{\sigma y} + \alpha \left(\frac{\sigma_{max} - \sigma_x}{\sigma y} \right)^r \right] \right. \qquad 2.15$$

where μ is the ductility factor for strains defined as:

$$\mu = \frac{\varepsilon_{max}}{\varepsilon y} = \frac{\sigma_{max}}{\sigma y} + \alpha \left(\frac{\sigma_{max}}{\sigma y} \right)^r \qquad 2.16$$

The resultant force F over half the section, i.e., to one side of the neutral axis, is obtained by integrating equation 2.14 from $\sigma_x = 0$ to $\sigma_x = \sigma_{max}$ yielding:

$$F = \sigma_{max} Bt \left\{ 2\left(1 - \frac{t}{B}\right) - \frac{1}{2\mu} \left[\frac{\sigma_{max}}{\sigma y} + \frac{2\alpha}{r+1} \left(\frac{\sigma_{max}}{\sigma y} \right)^r \right] \right\} \qquad 2.17$$

In order to obtain the total moment M, equation 2.15 is integrated over the whole section yielding:

$$M = \sigma_{max} \frac{B^2 t}{2} \{3 - 6 \frac{t}{B} + 4 \frac{t^2}{B^2}) - \frac{1}{\mu^2} [\frac{1}{3} (\frac{\sigma_{max}}{\sigma y})^2 + \frac{2\alpha}{r+2} (\frac{\sigma_{max}}{\sigma y})^{r+1} + \frac{\alpha^2}{2r+1} (\frac{\sigma_{max}}{\sigma y})^{2r}]\} \qquad 2.18$$

The maximum curvature ϕ_{max}, corresponding to the previous moment M is obtained by dividing the extreme fibre strain ε_{max} by its distance from the neutral axis.

$$\phi_{max} = \frac{2\varepsilon_{max}}{B} = \frac{2\varepsilon y}{B} [\frac{\sigma_{max}}{\sigma y} + \alpha (\frac{\sigma_{max}}{\sigma y})^r] \qquad 2.19$$

The stress center $\bar{y}$ for the full section is obtained as:

$$\bar{y} = \frac{M}{2F} \qquad 2.20$$

Substituting equations 2.17 and 2.18 into 2.20, yields:

$$\bar{y} = \frac{B}{4} \frac{(3 - 6 \frac{t}{B} + 4 \frac{t^2}{B^2}) - \frac{1}{3\mu^2} [Z_m^2 + \frac{6\alpha}{r+2} Z_m^{r+1} + \frac{3\alpha^2}{2r+1} Z_m^{2r}]}{2 (1 - \frac{t}{B}) - \frac{1}{2\mu} [Z_m + \frac{2\alpha}{r+1} Z_m^r]} \qquad 2.21$$

where:

$$Z_m = \frac{\sigma_{max}}{\sigma y} \qquad 2.22$$

When the section approaches the fully plastic condition of stress, the ductility ratio for strain μ tends to increase considerably. Thus equation 2.21 could be approximated to:

$$\bar{y} = \frac{B}{8} \frac{(3 - 6\frac{t}{B} + 4\frac{t^2}{B^2})}{(1 - \frac{t}{B})} \qquad 2.23$$

For the elastic distribution of stress, the expression for the stress center becomes:

$$\bar{y} = \frac{B}{9}(4 - 3\frac{t}{B}) \qquad 2.24$$

The values of the stress center y determined by equations 2.23 and 2.24 are the limiting values for the square hollow section of Figure 2.4.

Now, the moment-curvature relationship of the Ramberg-Osgood type could be written as follows:

$$\frac{\phi}{\phi y} = \frac{M}{M_y}\left[1 + \alpha'\left(\frac{M}{M_y}\right)^{R-1}\right] \qquad 2.25$$

where ϕ is the curvature, ϕy is the yield curvature, M is the moment, M_y is the yield moment, α' and R are the Ramberg-Osgood parameters.

The actual moment-curvature relationship could be calculated from equations 2.18 and 2.19 for different values of the extreme fibre stress σ_{max} and for given values of σy, εy and μ.

The parameters α' and R could be obtained by fitting equation 2.25 to the previous moment-curvature relationship using the method of least squares with the aid of a computer.

2.3 Cyclic Energy Dissipation

The dynamic behaviour of a structure is greatly influenced by the amount of energy absorbed during motion. Since dynamic response is usually described in terms of displacement, it is of interest to know how the cyclic energy dissipation is related to displacement.

Considering the response of a one degree-of-freedom structure to sinusoidal excitation, equation 2.3 describing the hysteresis loop, could be utilized in computing the energy dissipated during one complete cycle as follows:

$$2W = \oint P(\Delta)\, d\Delta \qquad 2.26$$

where 2W is the energy dissipated in a complete load cycle. Taking point (Δ_o, P_o) and $(-\Delta_o, -P_o)$ to be the extremes of the hysteresis loop,

it would be convenient to separate the previous integral 2.26 into the parts corresponding to the ascending and descending portions of the hysteresis loop respectively, and writing $d\Delta$ as $(d\Delta/dp)dp$:

$$2W = \int_{-P_o}^{P_o} p(\Delta) \frac{d\Delta}{dp} dp + \int_{P_o}^{-P_o} P(\Delta) \frac{d\Delta}{dp} dp \qquad 2.27$$

$d\Delta/dp$ represents slope on the ascending branch in the first integral and the slope of the descending branch in the second integral. Both of those slopes could be calculated from equation 2.3. Inserting these values in equation 2.27 and making a change of variables produces:

$$\frac{2W}{\frac{1}{2} P_p \Delta_p} = \frac{2}{\beta} \int_{-P_o/P_p}^{P_o/P_p} \frac{P}{P_p} \left[1 + \alpha r \left(\frac{P+P_o}{2P_p} \right)^{r-1} \right] d \left(\frac{P}{P_p} \right) \qquad 2.28$$

$$+ \frac{2}{\beta} \int_{P_o/P_p}^{-P_o/P_p} \frac{P}{P_p} \left[1 + \alpha r \left(\frac{P-P_o}{2P_p} \right)^{r-1} \right] d \left(\frac{P}{P_p} \right)$$

Considering the left side of equation 2.28 the dimensionless term $W/ 1/2 P_p \Delta p$ would be defined as the "Energy Ratio", which is the ratio of the energy dissipated in a single load excursion (half-cycle) to the characteristic term $(1/2 P_p \Delta p)$, thus:

$$e = W/(1/2 P_p \Delta_p) \qquad 2.29$$

Expanding the previous integrals in equation 2.28 and letting:

$$Z1 = \frac{P+P_o}{2P_p} \qquad 2.30a$$

and

$$Z2 = \frac{P-P_o}{2P_p} \qquad 2.30b$$

yields

$$\frac{2W}{\frac{1}{2}P_p\Delta p} = \frac{2}{\beta}\int_{-P_o/P_p}^{P_o/P_p}\frac{P}{P_p}\,d\left(\frac{P}{P_p}\right) + \frac{2}{\beta}\int_{P_o/P_p}^{-P_o/P_p}\frac{P}{P_p}\,d\left(\frac{P}{P_p}\right) \qquad 2.31$$

$$+ \frac{8\alpha r}{\beta}\int_0^{2P_o/P_p} Z1^{r-1}\left(Z1 - \frac{P_o}{2P_p}\right)dZ1 + \frac{8\alpha r}{\beta}\int_0^{2P_o/P_p} Z2^{r-1}\left(Z2 - \frac{P_o}{2P_p}\right)dZ2$$

The first two integrals in the previous expression represent the elastic portion of the work done in the half cycles and are equal to zero. Evaluating the remaining two integrals equation 2.31 yields:

$$\frac{2W}{\frac{1}{2}P_p\Delta_p} = \frac{8\alpha}{\beta}\left(\frac{r-1}{r+1}\right)\left(\frac{P_o}{P_p}\right)^{r+1} \qquad 2.32$$

Equation 2.32 gives the energy dissipated in a single cycle as a function of the force amplitude P_o/P_p. Although, in general, W cannot be expressed explicitly as a function of Δ_o/Δ_p approximate expressions for the cases of very small or very large deflections could be derived. Considering equation 2.1, the linear term could be neglected, for large displacements. Substituting the value of P/P_p into equation 2.32 produces a large amplitude approximation depending on displacement only:

$$\frac{2W}{\frac{1}{2}P_p\Delta_p} = \frac{8}{r\sqrt{\alpha}\,\beta}\left(\frac{r-1}{r+1}\right)\left(\frac{\Delta_o}{\Delta_p}\right)^{r+1/r}, \text{ as } \frac{\Delta_o}{\Delta_p} \to \infty \qquad 2.33$$

Similarly, for the small displacement amplitudes equation 2.32 can be written as:

$$\frac{2W}{\frac{1}{2}P_p\Delta_p} \approx \frac{8\alpha}{\beta}\left(\frac{r-1}{r+1}\right)\left(\frac{\Delta_o}{\Delta_p}\right)^{r+1}, \text{ as } \frac{\Delta_o}{\Delta_p} \to 0 \qquad 2.34$$

Equation 2.33 shows that for large amplitudes the energy dissipated is proportional to the displacement amplitude raised to a power between one and two. This power approaches one as r increases and equals two for the linear case when r equals one. Also the influence of α diminishes rapidly as r increases.

Equation 2.34 shows also that the energy dissipated is proportional to α and approaches zero as the value Δ_o/Δ_p diminishes.

Equation 2.32 is very advantageous in terms of determining the

α, β and r parameters, knowing the predetermined values of P_p and Δ_p and the amount of energy dissipated for a certain structural member during a cyclic program. This method excels the one of least squares suggested earlier which is quite lengthy and time consuming.

2.4 Ductility Factors

The term "ductility factor" is a measure of the amount of yielding occurring in a system. However, a ductility factor has no precise significance until the method of measuring it has been defined. The widely used definition of the term is the ratio of total deformation to elastic deformation at yield; it could be defined as that ratio for strains, rotations and displacements. For strains the value depends mainly on the material, while for rotation the effects of the shape and size of cross section are included. The ratio for displacements involves the total configuration of the structure and loading. It is also necessary to state whether the ductility factor is measured from the initial configuration of the system, or from the immediately preceding no-load position.

Giberson[13] presented two more definitions of the term other than the one described above. These definitions are presented here after being modified to suit plastic design purposes by using the elastic deflection Δ_p, corresponding to the plastic load P_p, instead of the yield deflection Δy.

These definitions apply to the non-linear spring of the simple yielding system of Figure 2.5. Ductility factors could be applied either to the bilinear hysteresis loop shown in Figure 2.6 or to the more general curvilinear hysteresis loop of Figure 2.7.

The only possible hysteresis loop for the non-linear spring of the system of Figure 2.5, is the path 0, a, b, c, d, e, f, in Figure 2.6. The path consists of the linear portion oa, where point a is the yield point and the non-linear portion ab in which the additional displacement, Δ_o occurs after yielding where:

$$\Delta_o = |\Delta|_{max} - \Delta_p \qquad 2.35$$

Δ_o consists of a linear and a non-linear component. Considering the geometry of Figure 2.6:

$$\Delta_n = (1 - \frac{K_2}{K}) \Delta_o \qquad 2.36$$

Thus, the additional linear displacement occurring from point a to b is:

$$\Delta_o - \Delta_n = (\frac{K_2}{K}) \Delta_o \qquad 2.37$$

Therefore, the total linear displacement contained in traversing from point 0 to a to b is:

$$\Delta_\ell = \Delta_p + (\frac{K_2}{K}) \Delta_o \qquad 2.38$$

Now, the three definitions of ductility factor are defined below:

(i) Elastic-Plastic Model

The ratio of the maximum absolute displacement at point b, $|\Delta|_{max}$, to the elastic deflection, Δ_p, without regard to the second slope, K_2 Figure 2.6:

$$\mu_1 = \frac{|\Delta|_{max}}{\Delta_p} \qquad 2.39$$

Equation 2.39 can be used to measure the yielding of any hysteresis loop, its most appropriate application is to ideally elastoplastic loops which are bilinear hysteresis loops with the second slope equal to zero, $K_2 = 0$, i.e.,

$$\Delta_n = \Delta_o = |\Delta|_{max} - \Delta_p, \ (K_2 = 0) \qquad 2.40$$

and the total linear displacement at point b is the elastic displacement, Δ_p:

$$\Delta_\ell = \Delta_p \ (K_2 = 0) \qquad 2.41$$

(ii) Bilinear Material with Strain Hardening

The second definition of ductility factor suits systems with $K_2 \neq 0$. It measures the nonlinear displacement (instead of the maximum absolute

displacement) at point b with respect to the elastic displacement, Δ_p:

$$\mu_2 = 1 + \frac{\Delta_n}{\Delta_p} \quad . \qquad 2.42$$

which, by substituting equation 2.37 for Δ_n becomes:

$$\mu_2 = 1 + (1 - \frac{K_2}{K}) \frac{\Delta_o}{\Delta_p} \qquad 2.43$$

These two definitions of ductility factor, need a well-defined yield level. However, most curvilinear hysteresis loops may not have a well defined yield point. Nevertheless, for most hysteresis loops, except those with a vertical initial tangent, the linear and non-linear displacements are well defined.

(iii) General Hysteresis Loop Model

For these loops a third definition of ductility factor relates the maximum absolute displacement, $|\Delta|_{max}$, at point b to the linear displacement, Δ_ℓ, as can be seen in Figure 2.6.

$$\mu_3 = \frac{|\Delta|_{max}}{\Delta_\ell} \qquad 2.44$$

or

$$\mu_3 = 1 + \frac{\Delta_n}{\Delta_\ell} \qquad 2.45$$

For bilinear hysteresis loops, and substituting equations 2.36 and 2.38 for Δ_n and Δ_ℓ, respectively, the third definition becomes:

$$\mu_3 = 1 + \frac{(1 - \frac{K_2}{K})\Delta_o}{\Delta_p + (\frac{K_2}{K})\Delta_o} \qquad 2.46$$

Table 2.1 shows values for the three definitions for bilinear hysteresis loops with the following arbitrary values: $\Delta_p = 0.30$ and $|\Delta|_{max} = 1.60$ for systems with $K_2/K = 0.05$ and $K_2/K = 0.95$. When $K_2 = 0$, $\mu_1 = \mu_2 = \mu_3$. From these examples, it is obvious that the choice of the definition of ductility factor makes a significant difference on the resulting numerical values.

2.5 Plasticity Ratio

The above definitions of ductility factor do not clearly differentiate between the recoverable deformation and the permanent, or plastic deformation. In addition, they are best suited to steady-state responses because of the inability of obtaining a direct indication of the residual displacement at no load. Thus, ductility factors cannot be used as cumulative damage indicators. For these reasons the term "plasticity ratio", π_d, with the subscript d, denoting deflection measure, is introduced as follows:

$$\pi_d = \frac{\Delta'}{\Delta_p} \qquad 2.47$$

where Δ' is the residual plastic deformation, and Δ_p is the elastic deformation corresponding to the plastic load P_p.

Popov[5] plotted the relationship between e and π_d (which is an indication of the permanent deformation), for each excursion, for every specimen. The relationship yielded a straight line of the following equation:

$$e = 1.77\ \pi_d \qquad 2.48$$

Equation 2.48 strictly describes the behaviour of the group of specimens tested by Popov[5]. That equation indicates that the strength of the connections did not deteriorate as the applied displacements and consequently the residual deformations were increased. Such information can be useful in actual practice in assessing the strength of a structural member after an eqrthquake, if the amount of residual deflections is known.

2.6 Cumulative Energy Dissipation

Energy dissipation is a measure of the cumulative damage. The decrease of the rate of energy dissipation, for a certain structural member would mean that it is not participating in resisting the straining

actions. Thus, the adjacent members are required to absorb the excess in energy input.

2.7 Total Energy Dissipation

The total energy absorbed by each specimen is a direct indication of its capability of resisting cyclic effects generated during an earthquake. A more generalized term is the accumulated energy ratio Σe, which was proportional to $\Sigma \pi_d$ in Popov's experiments.

The previous measures are going to be utilized in assessing the capabilities of HSS in cyclic loading as summarized in the following:

1. The load-deflection hysteresis loops are going to be examined for their stability and reproducibility under conditions of high cyclic strain limits.
2. The moment-curvature relationships would indicate the curvature patterns and their changes as testing advances. The residual curvatures will indicate the beam shape after cycling.
3. The energy dissipation through individual load cycles and its accumulation as the test proceeds would furnish a sufficient guide to judge the validity of the section for seismic applications.
4. The ductility and plasticity factors are going to be investigated, and would indicate the trends of the total and residual displacements through tests. The accumulation of the plasticity factor will indicate

the cumulative damage.

5. On the basis of the previous measures we can determine the minimum requirements of HSS that qualify them as earthquake resistant structural members.

TABLE 2.1

Three Definitions of Ductility Factors

for Bilinear Hysteresis Loop of Figure 2.6

Definition	$\frac{K_2}{K} = 0.05$	$\frac{K_2}{K} = 0.95$
μ_1, Eq. 2.39	5.33	5.33
μ_2, Eq. 2.43	5.12	1.22
μ_3, Eq. 2.46	4.38	1.04

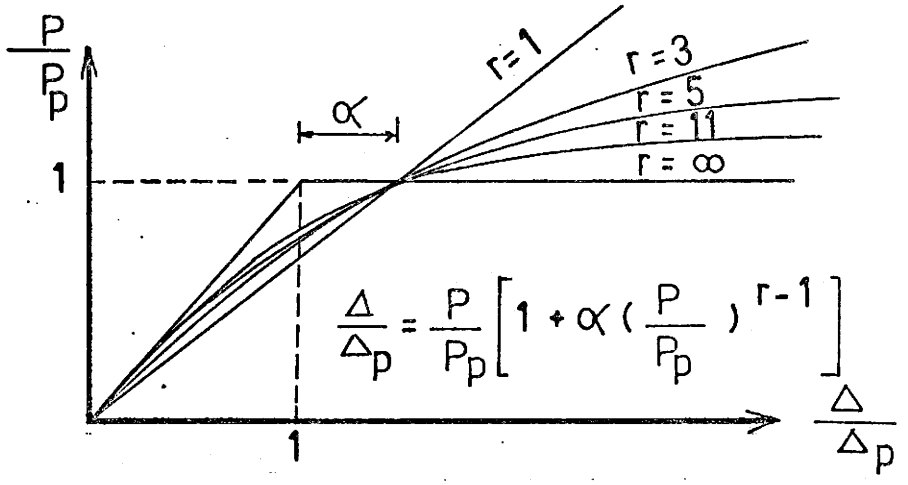

Fig.2.1 RAMBERG-OSGOOD FUNCTION.

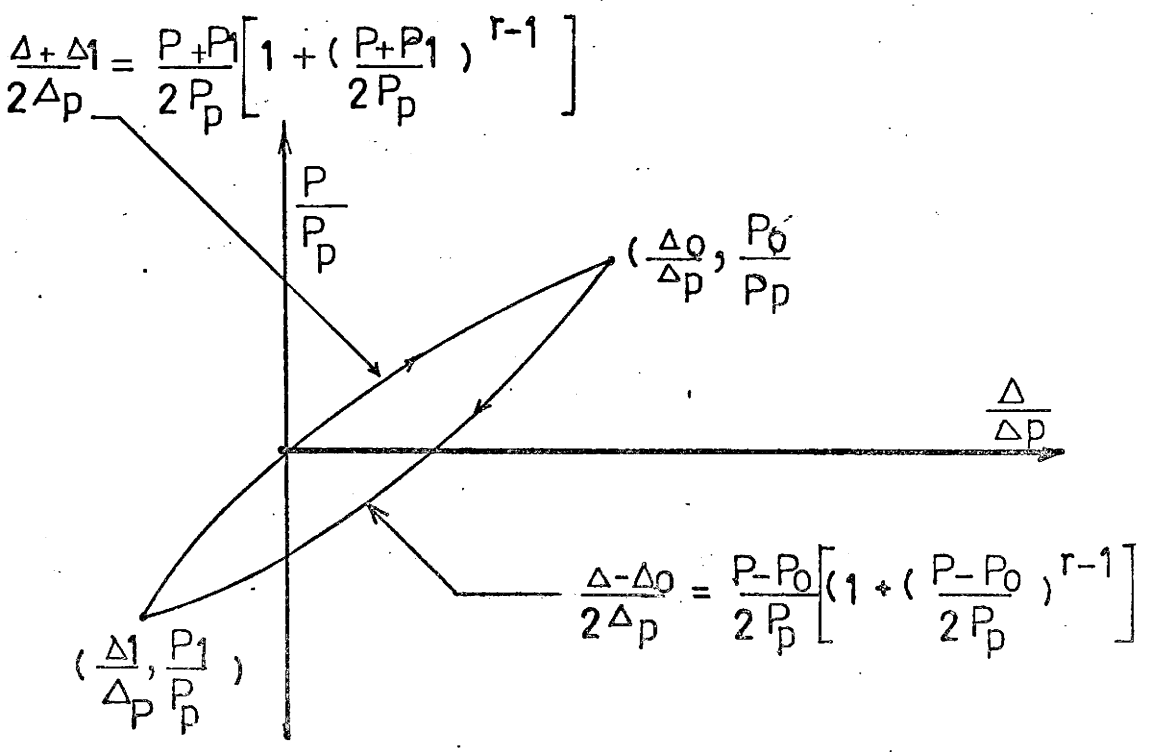

Fig.2.2-RAMBERG-OSGOOD

LOAD-DISPLACEMENT RELATIONS.

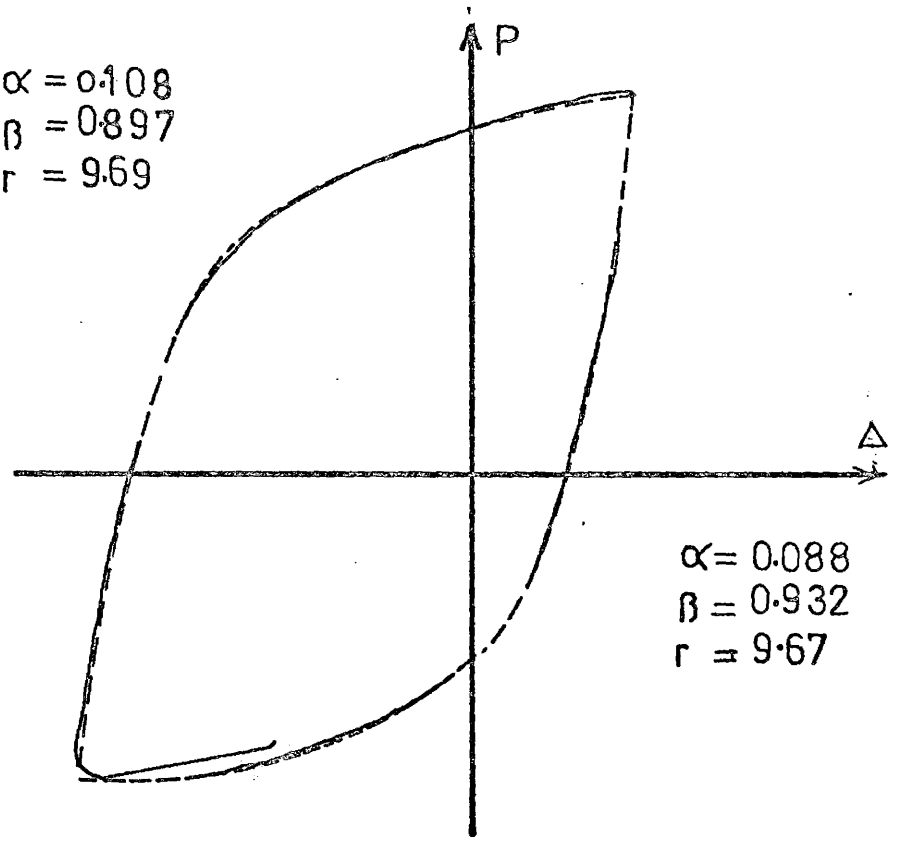

Fig: 2.3 - EXAMPLE OF LEAST SQUARES FIT.

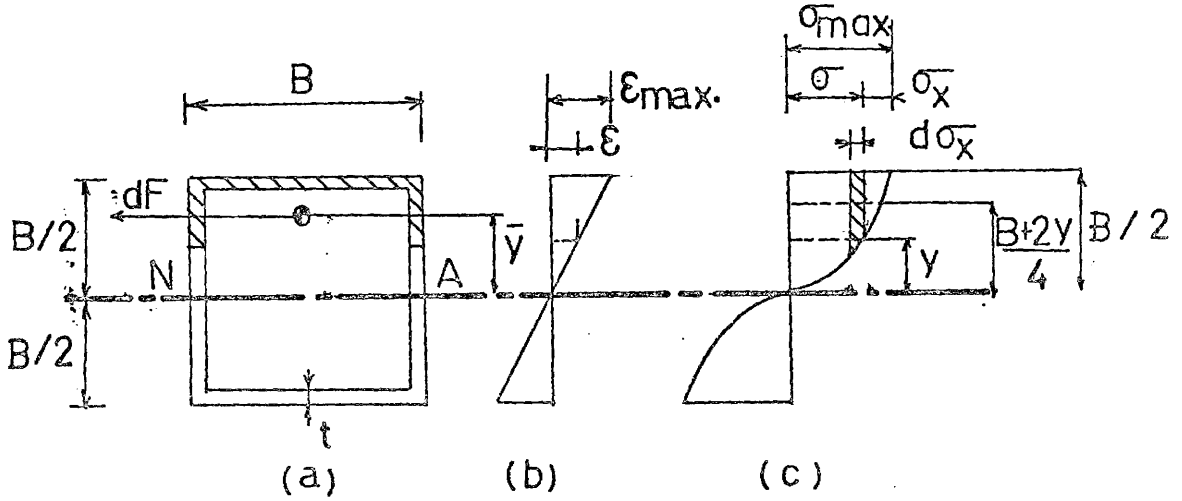

Cross-Sectional Area. Strain Distribution. Stress Distribution.

Fig. 2.4 – STRESS AND STRAIN DISTRIBUTION.

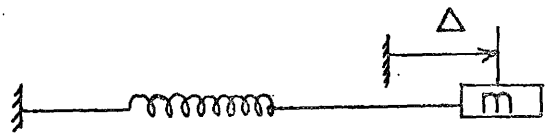

Fig. 2.5- SIMPLE YIELDING SYSTEM WITH NONLINEAR SPRING.

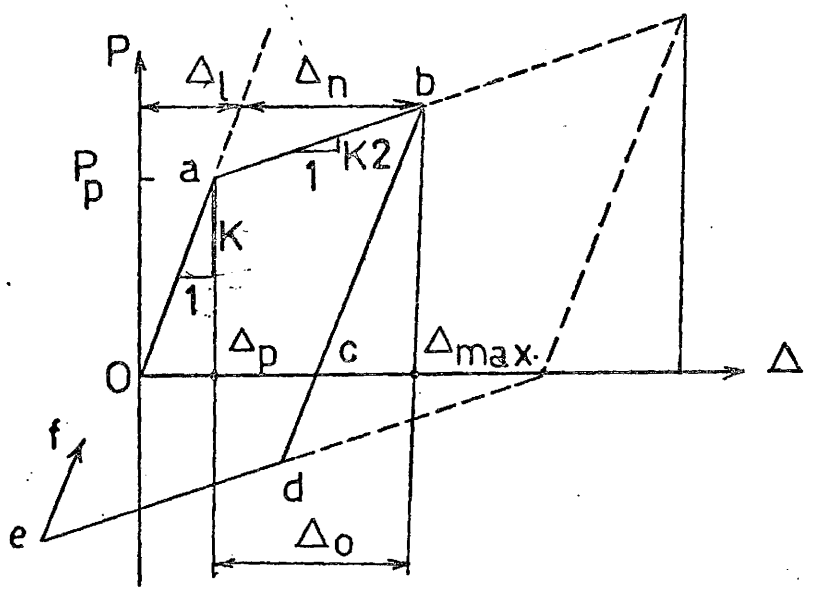

Fig. 2.6-BILINEAR HYSTERESIS LOOP.

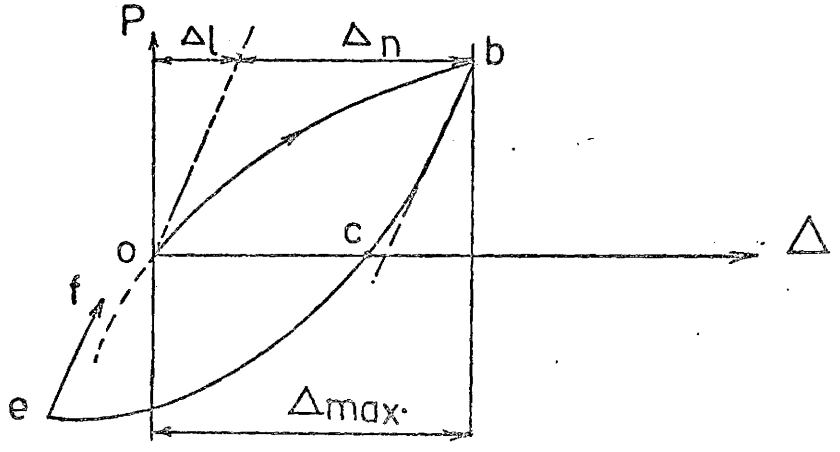

Fig. 2.7-CURVILINEAR HYSTERESIS LOOP.

CHAPTER III

EXPERIMENTAL PROGRAM

3.1 Testing Material

HSS are manufactured by the Steel Co. of Canada Ltd., suppliers of the tested sections in two ways:

(a) hot-forming if the periphery of the section does not exceed 16 inches, and

(b) cold forming if the periphery of the section exceeds 16 inches.

All the sections investigated were cold-formed. The flange slenderness ratio, b/t for the tested square sections was chosen so as to provide a range for plastic design, compact, non-compact and reduced stress cases.

The tested sections are listed in Table 3.1, along with their detailed structural properties. The elastic modulus of all sections is assumed to be 30,000 KSI. The minimum yield stress is specified as 50 KSI. Table 3.2 shows the structural properties of the tested beams.

3.2 Material Properties

A typical stress-strain curve obtained from a tensile test is shown in Figure 3.1. The yield stress, σy, is defined herein as that stress corresponding to a total strain of 0.5%. This stress corresponds to the constant stress at yielding, and is close to the value obtained by the 0.20% offset method.

The idealized bilinear stress-strain relationship is defined by the yield strength, σ_y, the modulus of elasticity E and the strain-hardening modulus E_{st} obtained from the tension test. This data is used to predict the moment curvature and load-deflection relationships.

HSS material tested by Hudoba[14] did not vary significantly along the periphery of the cross-section and the material taken at right angles to the seam of the section represented a reasonable sample to assess the material properties. The tensile specimens were cut accordingly conforming with ASTM standards[15] E8-66. Table 3.3 gives the area of cross section, the maximum load and the ultimate stress for each tensile specimen.

3.3 Testing Arrangement

(a) Test Set Up

The test set up was designed to allow for a simply supported beam of 97.50 inches span. The testing objective was to establish the

static load deflection curve of the beam, and then apply twenty full cycles of 2.0% control strain by means of a hydraulic jack with its ram mounted at the midspan of the beam. At the end of the cycling program the flexural capacity of the beam was tested again in order to assess the loss in strength due to the previous dynamic testing.

Three strain gauges were located on each top and bottom flange of the beam, two inches from midspan. The strain gauges were located at the center of the flange and at both corners. Deflections were measured by means of two dial gauges installed 5 3/4 inches from the midspan and at the end support. The accuracy of the dial gauge was $\pm$ 0.001 inches.

(b) Description of Test Apparatus

1. Electronic Controller

The controlling unit used to govern the hydraulic jack is Model 406.11 Controller produced by the MTS (Materials Testing Systems) Corp. It is an electronic sub-system containing the principal servo control, failsafe, and readout functions for one channel in an electrohydraulic testing system. The system's hydraulic actuator drives the hydraulic jack used for applying load to a specimen, and to a transducer connected to the load cell in order to evaluate the amount of load applied. Transducer conditioner 1 supplies AC excitation to its associated transducer and provides a DC output proportional to the mechanical input to the transducer. Transducer conditioner 2 also supplies a DC output proportional to the mechanical input to its transducer. Full scale conditioner output is $\pm$ 10 VDC.

The feedback selector allows selection of either transducer conditioner connected to the LVDT (Linear Variable Differential Transformer) system indicating the hydraulic jack's stroke reading, or the external transducer conditioner signal received from the load cell indicating the load reading.

The servo controller compares feedback with a command signal to develop a control signal that operates the servovalve. Command is the sum of an external program signal and an internal set point level and has a full scale input amplitude of $\pm$ 10 VDC. The servo controller has an error detector circuit that can open a system failsafe interlock to stop the test if error between command and feedback exceeds a preset limit.

2. Hydraulic Jack

The hydraulic jack is of 250 kips capacity, with a peak to peak ram stroke of 8 inches. The ram travel is controlled by the LVDT system according to the command signal sent from the controller unit. The jack weighs 1600 lbs. and is manufacted by the MTS Corporation.

3. Load Cell

The load cell could be used for both tension and compression purposes with a maximum capacity of 450 kips. Load value is indicated by means of an electronic transducer connected to the controller unit, in the form of DC voltage. The cell weighs 140 lbs. and has two threaded ends of 5 inch diameter.

4. The LVDT (Linear Variable Differential Transformer) System

Differential transformers are electromagnetic devices for translating the displacement of a magnetic armature into an AC voltage which is a linear function of the displacement. Although the physical configurations vary between the manufacturers, they are basically composed of primary and secondary coils wound on an air core and a moveable armature is used to control the electrical coupling between them. This device, after being calibrated, was used to indicate the hydraulic jack's stroke reading as mentioned before.

5. Loading Plates

There were two loading plates mounted to the top and the bottom of the specimen midspan by means of six 1.25 inch and four 1.00 inch bolts. The top loading plate was 1.00 inch thick and was connected to the load cell by means of a 5 inch diameter female thread welded to the top of the plate. The bottom plate was 2.0 inches thick and was connected to the top plate by means of the bolts.

(c) Preparation of Test Apparatus

The hydraulic jack was calibrated for stroke readings against the DC voltage signals representing the set point commands applied to the controller. The three variables, stroke, DC voltage and the set point changes proved to be linearly related with a great level of accuracy.

The load cell was also calibrated in the 120 kips Tinius Olsen testing machine, for both tensile and compressive load values in the

range of ± 120 kips. Load readings and the DC voltage readings of the cell's electric transducer were also of a linear relationship.

(d) Preparation of Specimens for Testing

All specimens were supplied with a steel collar for loading purposes at midspan. The collar was 3 inches wide and 0.50 inch thick, mounted on the outside periphery of each specimen. The collar helped to guarantee a uniform load on the whole cross section to prevent areas of stress concentration which could lead to premature local buckling.

Two specimens of size (12.0 x 12.0 x 0.3120) inches were provided with a three inch thick block of timber filling the midspan cross section within the limits of the collars. A chemical cementing material called Colma-Dur was used to develop complete adhesion between the timber block and the steel section. That provision helped in preventing premature local buckling in the midspan where the load capacity is of prime concern.

(e) Provisions of End Supports

The end supports were required to represent a simply supported condition; hence rotation of the specimen was permitted with vertical displacements prevented in both upward and downward directions. Four end brackets were used on each end of the specimen to connect it to the vertical supporting column. Also, two end bolts of 1.00 inch L9 Lamalloy high tensile steel were used, one on each side. During the actual testing, specimens experienced some vertical displacement at the ends in both

directions. These displacements were recorded by means of dial gauges of ± 0.001 inch accuracy which were vertically installed at the ends of each specimen to record these displacements. After the first three tests the end brackets were replaced by a more rigid system, in order to minimize end displacements. Four rollers were used, two at each end in order to facilitate the rotation of specimens during loading. Four steel box sections, and one inch diameter high tensile steel bolts ASTM A-325, were used as end support. Figures 3.2 and 3.3 show diagramatic drawings of the testing apparatus. Figure 3.4 shows photographs of the overall set up of the test and Figure 3.5 shows the modified roller end supports. Figures 3.6 through 3.11 show the failure shapes of Beams H1 through H7.

(f) Mounting of Strain-Gauges

The electric strain gauges which were used for strain measurements were:

EP-08-500 BH-120 option W, manufactured by Micro-Measurement Co., Romulus, Michigan, with the following specifications:

Resistance in ohms	120.0 ± 0.30%
Gauge factor at 75°F	2.055 ± 0.50%
Strain limits	Approximately 15%

For the gauge installation M-Bond GA-2 adhesive was used. This is a 100% solid epoxy system which has a preferred cure schedule of 40 hours

at 75°F. The surface preparation and installation were made as recommended in Instruction Bulletin B-137-2 March, 1973 provided by the manufacturer.

3.4 Testing Procedure

The load was applied to the specimen by means of a gradual increase of the stroke of the jack. A static loading test was carried out on each specimen before and after the cyclic program. The cyclic loading was started by the attainment of the maximum strain value of $\pm$ 2.0% in the first half cycle in compression. The resulting value of peak midspan deflection was maintained afterwards throughout the dynamic test, measured from the last position of zero load. For each cycle four main points were investigated, the two peak points of maximum compression and maximum tension, and the two points of zero load. At each of these stages, detailed readings of load, stroke, dial gauges and strain gauge readings were recorded. The cycling program was carried out twenty cycles unless failure of the specimen was noticed earlier. Detailed readings were recorded for each load increment during the static load tests.

TABLE 3.1

Hollow Structural Sections and Their Structural Properties

No.	Size (inches)	Wall Thickness (inches) t	Weight (pounds/ foot)	Area ($inches^2$) A	Moment of Inertia ($inches^4$) I	Section Modulus ($inches^3$) S	Radius of Gyration (inches) r	Shear Constant ($inches^2$) C_{RT}	Plastic Section Modulus ($inches^3$) Z	Location of Elastic and Plastic Neutral Axis
1	8.00x 8.00	0.2500	25.80	7.51	75.1	18.8	3.15	3.50	22.0	4.00
2	8.00x 8.00	0.3120	31.77	9.34	90.7	22.70	3.12	4.21	26.8	4.00
3	8.00x 8.00	0.5000	48.81	14.36	131	32.80	3.02	6.00	40.3	4.00
4	10.00x10.00	0.2810	36.45	10.72	167	33.40	3.95	4.99	38.80	5.00
5	10.00x10.00	0.4500	56.67	16.67	249	49.8	3.87	7.38	59.50	5.00
6	12.00x12.00	0.3120	48.74	14.34	323	53.9	4.75	6.71	62.60	6.00
7	12.00x12.00	0.3120	48.74	14.34	323	53.9	4.75	6.71	62.60	6.00

TABLE 3.2

Elastic and Plastic Properties of Beams Tested

Beam No.	Span (inches)	Yield Load (kips)	Yield Moment (kip-ft)	Yield Deflection (inch)	Elastic Stiffness (kip/inch)	Plastic Load (kips)	Plastic Moment (kip-ft)	Elastic Deflection at Yield (inch)	$1/2\ P_p\Delta_p$	Shape Factor
H1	97.50	38.60	78.40	0.338	114.0	45.20	91.50	0.396	8.95	1.165
H2	97.50	46.50	94.50	0.338	137.50	55.0	111.50	0.398	10.95	1.170
H3	97.50	67.40	138.00	0.338	200.00	82.60	169.00	0.415	17.20	1.230
H4	97.50	68.50	139.50	0.271	264.00	79.50	162.00	0.316	12.55	1.160
H5	97.50	102.00	207.00	0.271	395.00	122.00	248.00	0.324	19.70	1.20
H6 and H7	97.50	110.00	225.00	0.225	484.00	128.50	261.00	0.262	16.80	1.16

TABLE 3.3

Tensile Tests Data

No.	HSS	Area ($inch^2$)	P_{max} (kips)	Fu (ksi)
H1	8x 8x0.25	0.125	6.92	55.40
H2	8x 8x0.312	0.154	8.90	57.80
H3	8x 8x0.50	0.234	15.26	65.00
H4	10x10x0.281	0.125	6.92	55.40
H5	10x10x0.45	0.228	12.20	53.50
H6	12x12x0.312	0.1355	8.00	59.00
H7	12x12x0.312	0.160	9.82	61.40

Fig. 3.1 (a)

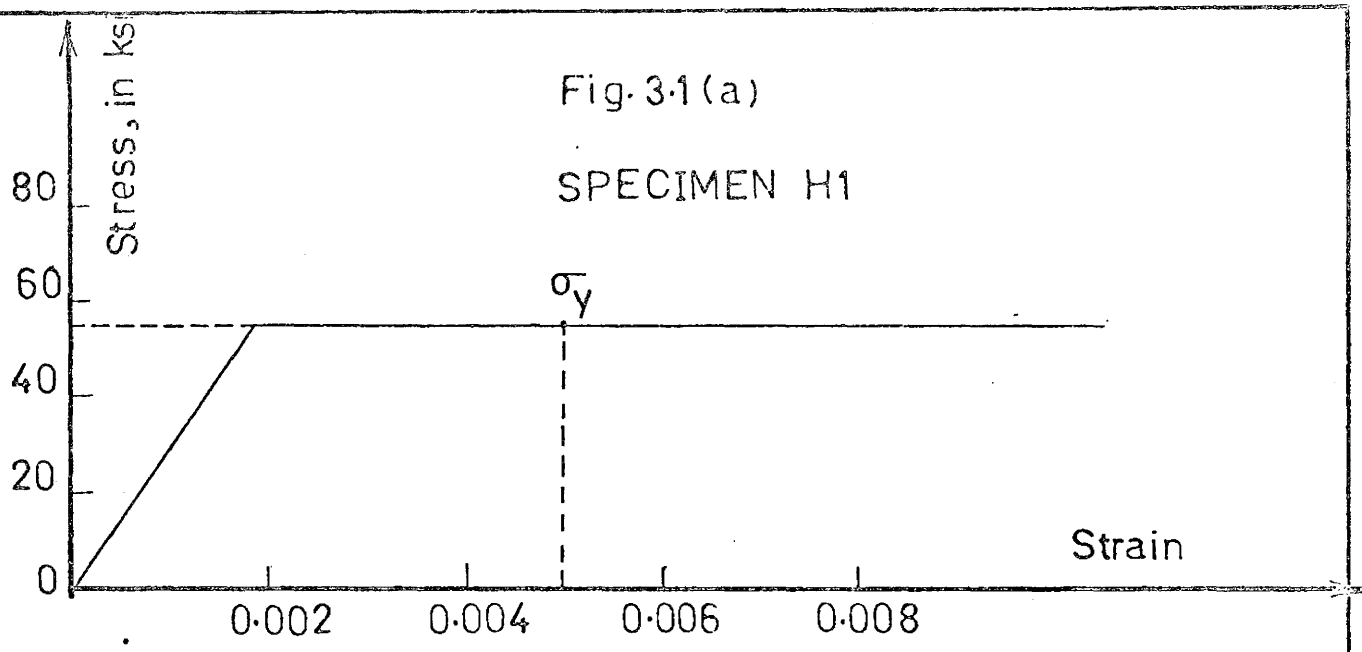

SPECIMEN H1

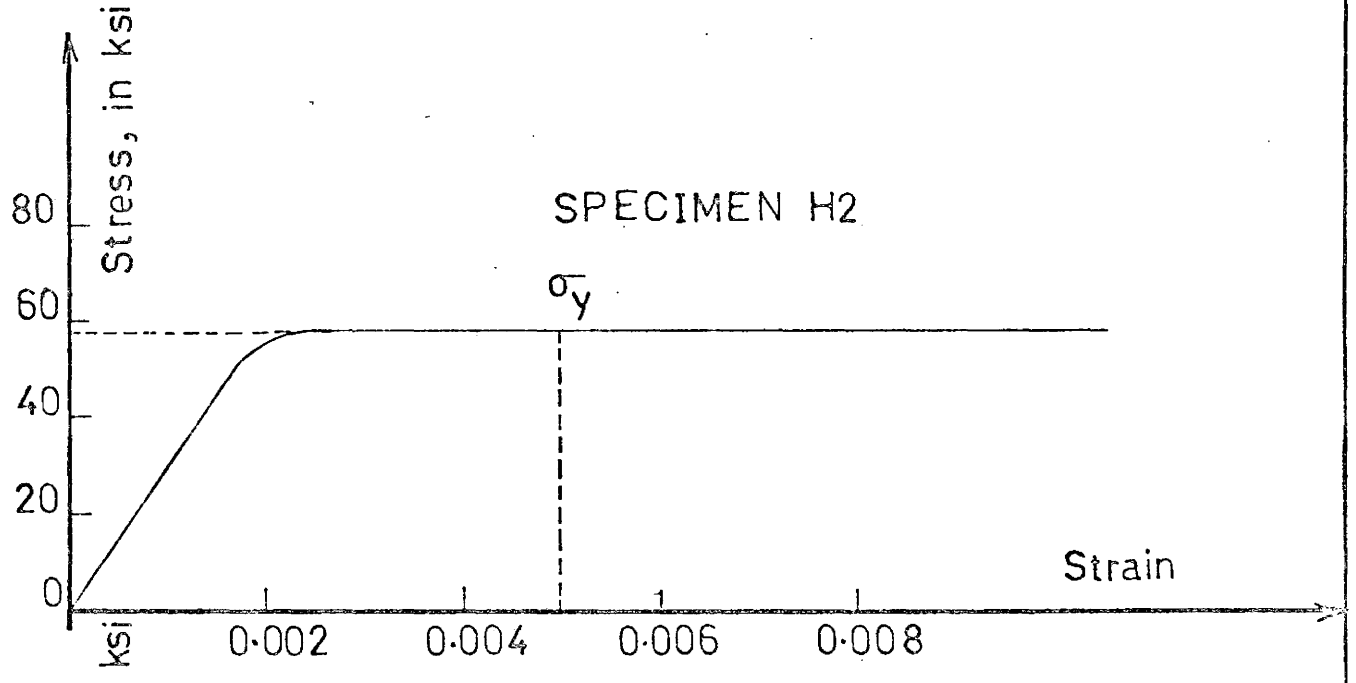

SPECIMEN H2

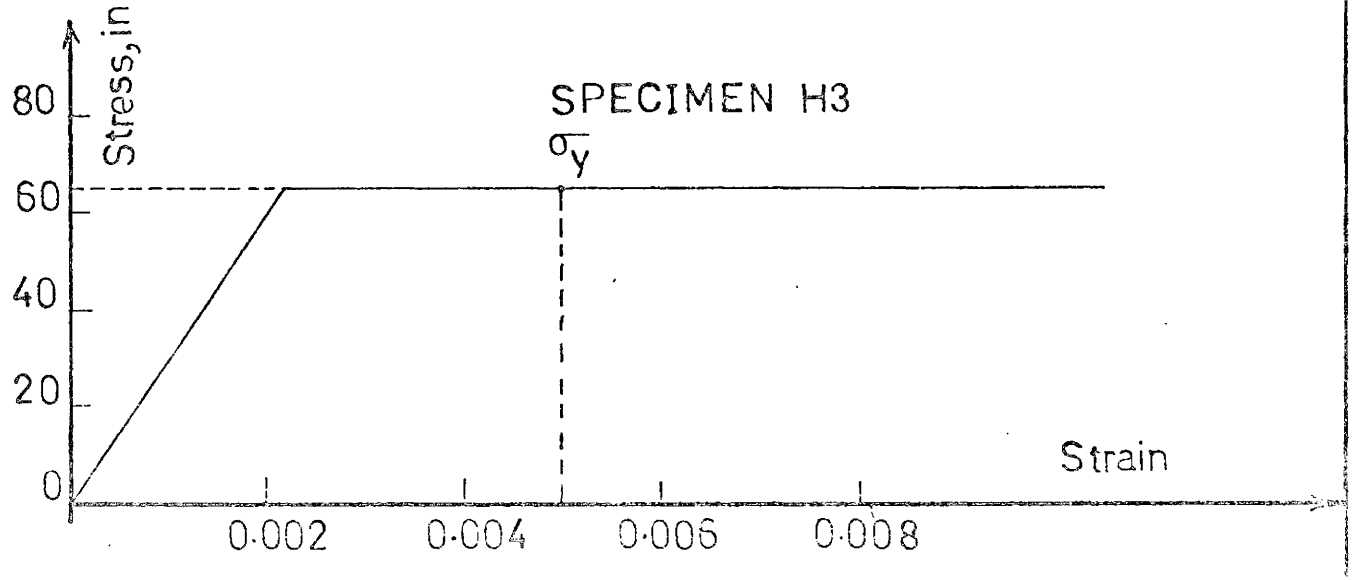

SPECIMEN H3

Fig·3·1(b)

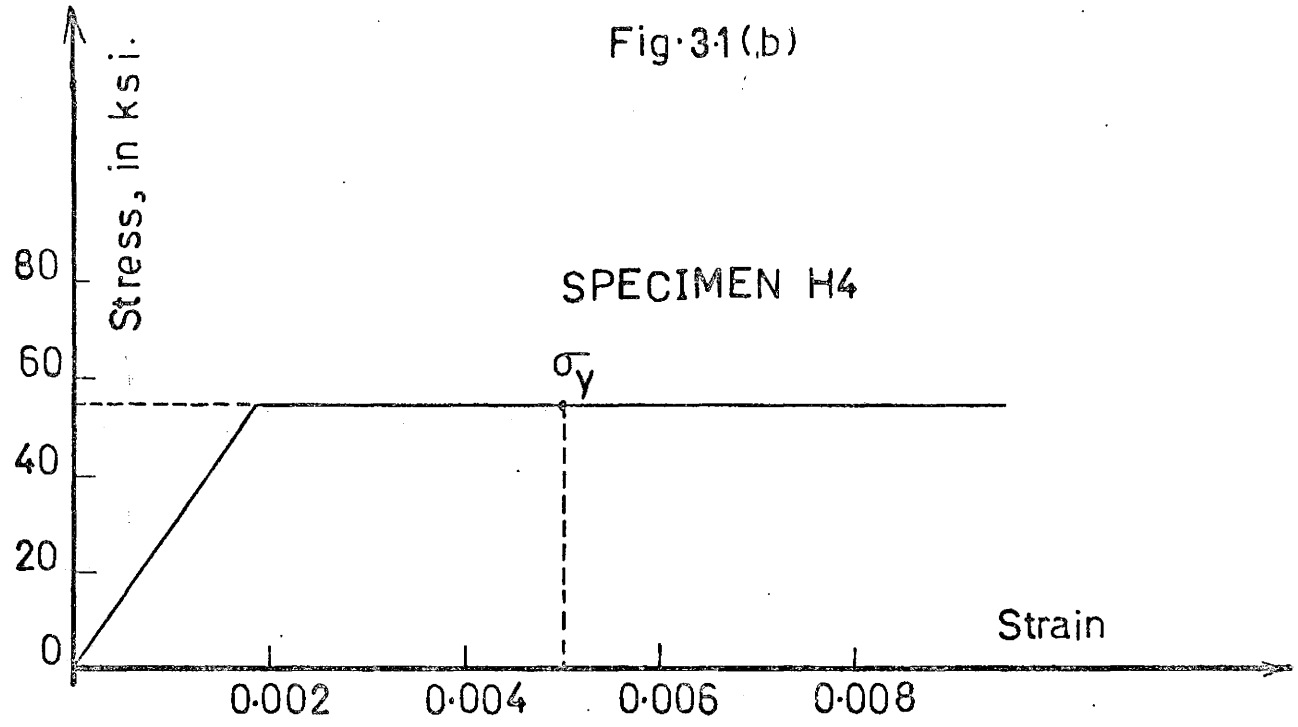
Stress, in ksi.
80
60
40
20
0
SPECIMEN H4
σ_y
Strain
0·002
0·004
0·006
0·008

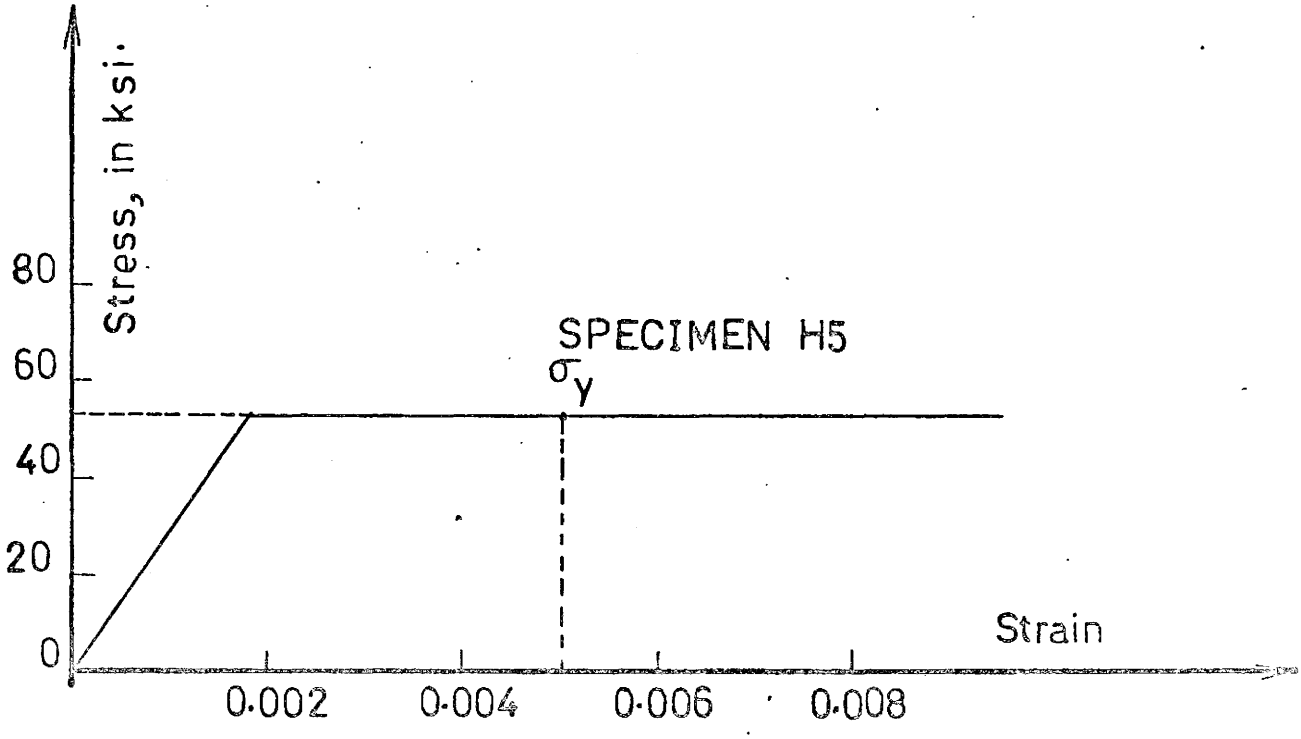
Stress, in ksi.
80
60
40
20
0
SPECIMEN H5
σ_y
Strain
0·002
0·004
0·006
0·008

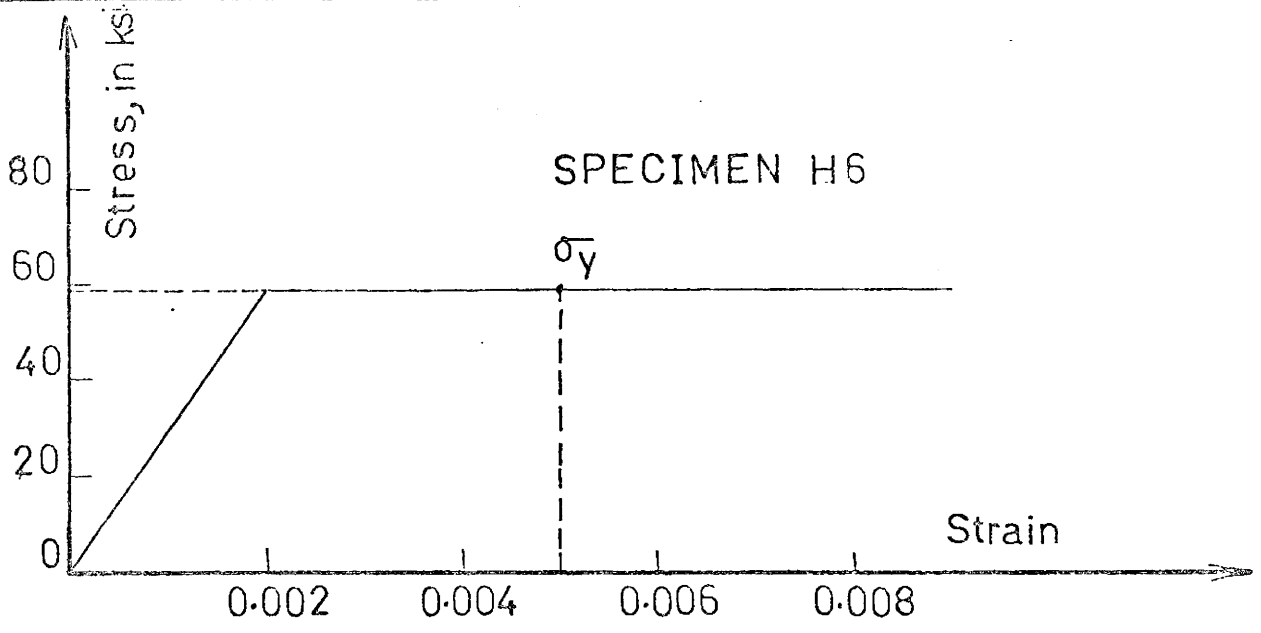

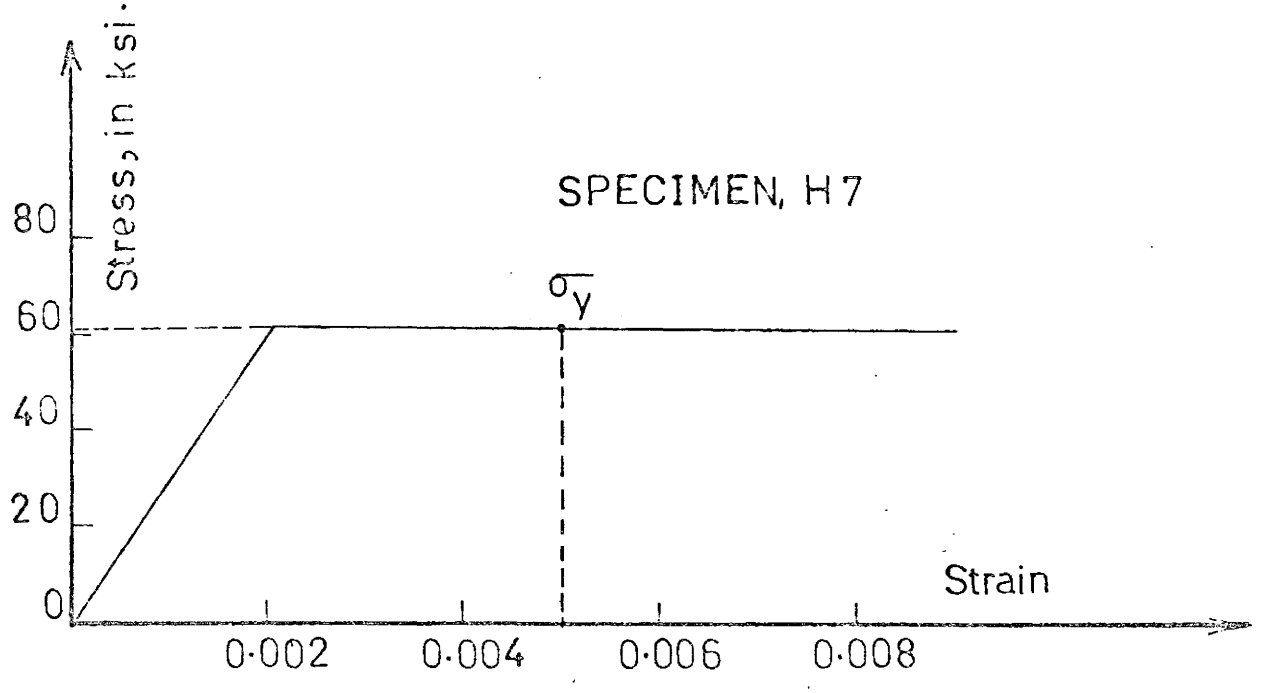

Fig·3·1-RESULTS OF TENSILE COUPONS·

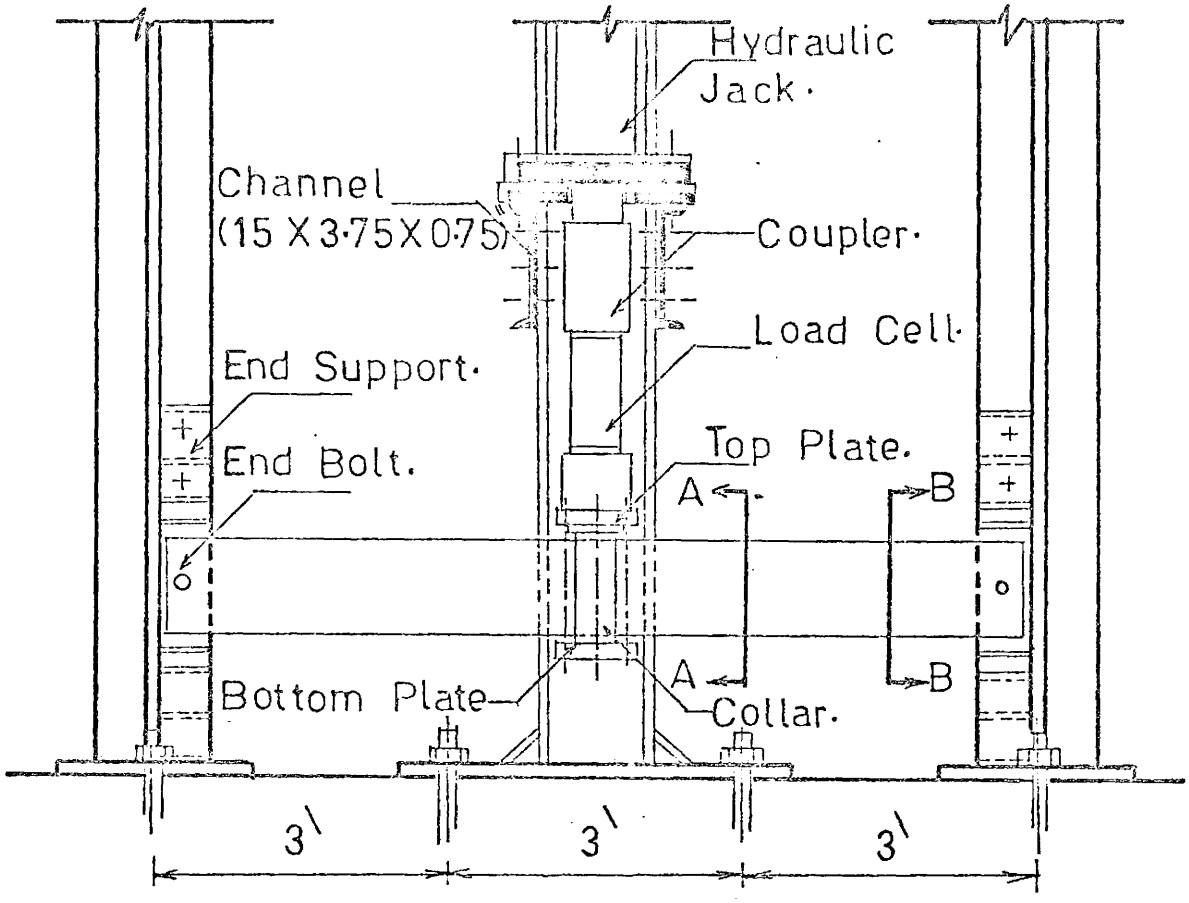

Sectional Elevation C-C.

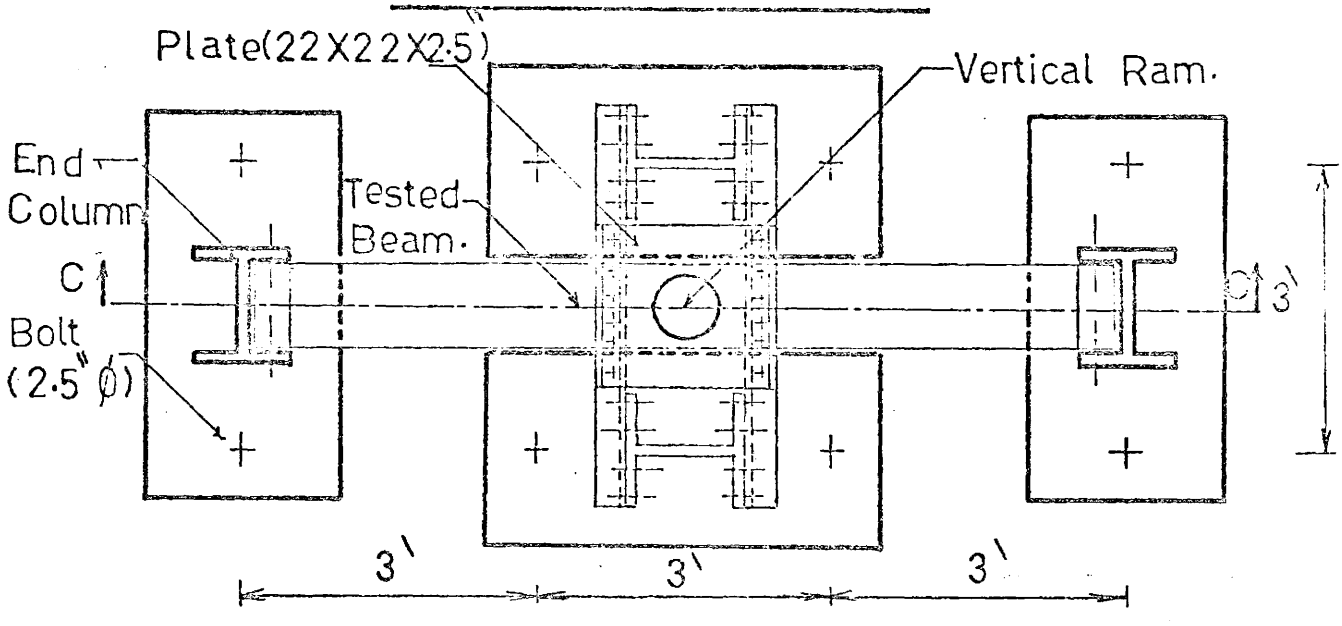

Plan of Test Set-Up.

Fig·32-DETAILS OF TEST APPARATUS.

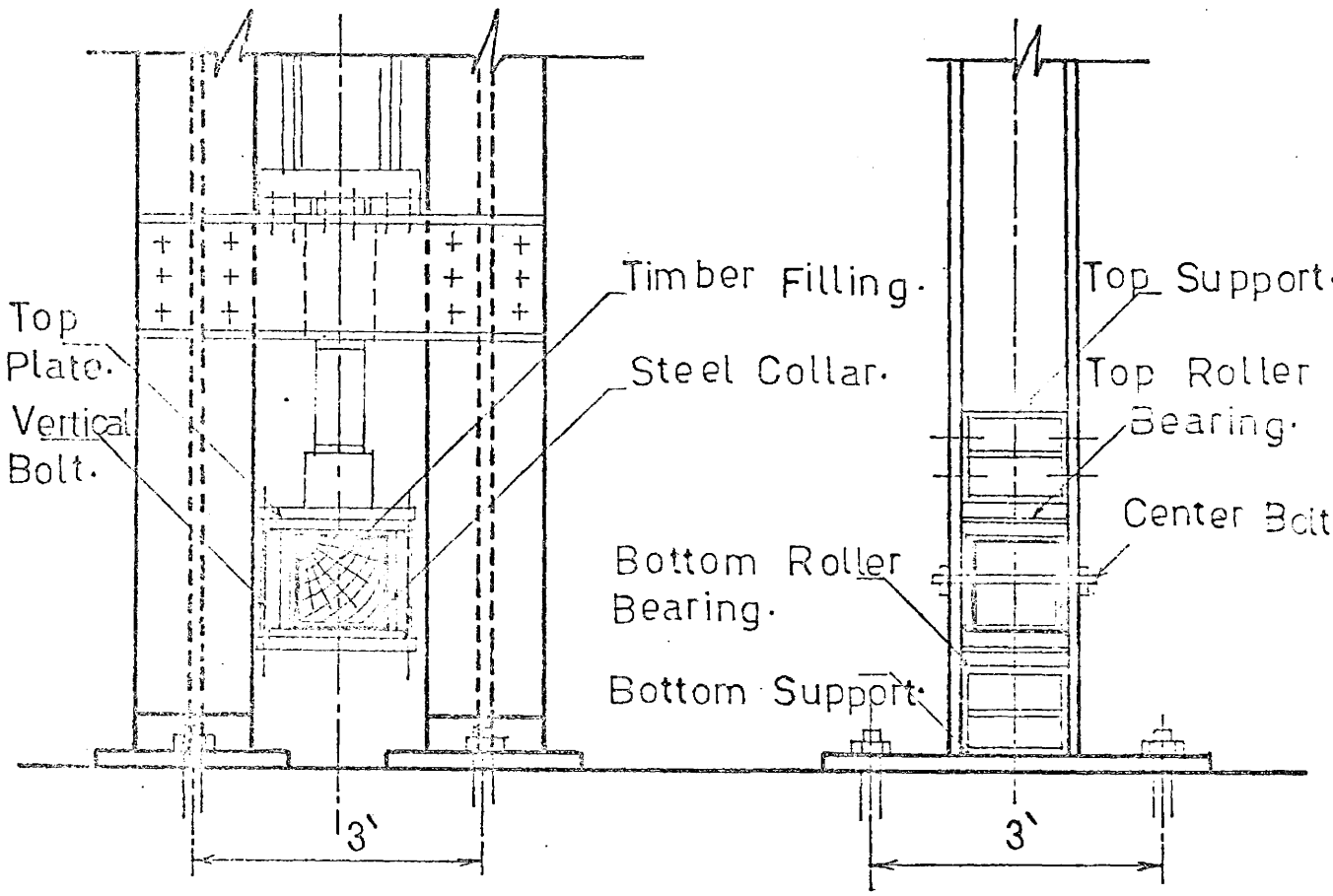

Fig.33-DETAILS OF LOADING PROVISIONS AND END SUPPORTS.

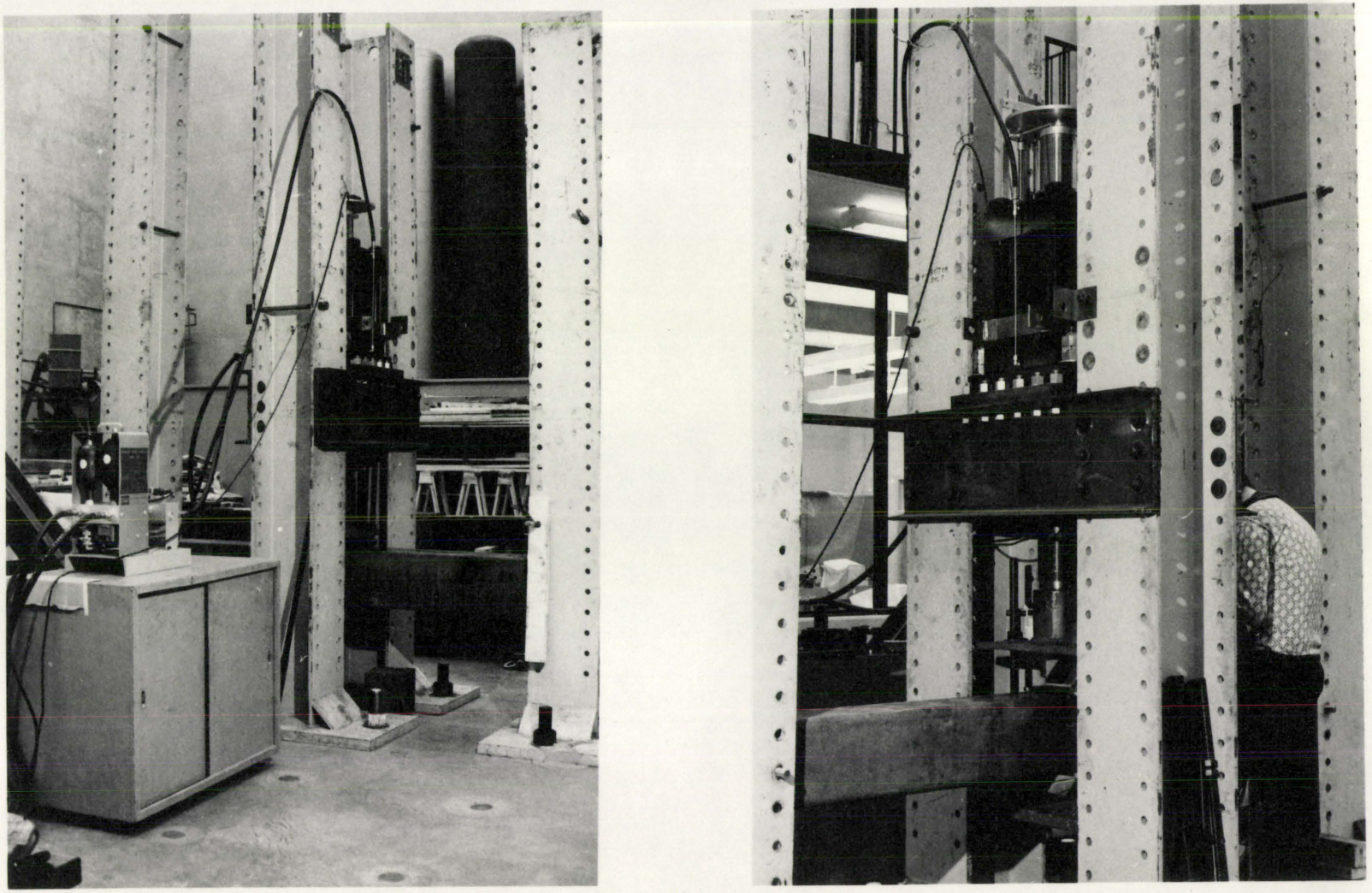

Fig.3.4 - OVERALL VIEW OF TEST APPARATUS AND INTERMEDIATE COLUMNS.

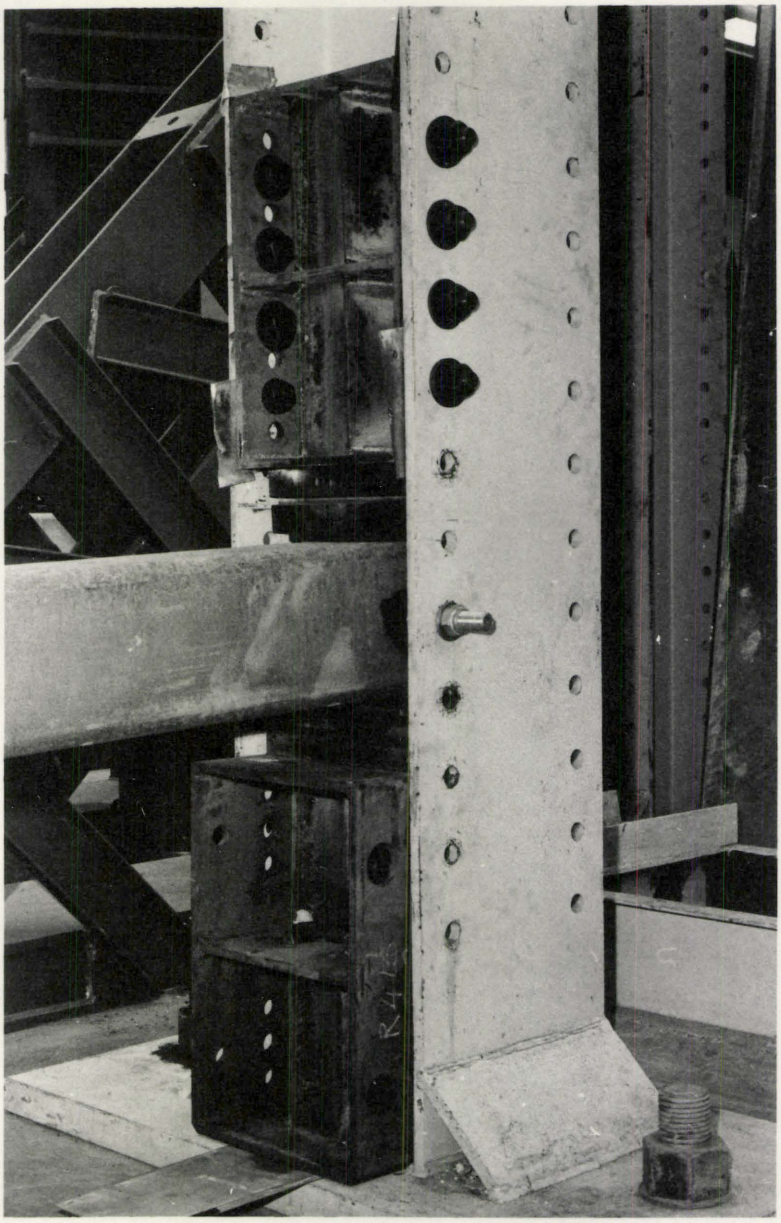

Fig·35-END SUPPORT·

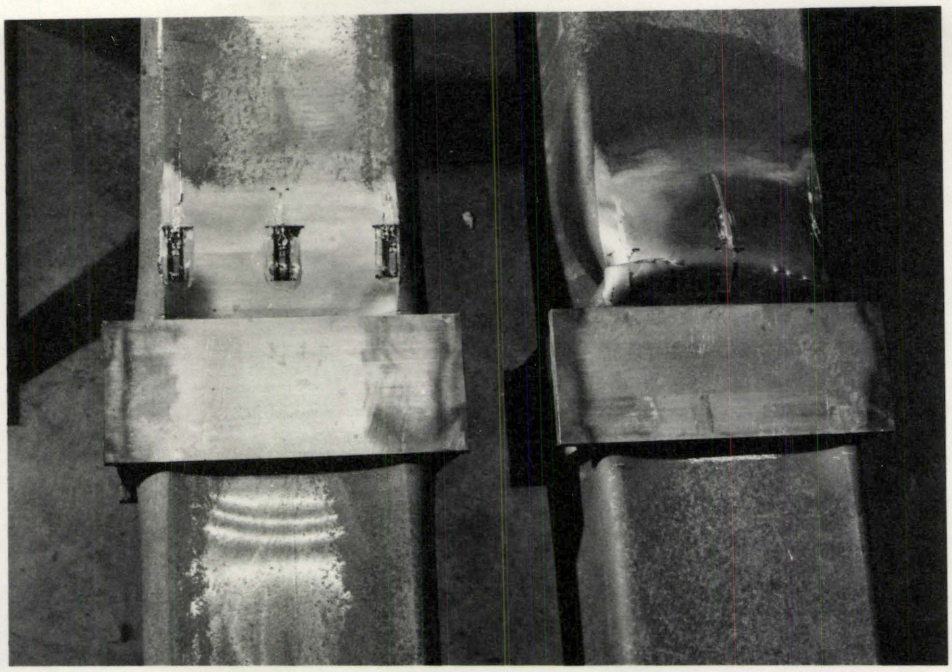

Fig·3·6(a)-PLAN OF BUCKLED BEAMS H1 (RIGHT) AND H3·

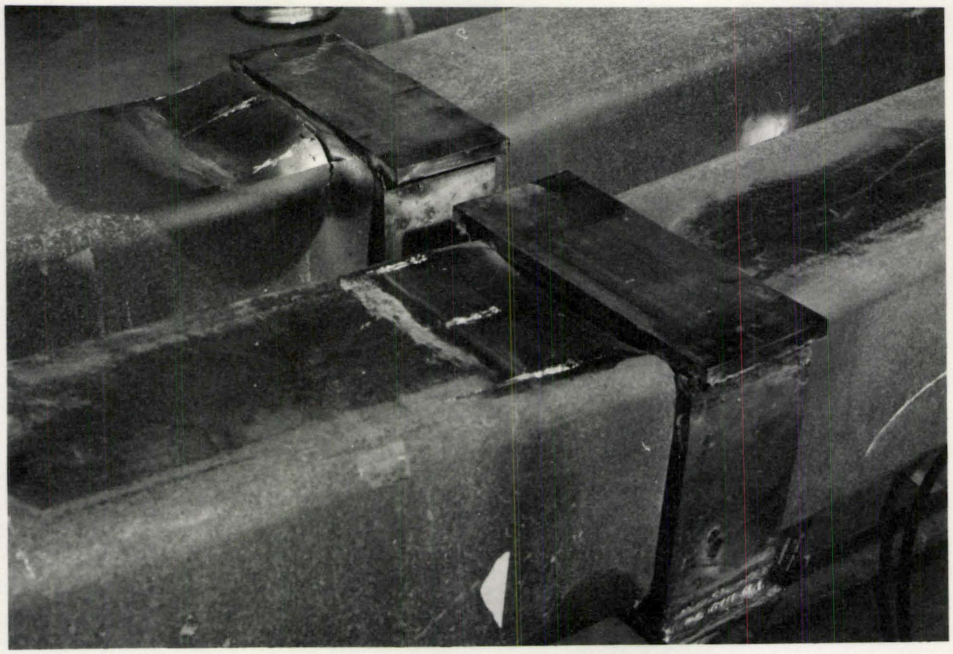

Fig·3·6-BEAM H1(TOP) AND BEAM H3 AFTER TEST·

Fig·3·7-BEAM H2 AFTER TEST·

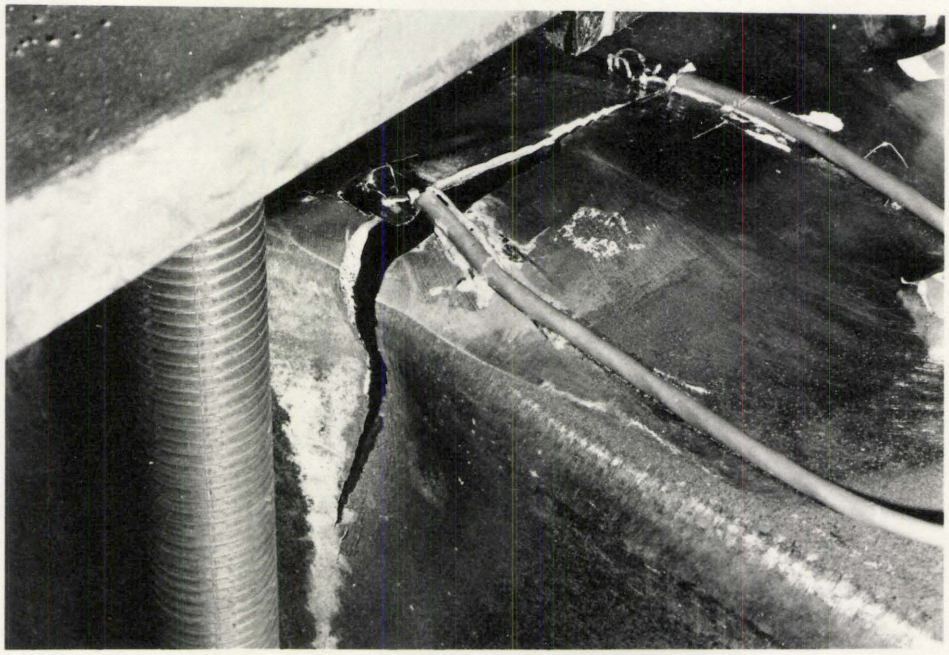

Fig·3·8-FRACTURED BEAM H4·

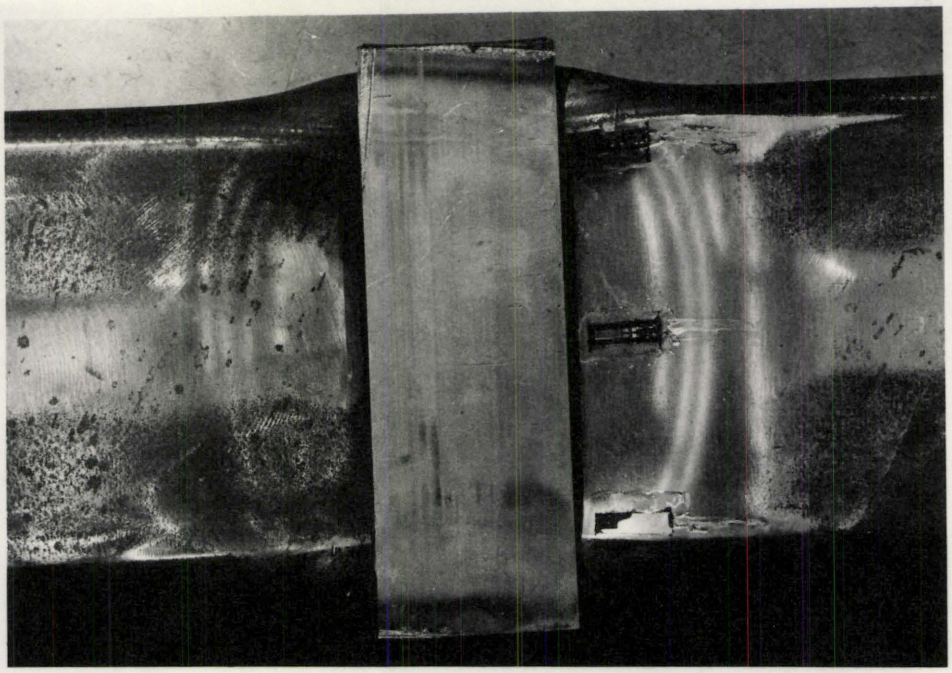

Fig 3.9 PLAN OF BEAM H5 AFTER TEST

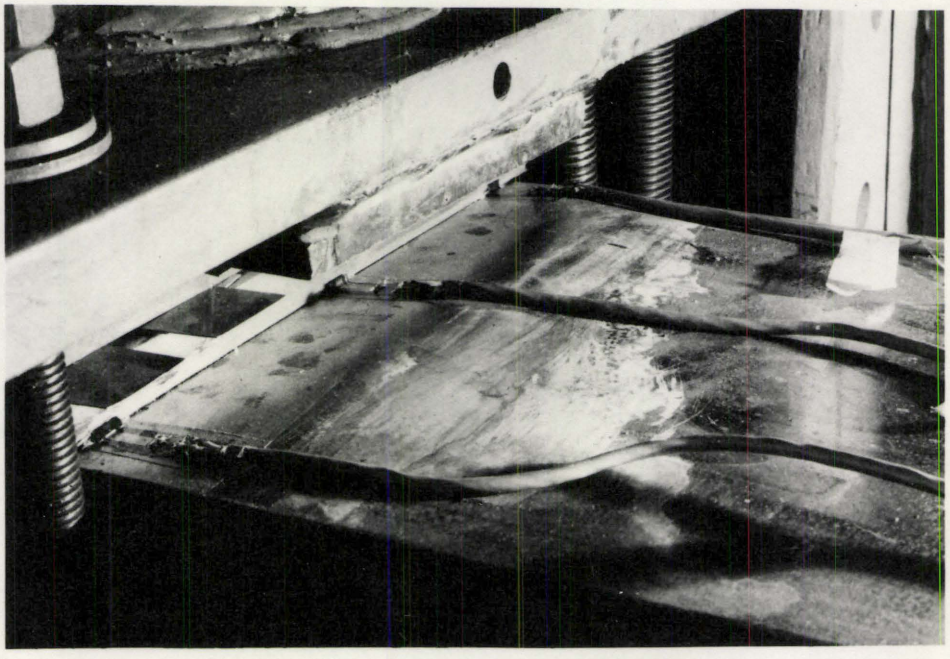

Fig. 3.10 BEAM H6 AFTER TWENTY CYCLES.

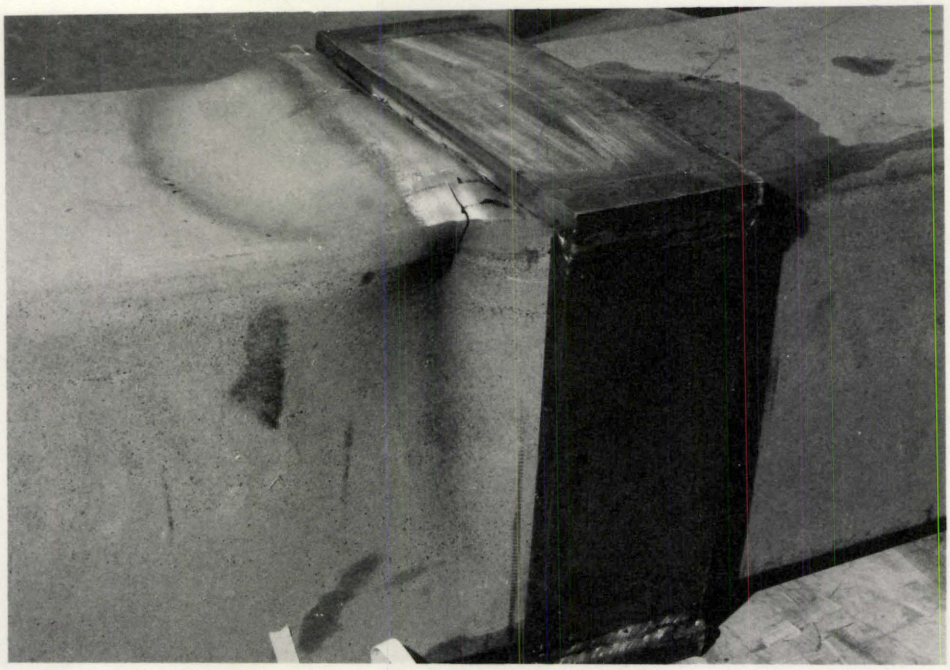

Fig·3·11(A)-WEB BUCKLING OF BEAM H7·

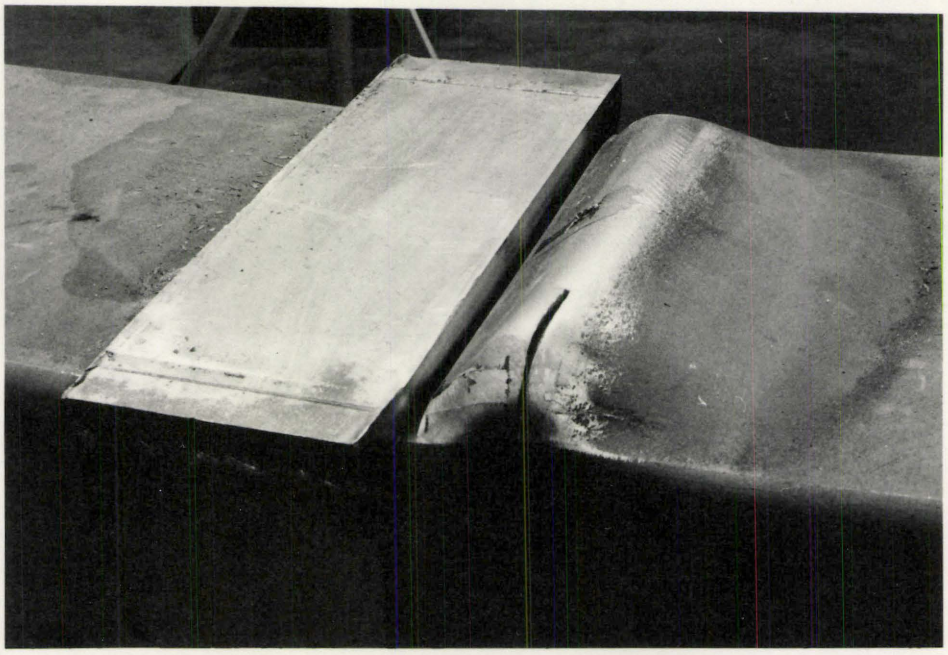

Fig·3·11(b)-TOP FLANG BUCKLING OF BEAM H7·

CHAPTER IV

EXPERIMENTAL RESULTS

4.1 Introduction

This chapter contains the experimental records and results of the tested beams. For each beam the graphical relationships, and detailed photographs showing the shapes of local buckling and failure modes after the cycling program are presented. All beams were loaded up to twenty cycles except beam H1 that failed after ten cycles only. All other beams except that designated H4 performed satisfactorily throughout the loading program within the limitations described later.

The test results are presented as follows.

4.2 Static Loading Curves

Figures 4.1 through 4.7 show the detailed static load deflection relationship for each beam before and after the cyclic testing was over. For each specimen three curves are described as follows: The solid line represents the pre-cycling load deflection curve. The dotted curve indicates static response after twenty cycles of loading have been applied. Such beam behaviour is important since it represents the possible resistance

to static loading situations after cyclic loading has occurred, such as from an earthquake. Finally, the dot-dash curve represents the idealized load deflection curve based on elastic plastic material properties. Initial departure from linearity occurs when the yield moment is reached. The fully plastic moment is only reached when very large deflections occur (ignoring second order effects). The previous notation applies for all specimens except beams H1 and H4. The cyclic test was terminated after 10 cycles for beam H1 as failure occurred at that stage. Beam H4 failed after ten cycles also, however the cyclic test continued to twenty cycles with a great deterioration in strength resulting in omitting the static test after the cycles were over.

In general the following observations are to be noted:

1. The static loading curves before cycling have similar shapes to the simple plastic theory case. As expected, the actual yield stresses are higher than the guaranteed value accounting for different leveling off values of load. In addition, these maximum load values are in excess of the estimated plastic loads, because of strain hardening. Beams H4 and H6 did not achieve the full plastic load as local buckling deteriorated their load carrying capacity. These results were predicted, however, since these sections are placed into the reduced sections category.

2. The flexural capacity deteriorated considerably after the cyclic

testing. The percentage of deterioration in strength with comparison to the static capacity before cycling ranged between about 15% for beam H3 and about 50% for beam H4. It is important to notice that the maximum flexural capacity after the load cycles were over developed at large deflections in the order of at least five times the elastic deflection at yeild. Local buckling appears to be the main factor contributing to the loss in load resistance. However, some reduction may be caused by material softening explaining the aforementioned observation of large deflections. This possibility was not specifically investigated.

Beam H7 was made of a stress relieved section. It developed a high level of flexural strength during the static test before the load cycles were applied. That maximum strength was approximately 20% higher than the calculated plastic capacity despite the high b/t ratio of the section of about 38.5. The previous increase in strength could be attributed to the absence of residual stresses. The behaviour of beam H7 was not significantly different than the others in the late stages of the cyclic test and in the static test after cycles were over.

4.3 Hysteresis Loops

Figures 4.8 through 4.14 show the shape of the load deflection hysteresis loops for the first and some of the subsequent cycles. The following observations need to be mentioned:

1. A noticeable difference between the shape of the first and the subsequent loops exists. However, these curves proved to be fairly reproducible on the whole, following the first cycle. There is a tendency of the curves to become flatter with an increase in the number of cycles.

2. The hysteresis loops tended to shift horizontally to a considerable extent with the result that residual deflections were noted after the first load cycle. A permanent kink formed in the section near the midspan during cycling. This appeared to be the primary reason for an increasing permanent residual displacement. The horizontal shifting of loops was in the negative direction of the displacement axis. This result is mainly because the cyclic loading was begun in the negative direction (defined as being downward).

3. The flexural capacity was fairly stable despite the high strain limits mentioned throughout the test.

4.4 Moment-Curvature Relationship

Figures 4.15 through 4.20 illustrate the moment curvature relationships for all the tested beams except beam H1 whose strain gauges performed poorly due to their damage early in the test. The following observations can be made, based on the curves of moment-curvature:

1. The curvature tended to increase at a constant level of moment at the first half cycle. This result was mainly because the ultimate moment value was reached, much earlier than the 2% strain limitation imposed. It is evident that the sections could in general sustain the peak moment for a considerable amount of curvature, an important property in plastic design considerations.

2. The fact that kinks happened to occur near the position of the strain gauges, caused the strain readings and consequently the curvatures to express the condition of the buckled portion rather than the whole beam. Thus, all of the beams except beam H3 did not experience negative curvatures at the position of the strain gauges despite the negative deflections associated with these curvatures, because the kinked areas always had a positive curvature. The accompanying photographs (Figures 3.6 through 3.11) emphasize the previous explanation. Because of the large wall thickness of beam H3, the kink was not severe and the recorded curvatures at the early stages of test

represented the shape of the whole beam and showed negative curvatures corresponding to negative deflections. As the test proceeded for beam H3 the kink became more pronounced and the beam's behaviour was similar to that of the other kinked beams.

3. All of the beams experienced an increasing amount of positive residual curvature at the position of the kink as the loading cycles proceeded. Beam H7 which was made of stress relieved section showed a larger moment capacity than beam H6 made of cold formed section having the same cross sectional dimensions. There was no significant difference in the curvature ranges of beams H7 and H6. In general, the moment-curvature curves conformed with those of the load-deflection.

4.5 Stability of the Load Levels

The load levels were found to be reasonably constant through tests as shown in Figures 4.21 to 4.23. Although there was a continual reduction in load level with excursions for all specimens, for specimen H3 the load value at the end of load cycling was greater than the plastic load value. For the other specimens load capacity deteriorated to a level below the plastic load limit.

The difference in performance may be attributed to the relatively low width to thickness ratio of specimen H3 which reduced the effect of local buckling.

4.6 Deflection Characteristics

Figures 4.24 to 4.26 show a diagramatic sketch of the midspan deflection with consecutive cycles. The four main points represented for each cycle are the two points of peak load, and the two intermediate points of zero load. The residual negative deflection is consistent in all of the tests, where downward deflection is being defined as negative. Deflection was controlled in such a way so as to maintain the first peak deflection attained in the first half cycle, denoted as ΔI in Figure 4.24 based on the preceding no load position throughout cycling. Positive deflections were of a much smaller magnitude compared to the negative deflections. They continued to decrease as test proceeded due to the increasing negative residual deflections. They were completely eliminated in later stages of tests as for beam H7.

4.7 Cumulative Residual Deflections

The cumulative plasticity ratio, $\Sigma\pi_d$, is plotted against the number of excursions in Figures 4.27 to 4.29. This relationship, being close to a straight line, indicates a constant residual deflection for most of the specimens, and emphasizes the repetative behaviour of beams throughout cycling.

These curves could be useful in actual design from the point of view of assessing the strength of a structural member after an earthquake on the basis of the resulting residual deformations compared to the maximum capacity of the member. The straight lines were noticed to be steeper for specimens of the same size with larger wall thicknesses indicating a lesser amount of residual deformations.

Figure 4.29 illustrates the difference between the behaviour of stress relieved section H7 and untreated cold formed section H6. Beam H7 experienced larger amounts of residual deflections than beam H6.

4.8 Cumulative Energy Dissipation

The energy accumulated through cycling was quite uniform especially for heavy specimens such as H3 and H5, as shown in Figures 4.30 through 4.32. Relating these curves to Figures 4.27 through 4.29, and assuming that the areas of the P-Δ hysteresis loops are functions of residual displacement and peak load, one can form an opinion about the strength history of the specimens and the uniformity of the P-Δ hysteresis loops. For example, if the loop areas are the same we get a straight line as in the case of H3 and H5. If peak load values drop, and the width of loops narrow we get a tendency of flatness of the relationship between the cumulative energy dissipation, ΣW, and the number of excursions. This is illustrated for beams H1, H4 and H6 in Figures 4.30 through 4.32.

4.9 Effect of Slenderness Ratio

Figure 4.33 summarizes the previous remarks, showing the trend toward proportionality between the decrease in slenderness ratio and cumulative energy with consequent greater resistance to local buckling. This information is based on five sections tested with width-thickness ratios varying between 16 and 38.5. Results of beam H1 were excluded as it was tested for ten cycles only, despite the other beams that were tested for twenty cycles. Results of beam H7 were also excluded as it was made of a stress relieved section unlike the rest of the beams. Beam H5 did not well adhere to the general shape of the previous curve of Figure 4.33.

4.10 Comparison Between the Three Ductility Factors

Tables A.1 through A.7 show the detailed information of the peak load, deflection, residual plastic deflection, and energy dissipated values. The generalized terms of the previous values are also presented as the load ratio, P, the ductility factor, μ_1 described in Chapter II, the plasticity ratio, π_d, and the energy ratio, e. The previous values are presented for each half cycle.

The μ_1 factor was calculated for each load excursion as shown in Tables A.1 through A.7 from equation 2.39. This value enables us to form

an opinion about the maximum deflections encountered during the test, therefore it was chosen rather than the other two definitions as a distinctive ductility measure. The plasticity ratio, π_d, as determined from equation 2.47, indicates the residual deflections and consequently the permanent damage.

Fig.4.1 - LOAD-DEFLECTION
H1 (8·0X8·0X0·25)

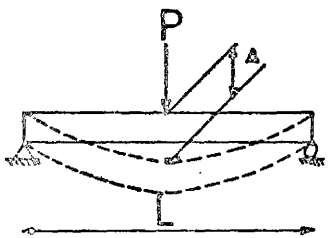

PRIOR TO CYCLING.

AFTER CYCLING.

SIMPLE PLASTIC THEORY.

Load, in kips.

100

75

50

25

0

0·25

0·50

0·75

1·00

1·25

1·50

1·75

2·00

2·25

Deflection, in inches.

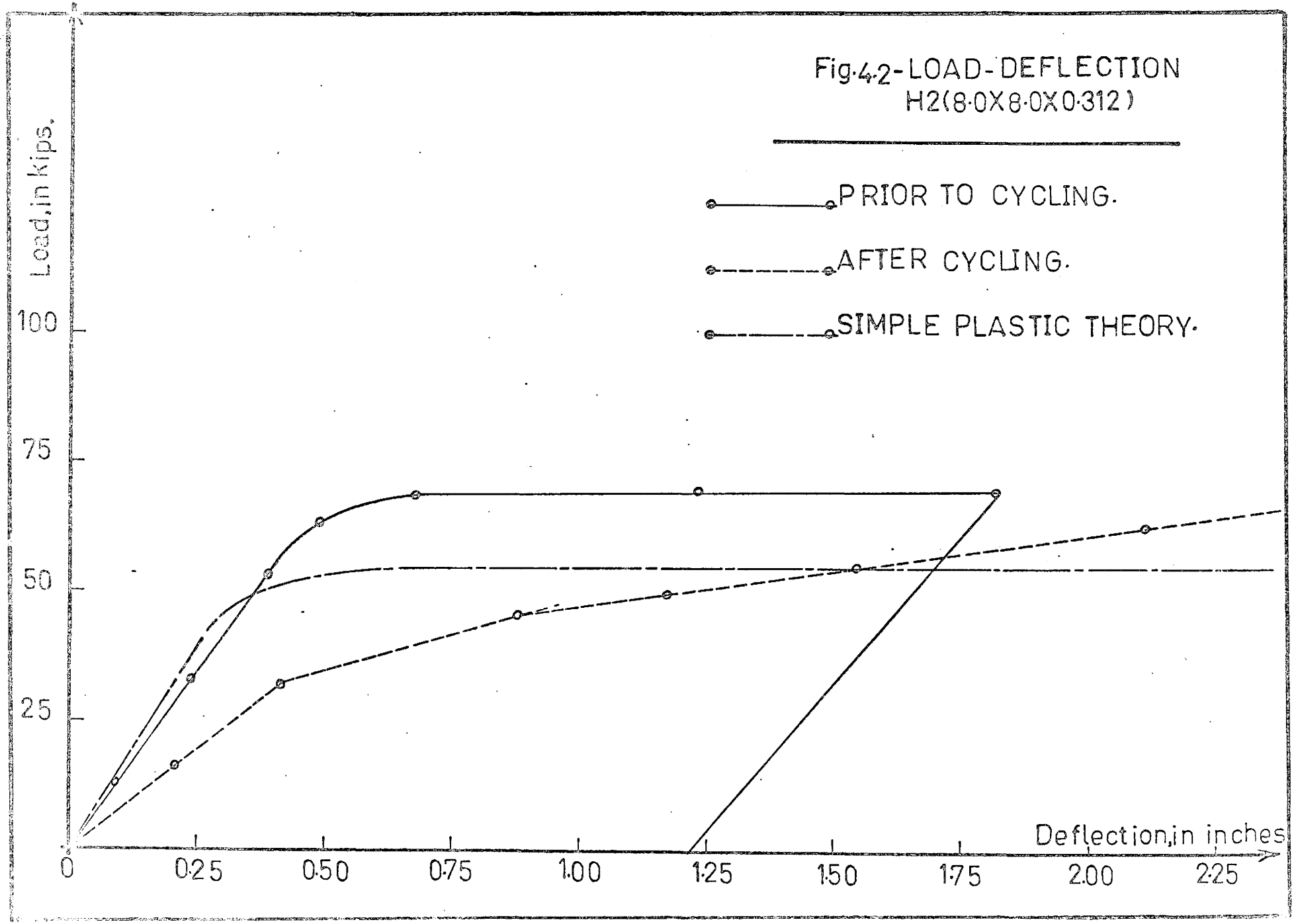
Fig.4.2-LOAD-DEFLECTION
H2(8·0X8·0X0·312)
PRIOR TO CYCLING.
AFTER CYCLING.
SIMPLE PLASTIC THEORY.
Load, in kips.
100
75
50
25
0
0·25
0·50
0·75
1·00
1·25
1·50
1·75
2·00
2·25
Deflection, in inches

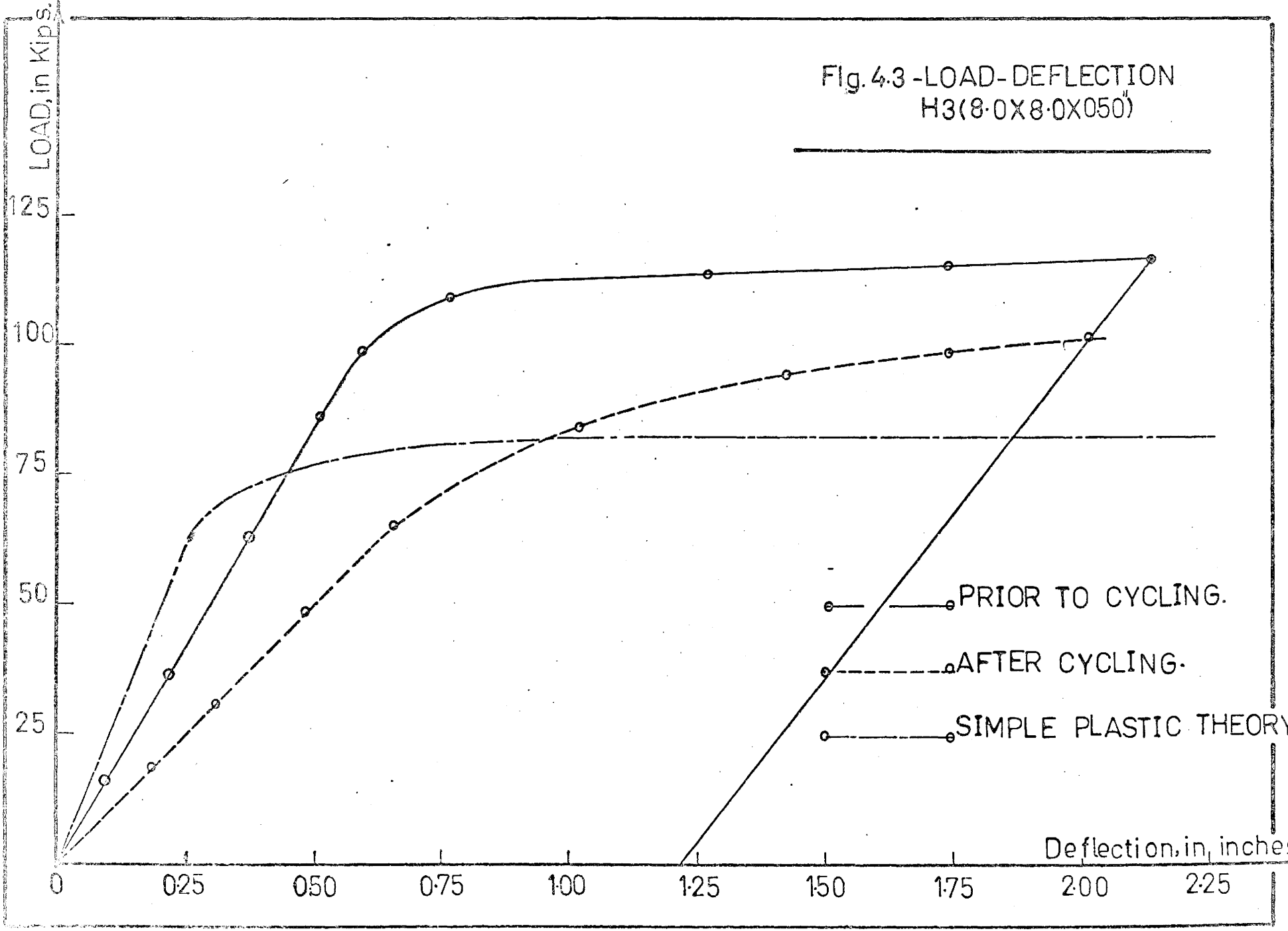
Fig. 4.3 - LOAD - DEFLECTION
H3 (8·0 X 8·0 X 050")
LOAD, in Kips.
125
100
75
50
25
0
0·25
0·50
0·75
1·00
1·25
1·50
1·75
2·00
2·25
Deflection, in inches.
PRIOR TO CYCLING.
AFTER CYCLING.
SIMPLE PLASTIC THEORY.

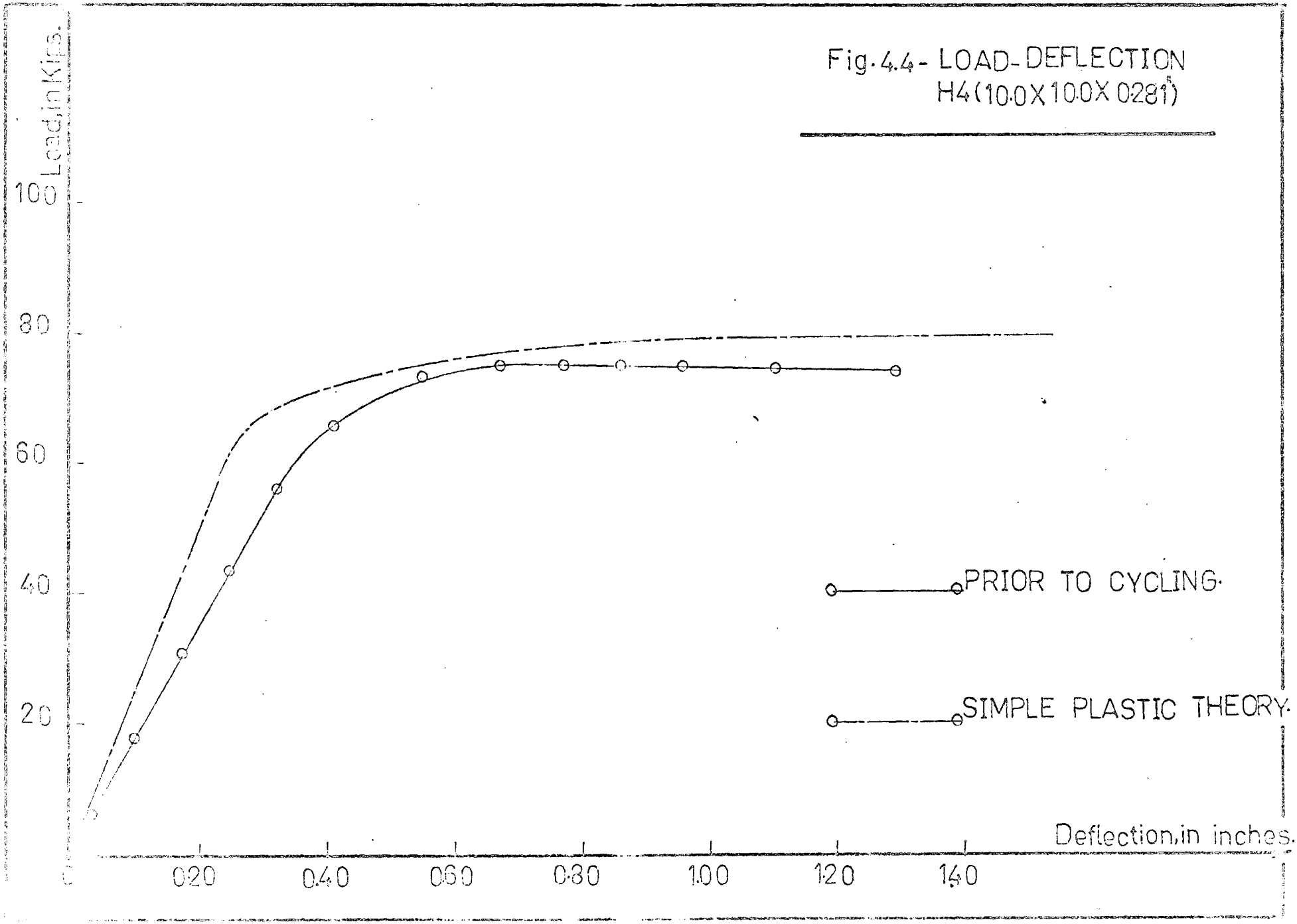
Fig. 4.4 - LOAD-DEFLECTION
H4 (10.0 X 10.0 X 0.281")
Load, in Kips.
100
80
60
40
20
PRIOR TO CYCLING.
SIMPLE PLASTIC THEORY.
Deflection, in inches.
0.20
0.40
0.60
0.80
1.00
1.20
1.40

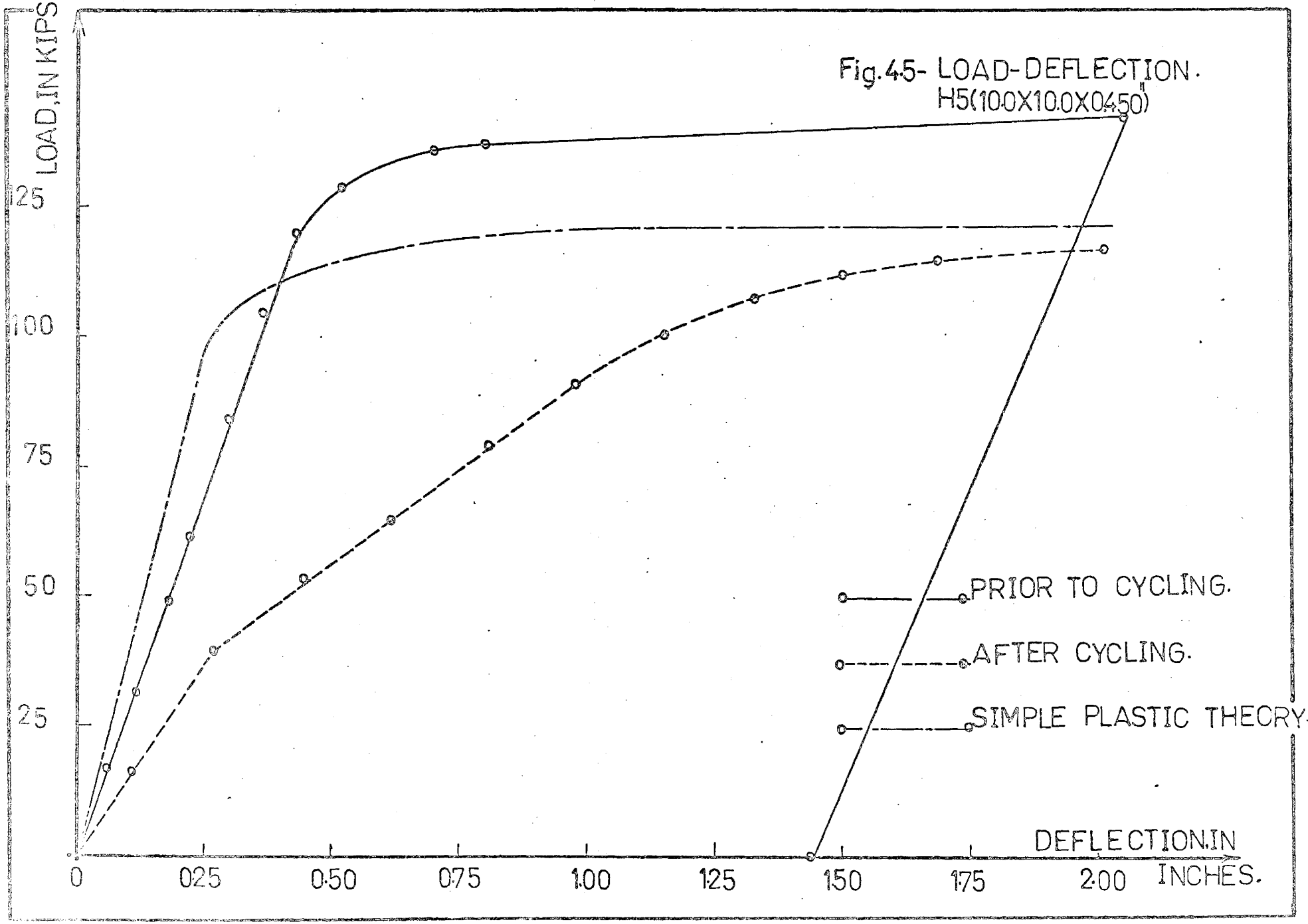
Fig.4.5- LOAD-DEFLECTION.
H5(10.0X10.0X0.450")
LOAD, IN KIPS.
125
100
75
50
25
0
0·25
0·50
0·75
1·00
1·25
1·50
1·75
2·00
DEFLECTION IN INCHES.
PRIOR TO CYCLING.
AFTER CYCLING.
SIMPLE PLASTIC THEORY.

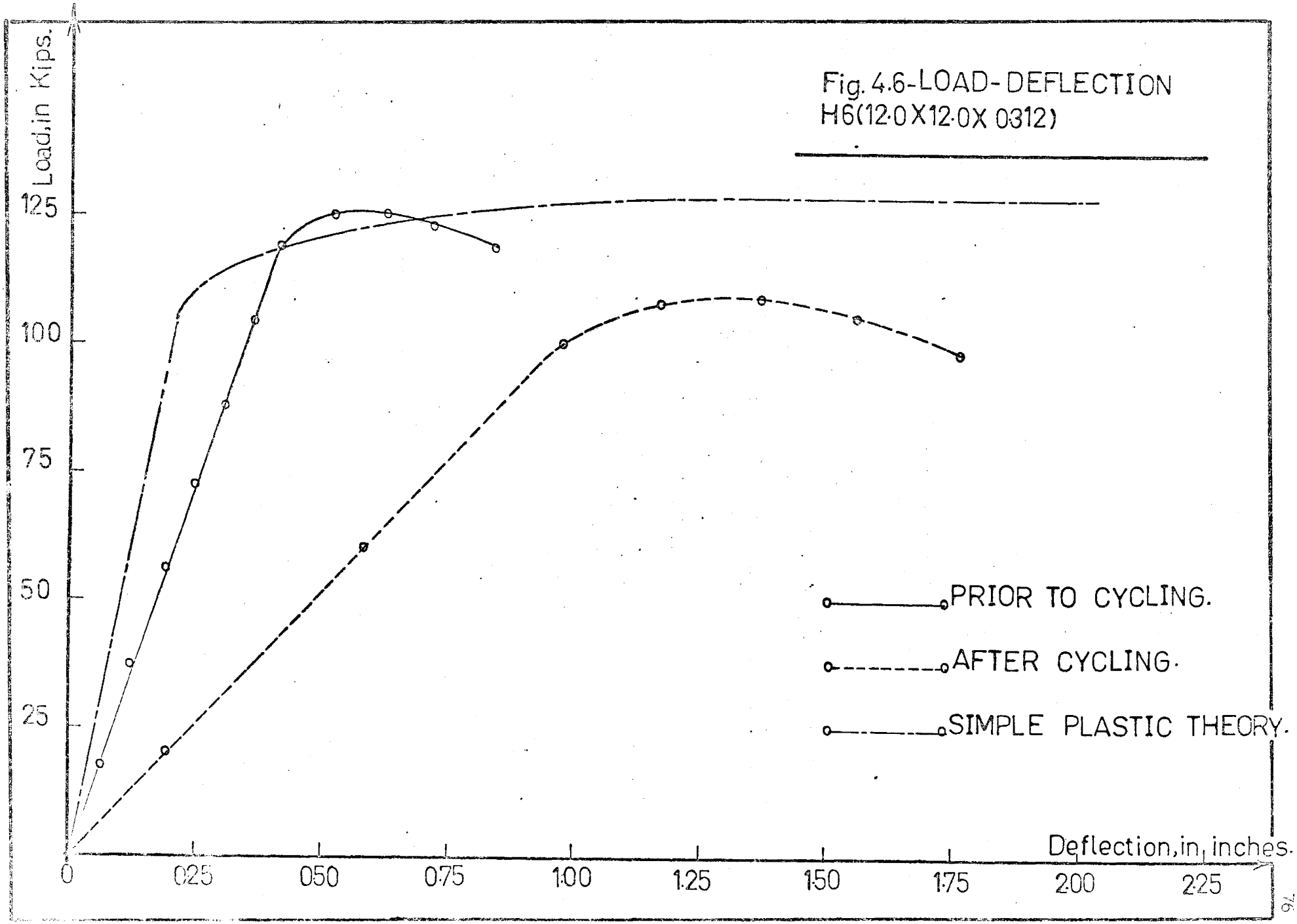

Fig. 4.6-LOAD-DEFLECTION
H6(12·0X12·0X 0312)

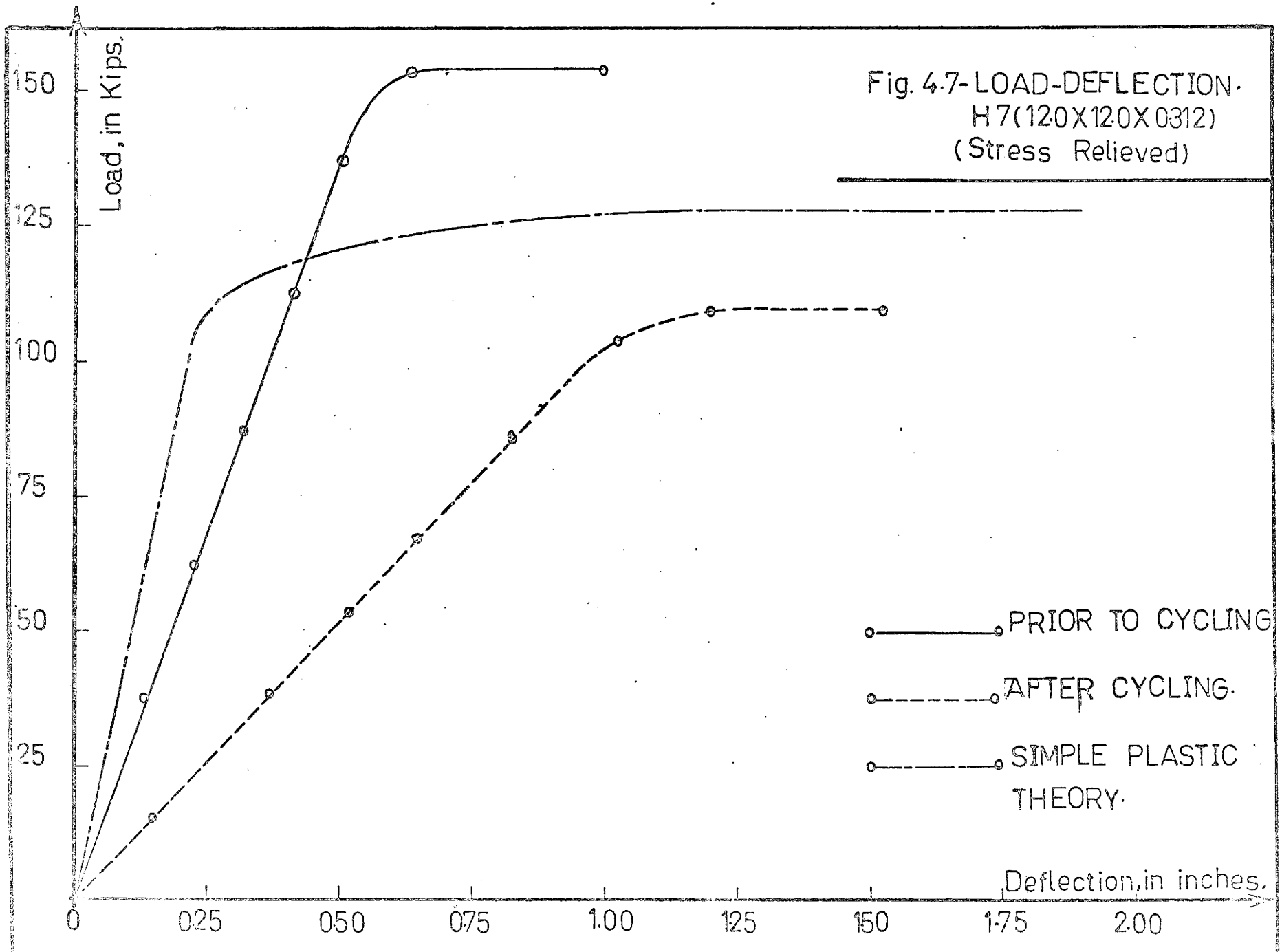
Load, in Kips.
150
125
100
75
50
25
0
0·25
0·50
0·75
1·00
1·25
1·50
1·75
2·00
Deflection, in inches.
Fig. 4·7- LOAD-DEFLECTION·
H 7 (12·0 X 12·0 X 0·312)
(Stress Relieved)
PRIOR TO CYCLING
AFTER CYCLING·
SIMPLE PLASTIC THEORY·

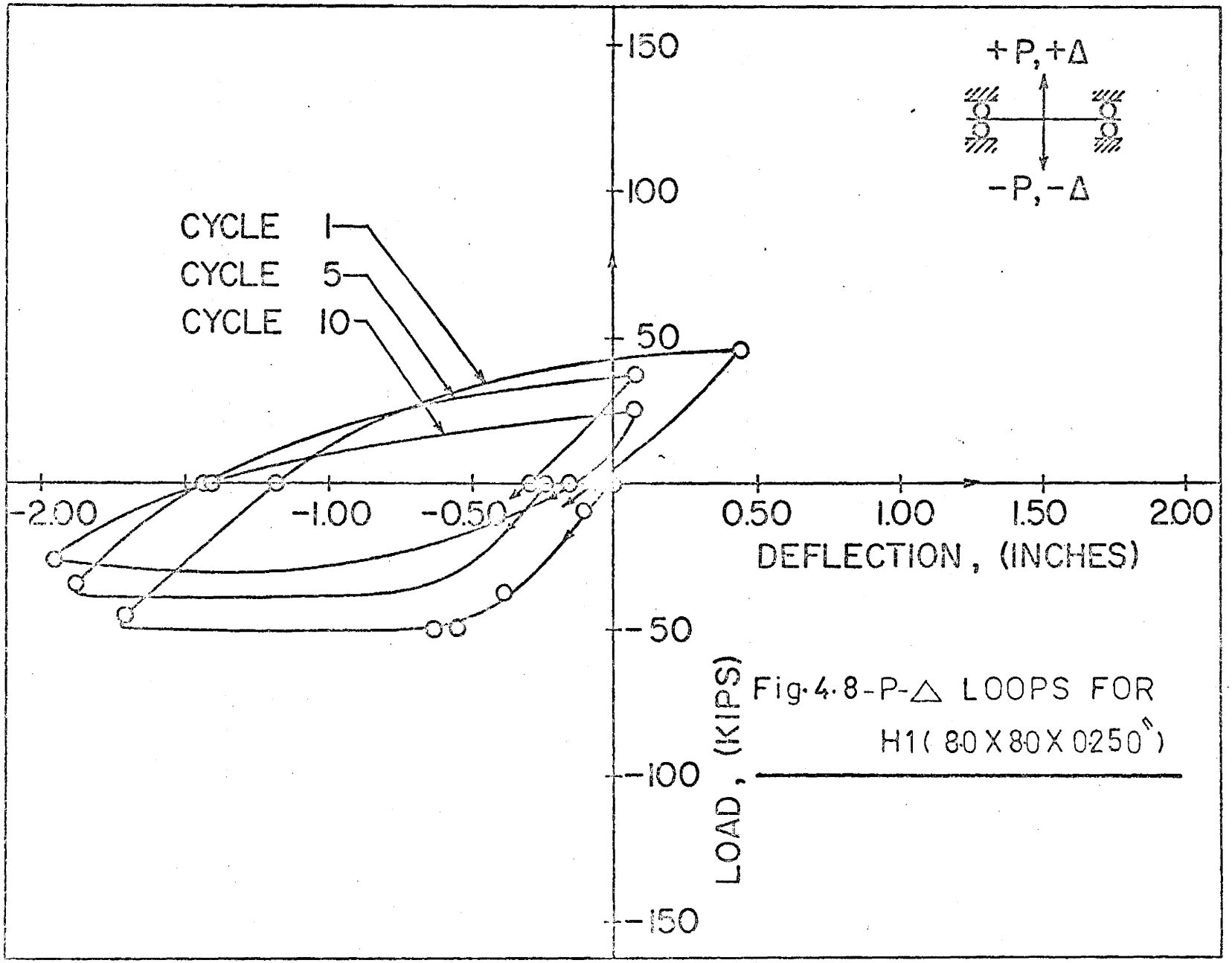

Fig.4.8-P-△ LOOPS FOR H1(8.0X8.0X0.250")

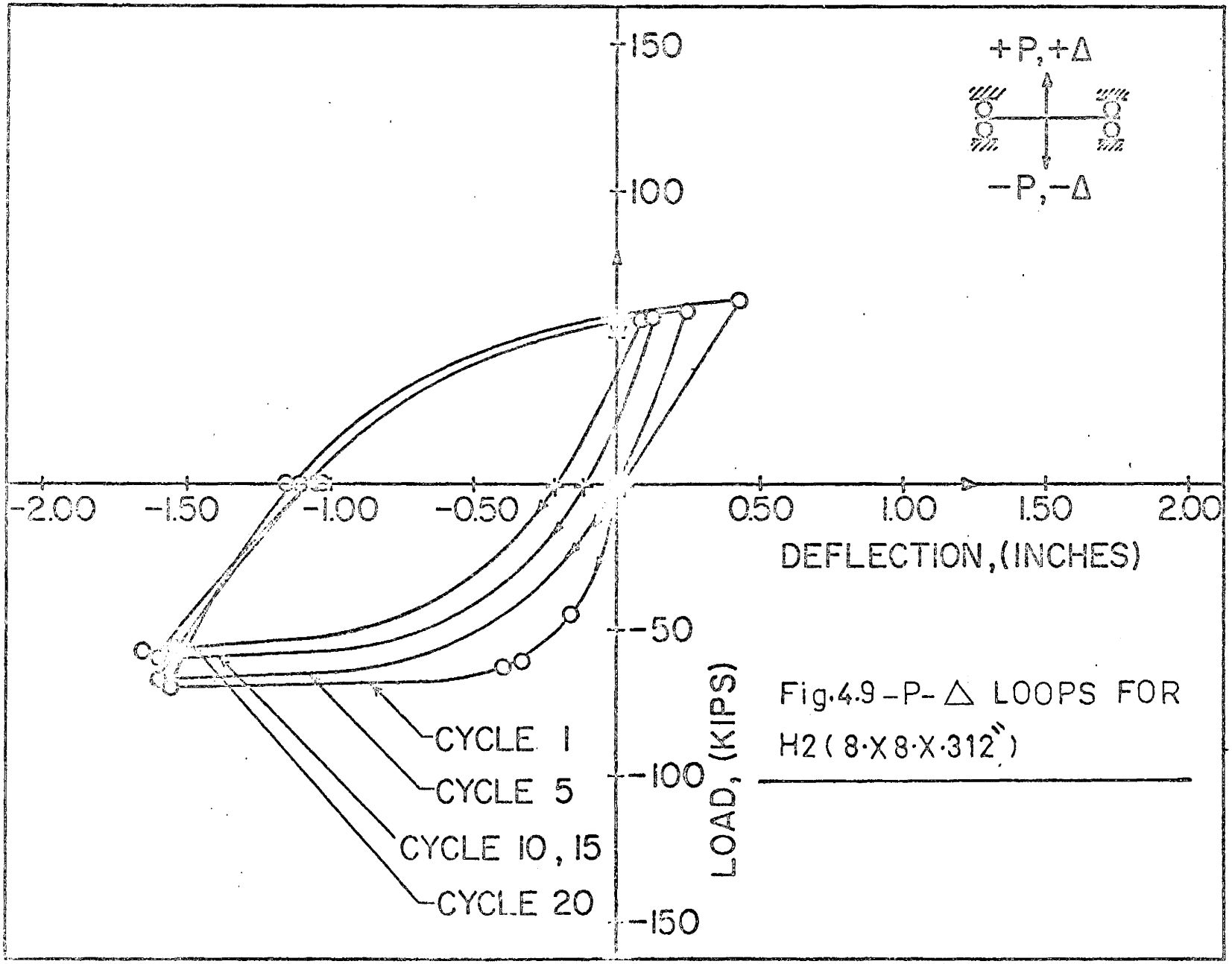

Fig.4.9 – P- Δ LOOPS FOR H2 (8·X 8·X·312")

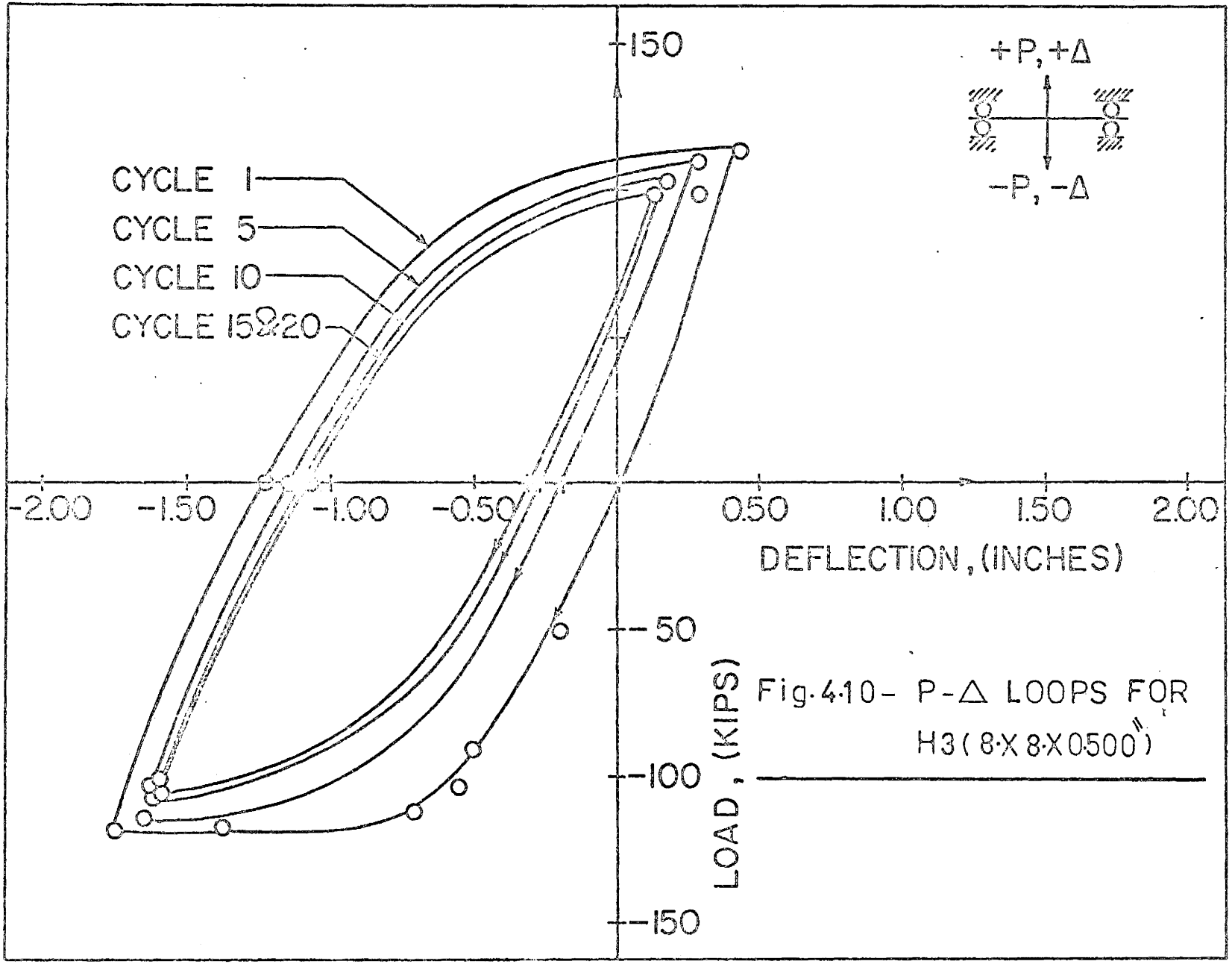

Fig. 4.10 - P-Δ LOOPS FOR H3 (8"X 8"X 0.500")

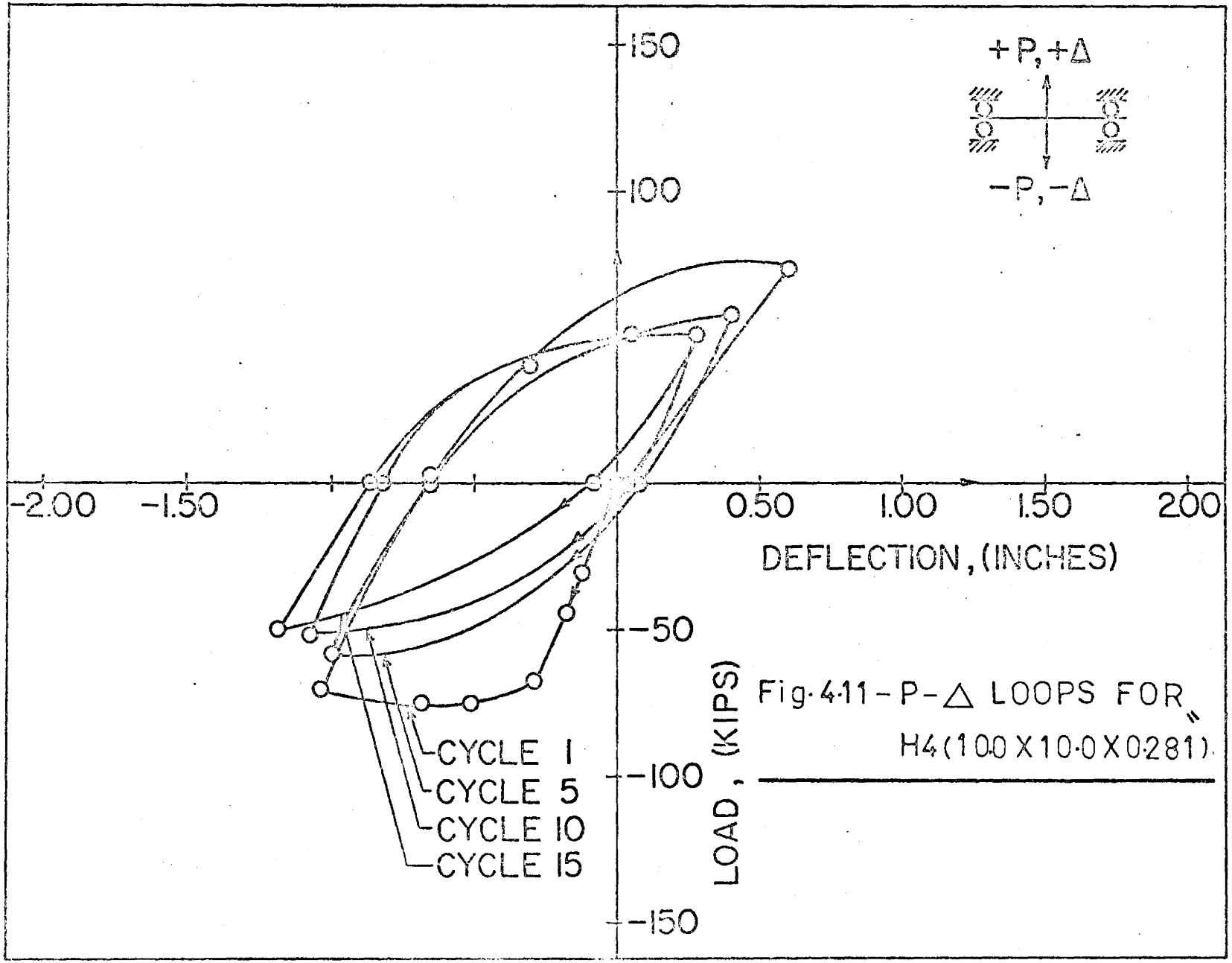

Fig. 4.11 - P-Δ LOOPS FOR H4 (10.0 X 10.0 X 0.281)

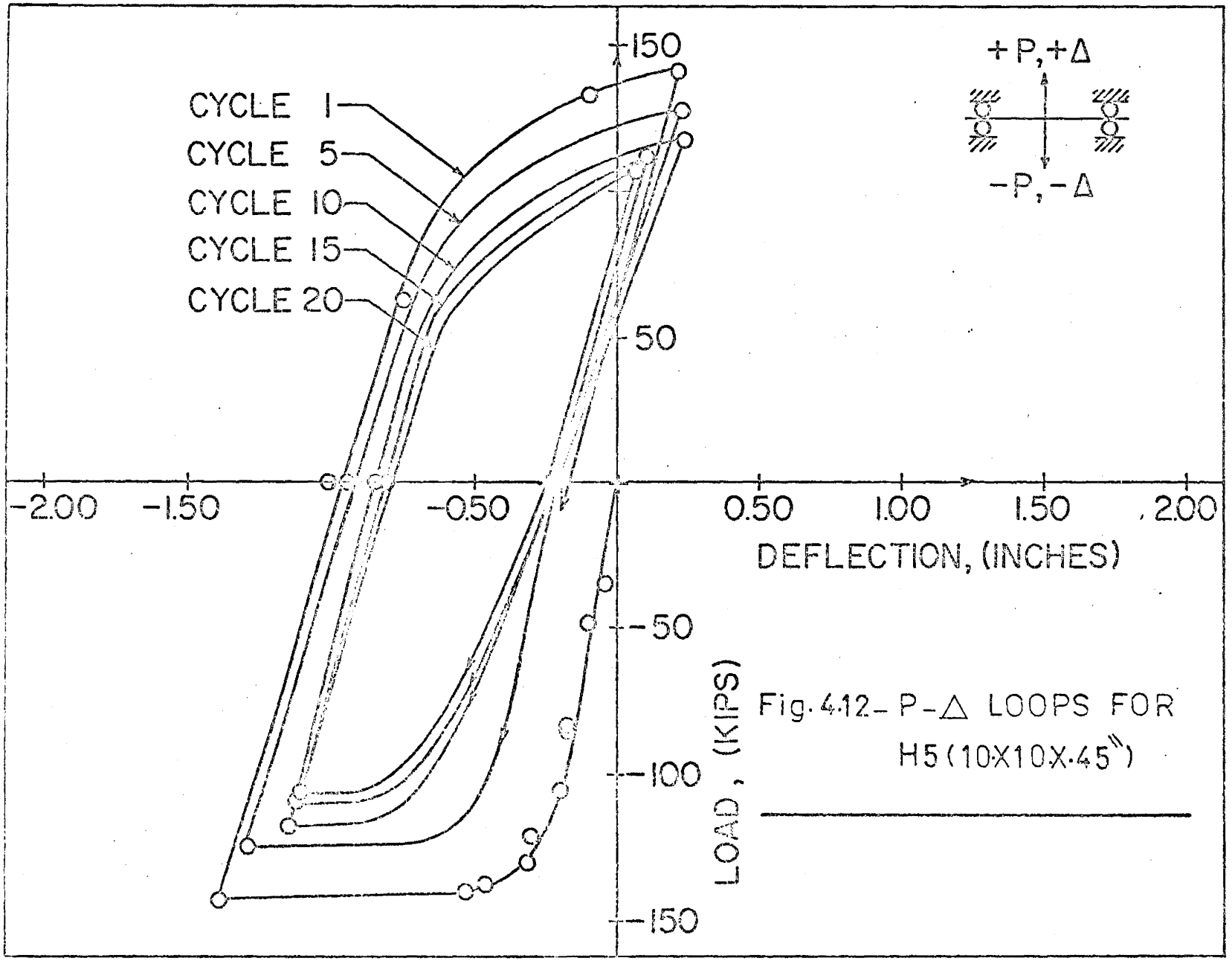

Fig. 4.12 - P-Δ LOOPS FOR H5 (10X10X.45")

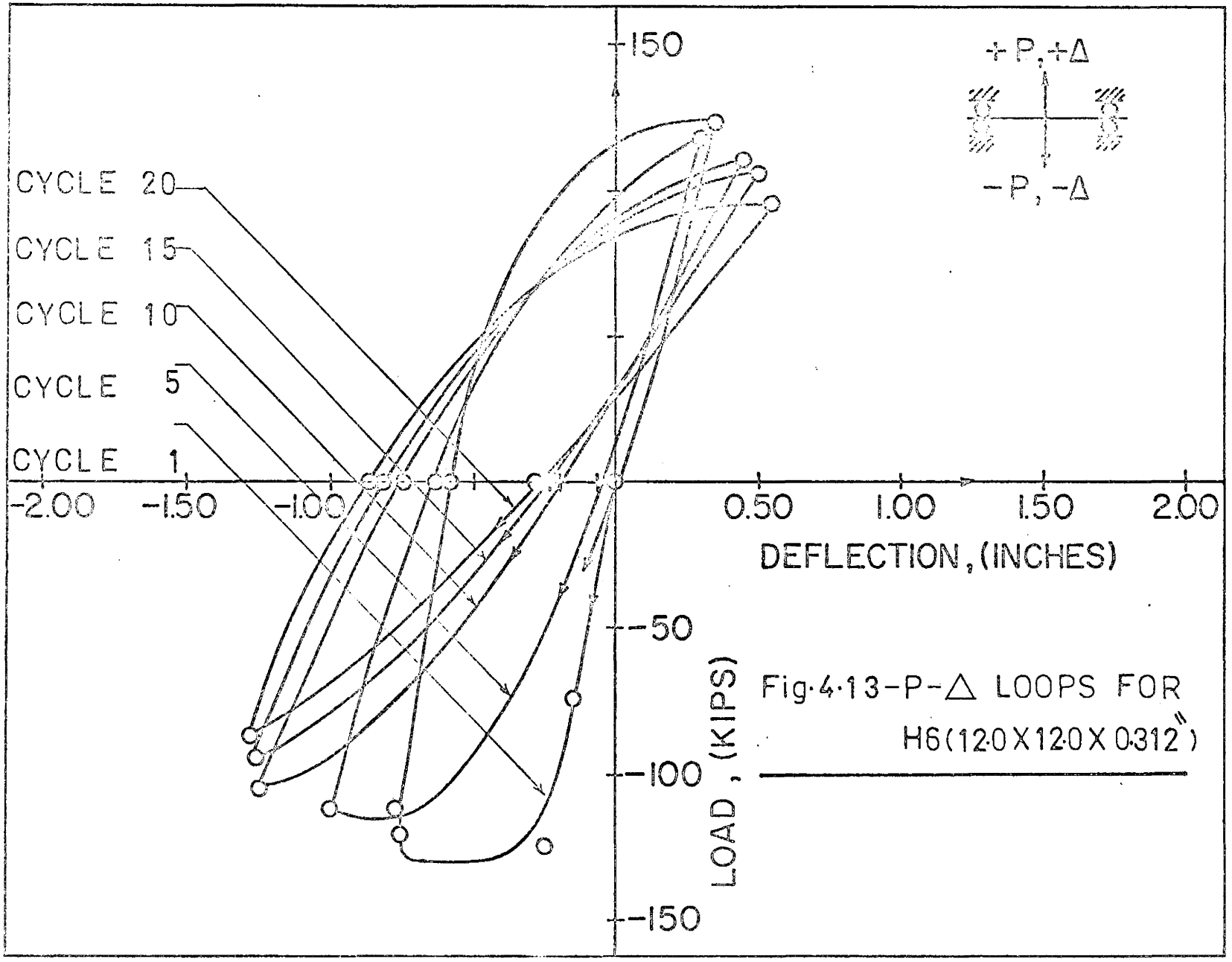

Fig·4·13–P–Δ LOOPS FOR H6(12·0 X 12·0 X 0·312")

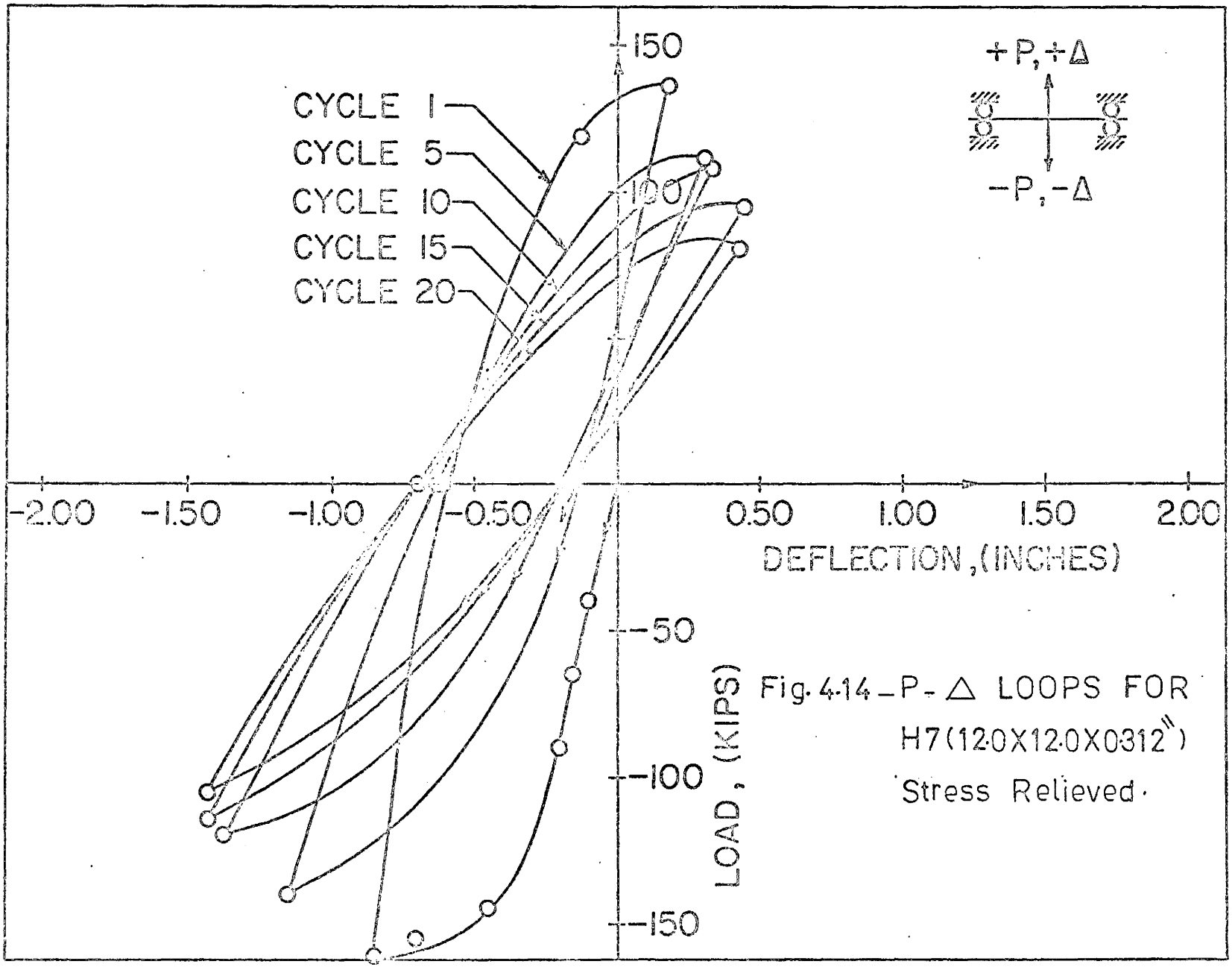

Fig. 4-14 – P - Δ LOOPS FOR H7 (12·0X12·0X0·312") Stress Relieved.

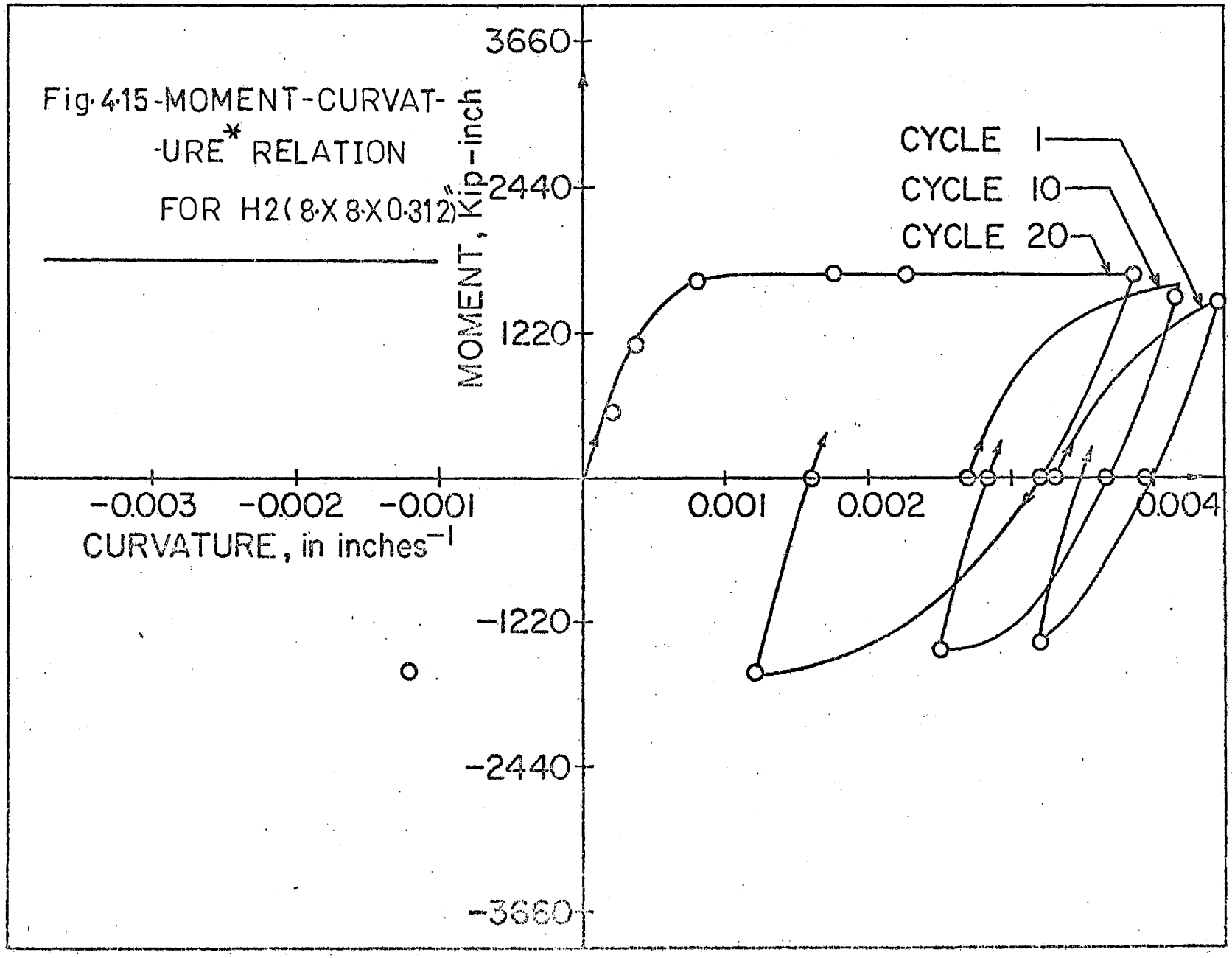

Fig. 4.15 - MOMENT-CURVATURE* RELATION FOR H2(8·X 8·X 0·312)

* The shown curve describes the behaviour of the buckled portion of the beam.

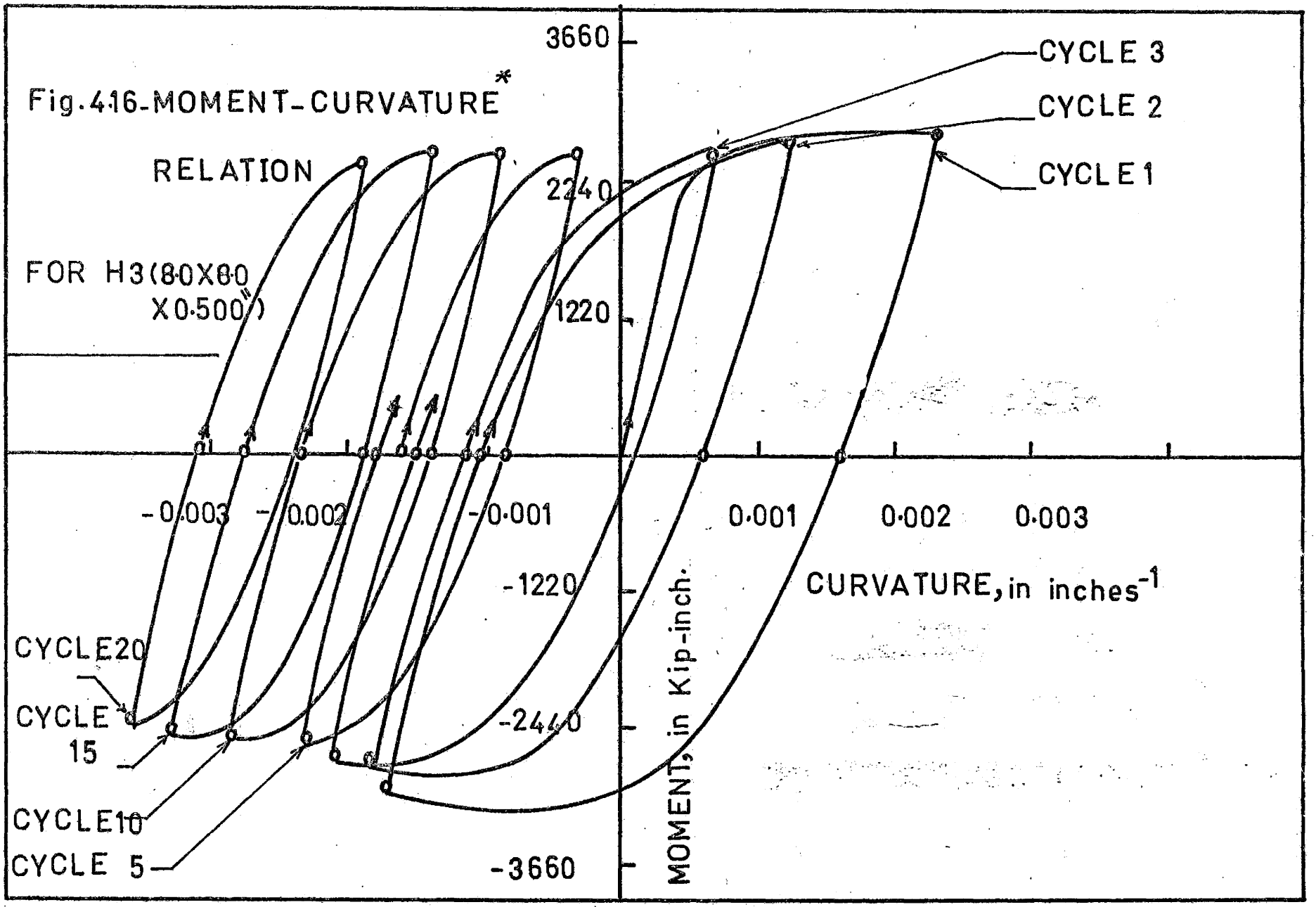

* The shown curve describes the behaviour of the buckled portion of the beam.

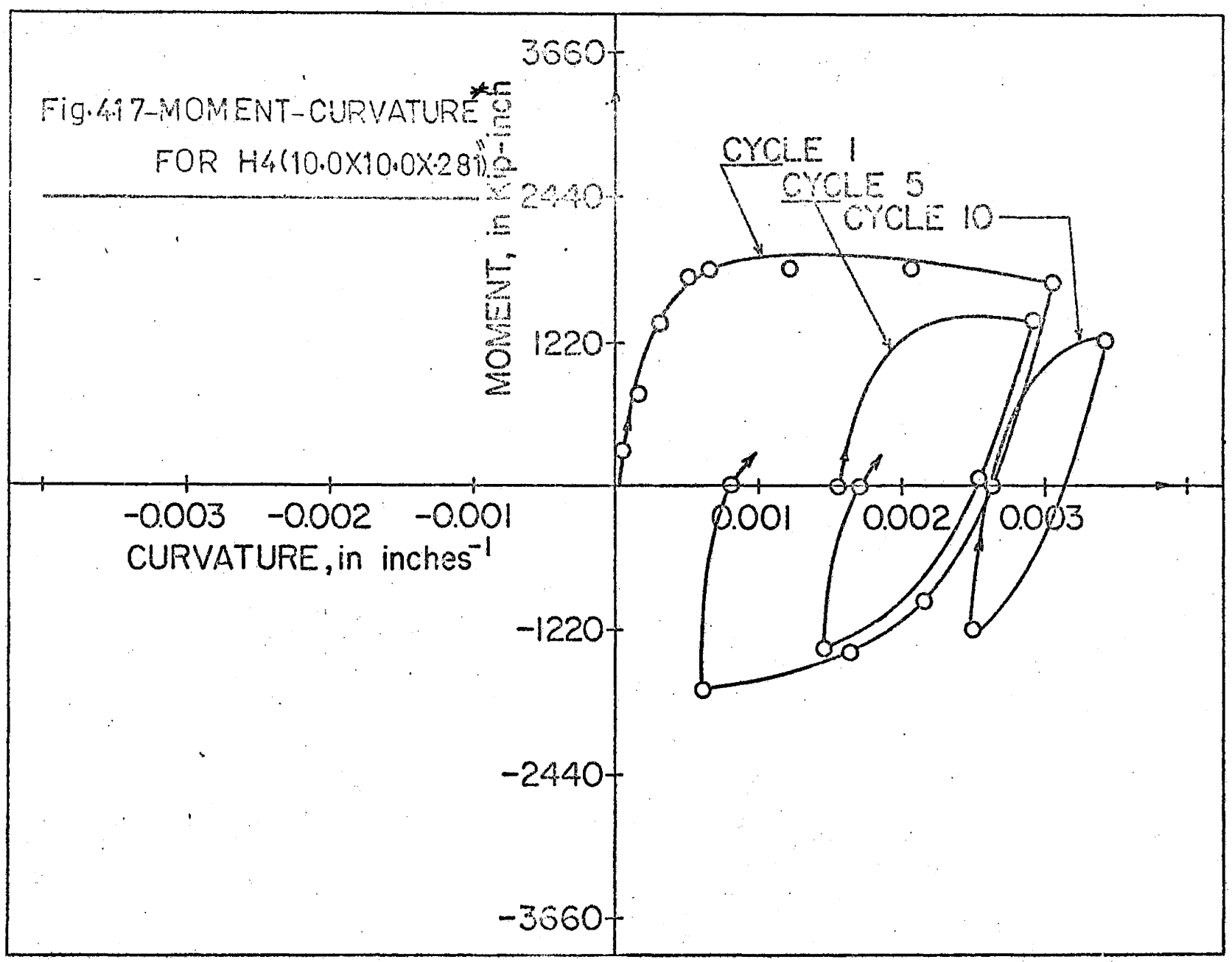

* The shown curve describes the behaviour of the buckled portion of the beam.

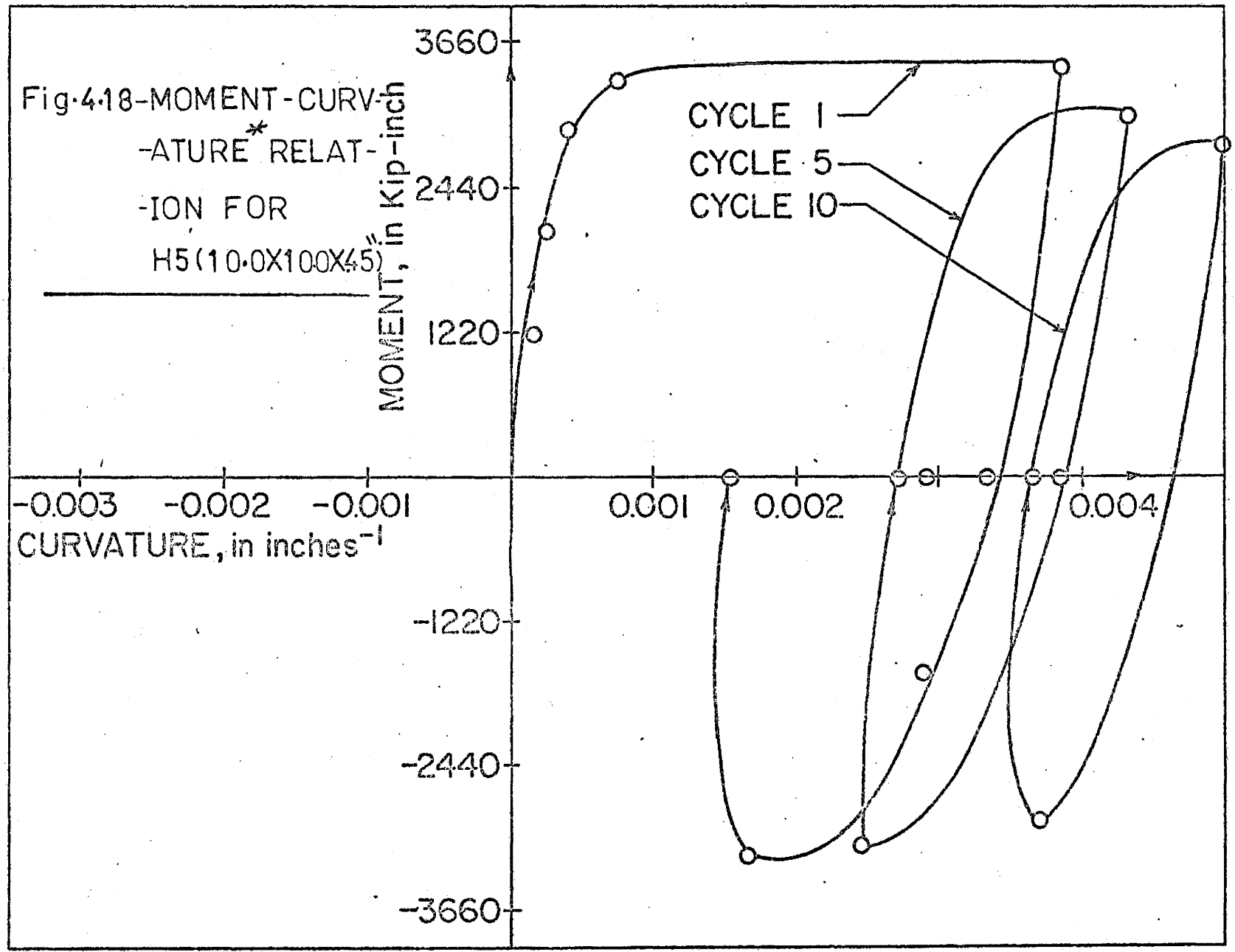

Fig·4·18-MOMENT-CURV-
-ATURE* RELAT-
-ION FOR
H5(10·0X100X45)

* The shown curve describes the behaviour of the buckled portion of the beam.

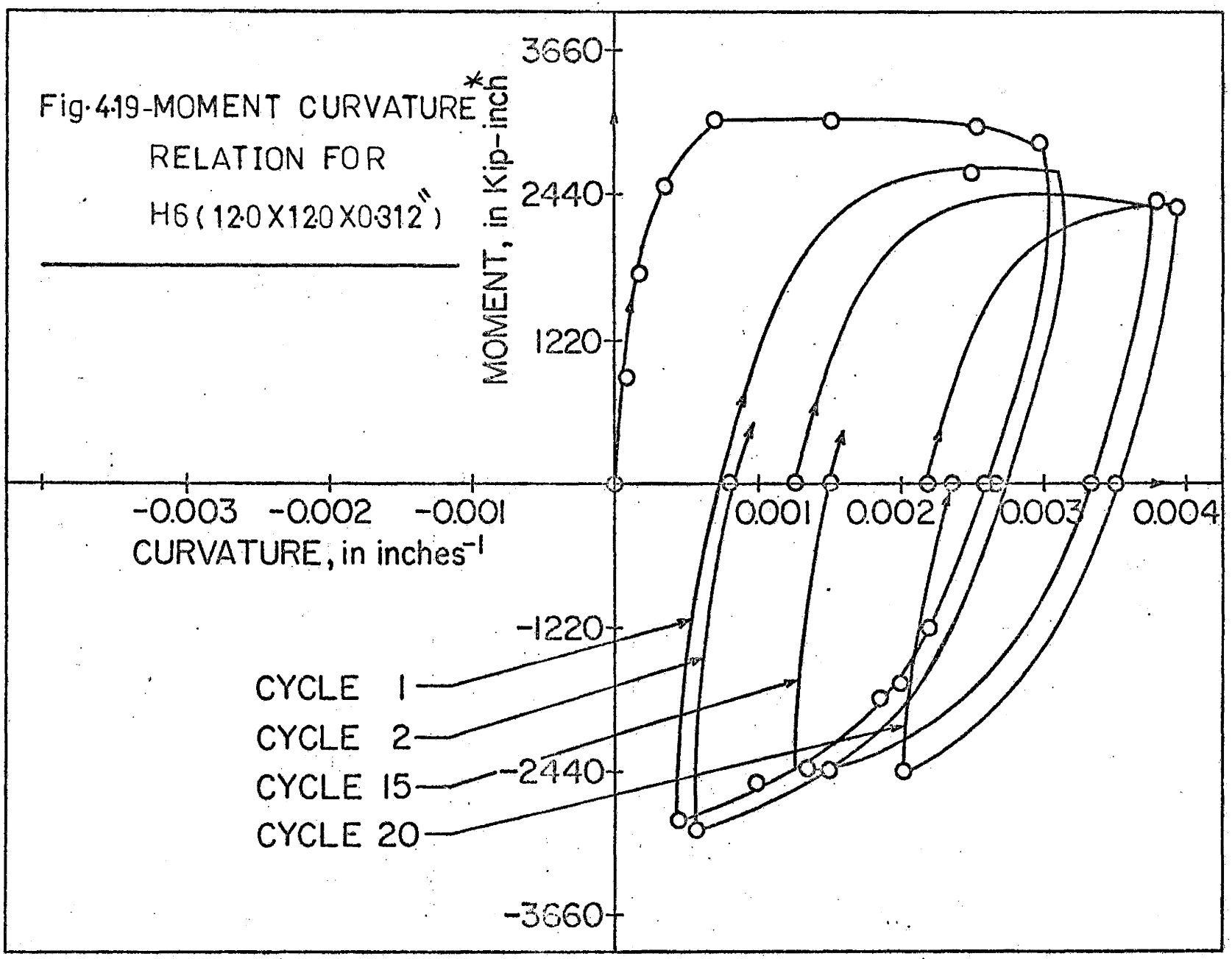

* The shown curve describes the behaviour of the buckled portion of the beam.

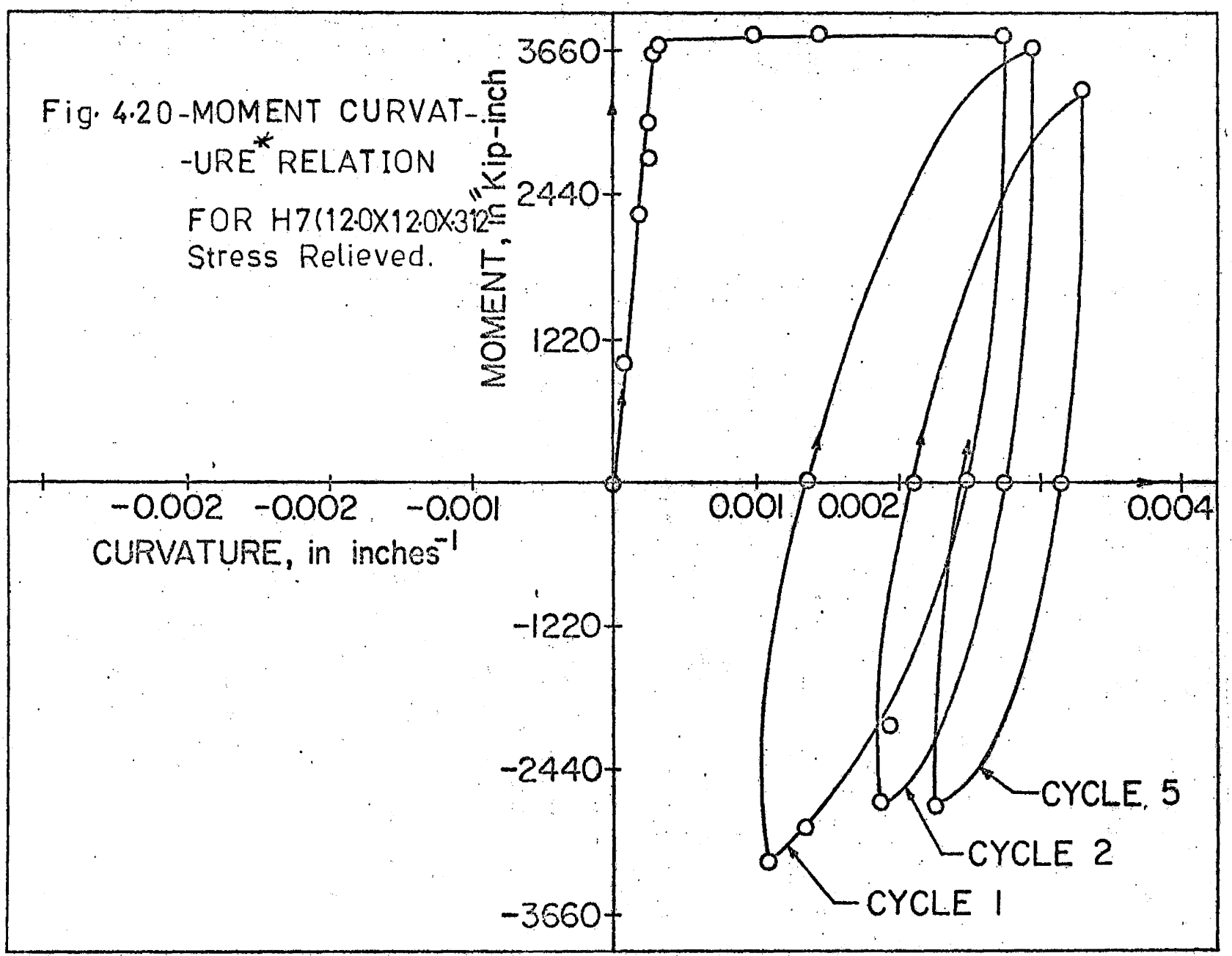

Fig. 4.20 - MOMENT CURVATURE* RELATION FOR H7(12.0X12.0X.312 Stress Relieved.

* The shown curve describes the behaviour of the buckled portion of the beam.

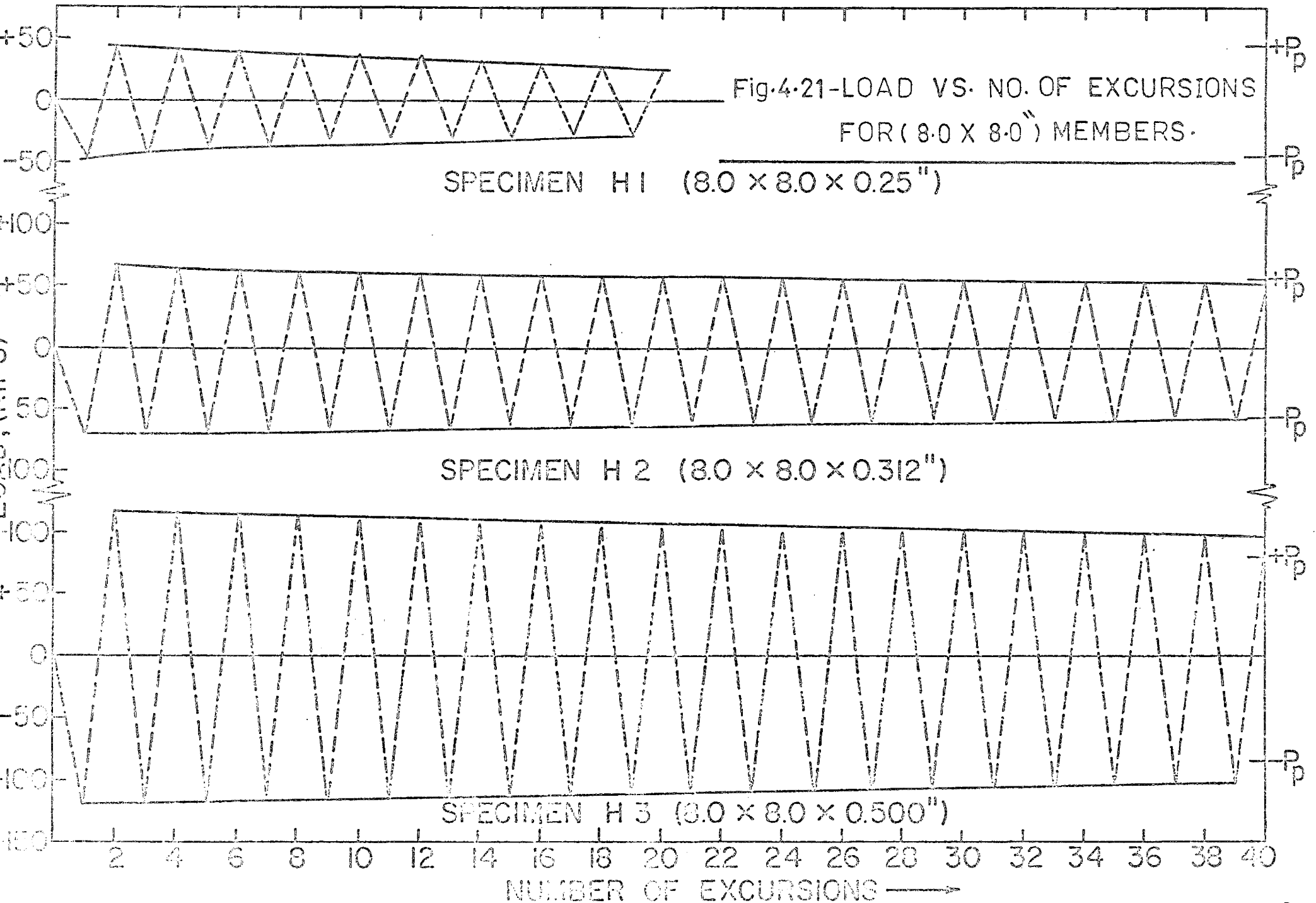

Fig·4·21-LOAD VS· NO. OF EXCURSIONS FOR (8·0 X 8·0") MEMBERS·

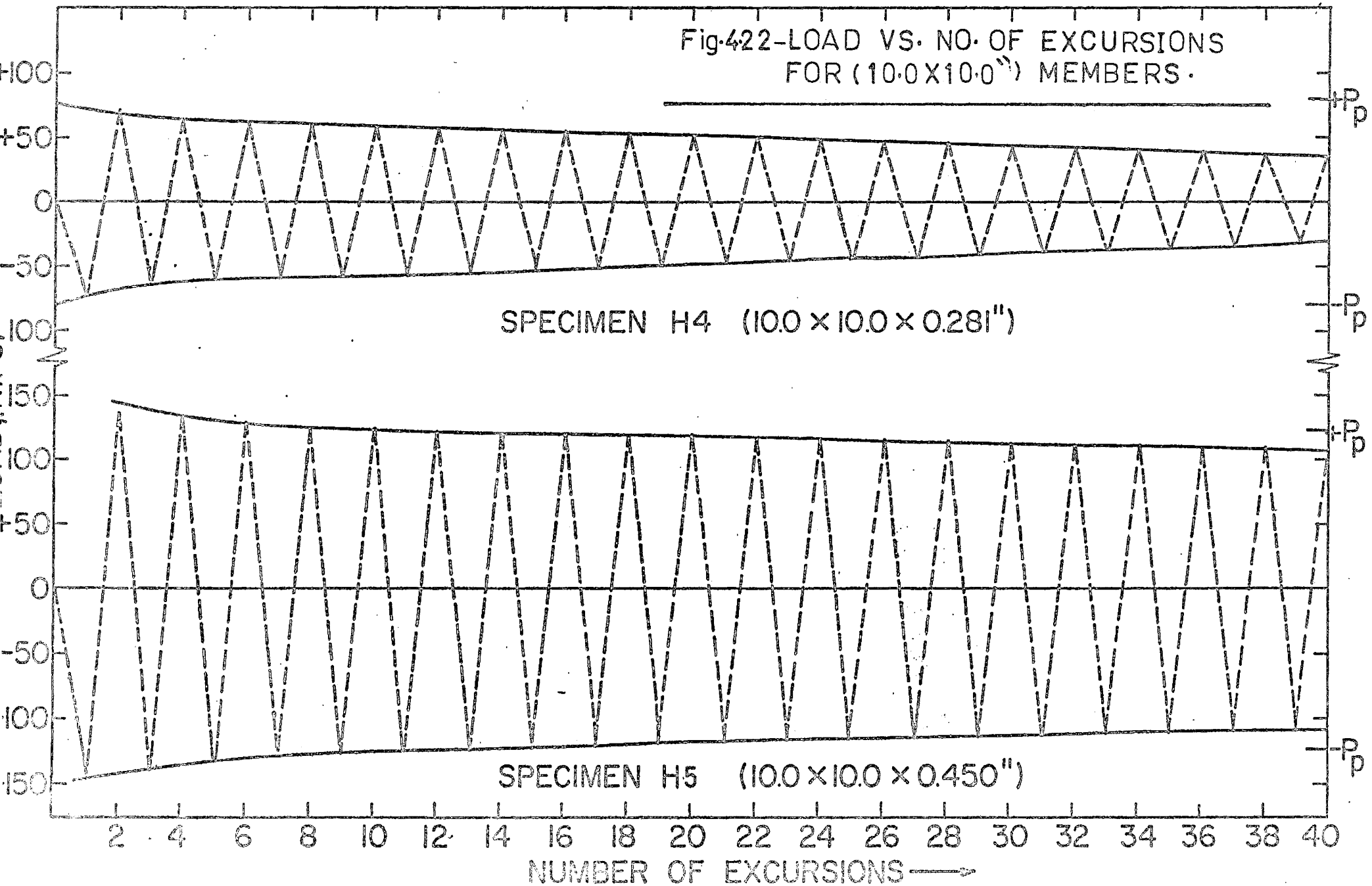
Fig·4·2 2-LOAD VS· NO· OF EXCURSIONS
FOR (10·0 X 10·0") MEMBERS·
+100
+50
0
-50
-100
+Pp
-Pp
SPECIMEN H4 (10.0 × 10.0 × 0.281")
-150
+100
+50
0
-50
-100
-150
+Pp
-Pp
SPECIMEN H5 (10.0 × 10.0 × 0.450")
2 4 6 8 10 12 14 16 18 20 22 24 26 28 30 32 34 36 38 40
NUMBER OF EXCURSIONS ⟶

Fig·4·23-LOAD VS. NO. OF EXCURSIONS FOR(12·0 X12·0") MEMBERS.

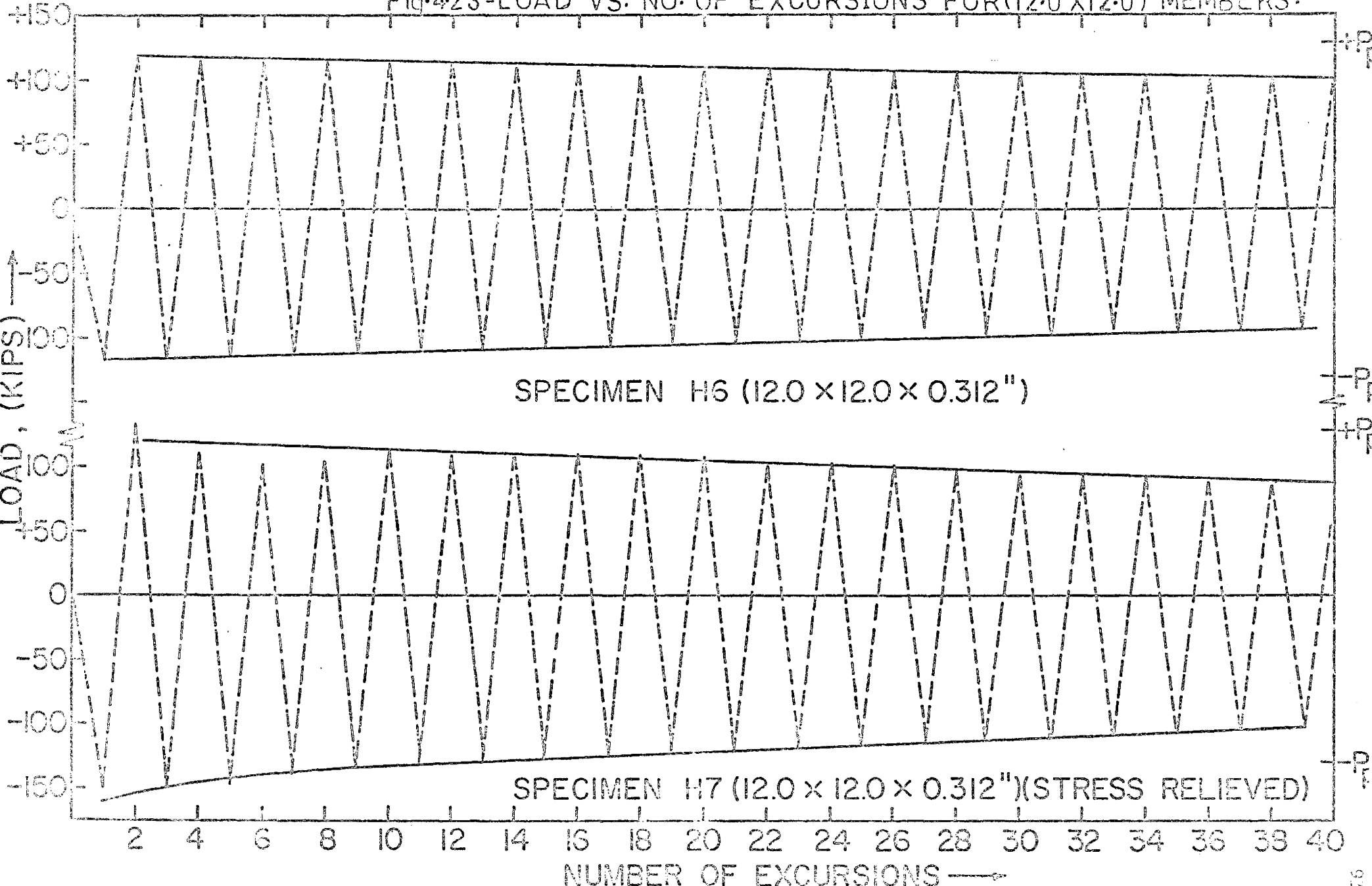

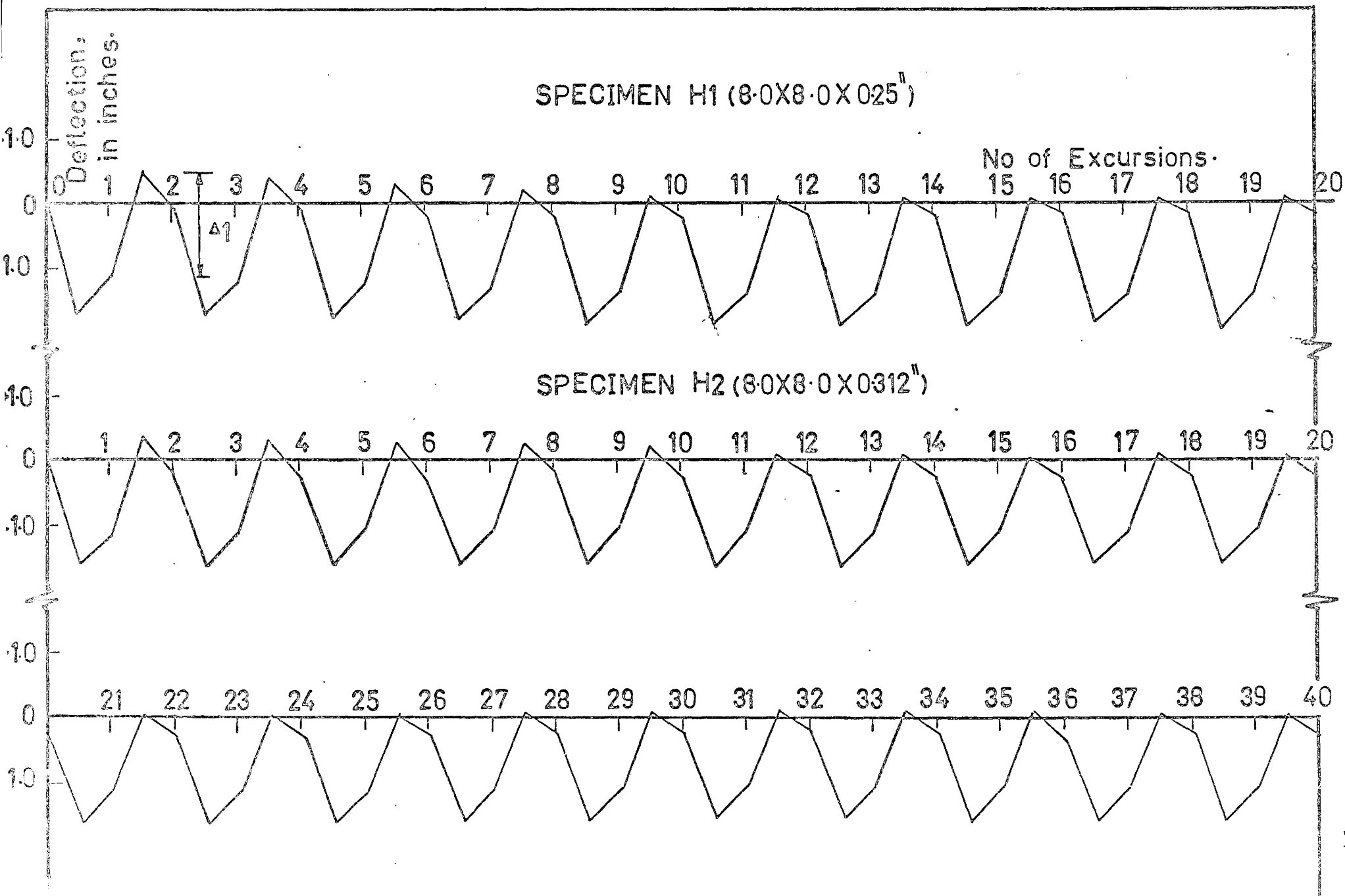
SPECIMEN H1 (8·0X8·0X·025")
Deflection, in inches.
No of Excursions.
·1·0
0
·1·0
Δ1
1 2 3 4 5 6 7 8 9 10 11 12 13 14 15 16 17 18 19 20
SPECIMEN H2 (8·0X8·0X·0312")
·1·0
0
·1·0
1 2 3 4 5 6 7 8 9 10 11 12 13 14 15 16 17 18 19 20
·1·0
0
·1·0
21 22 23 24 25 26 27 28 29 30 31 32 33 34 35 36 37 38 39 40

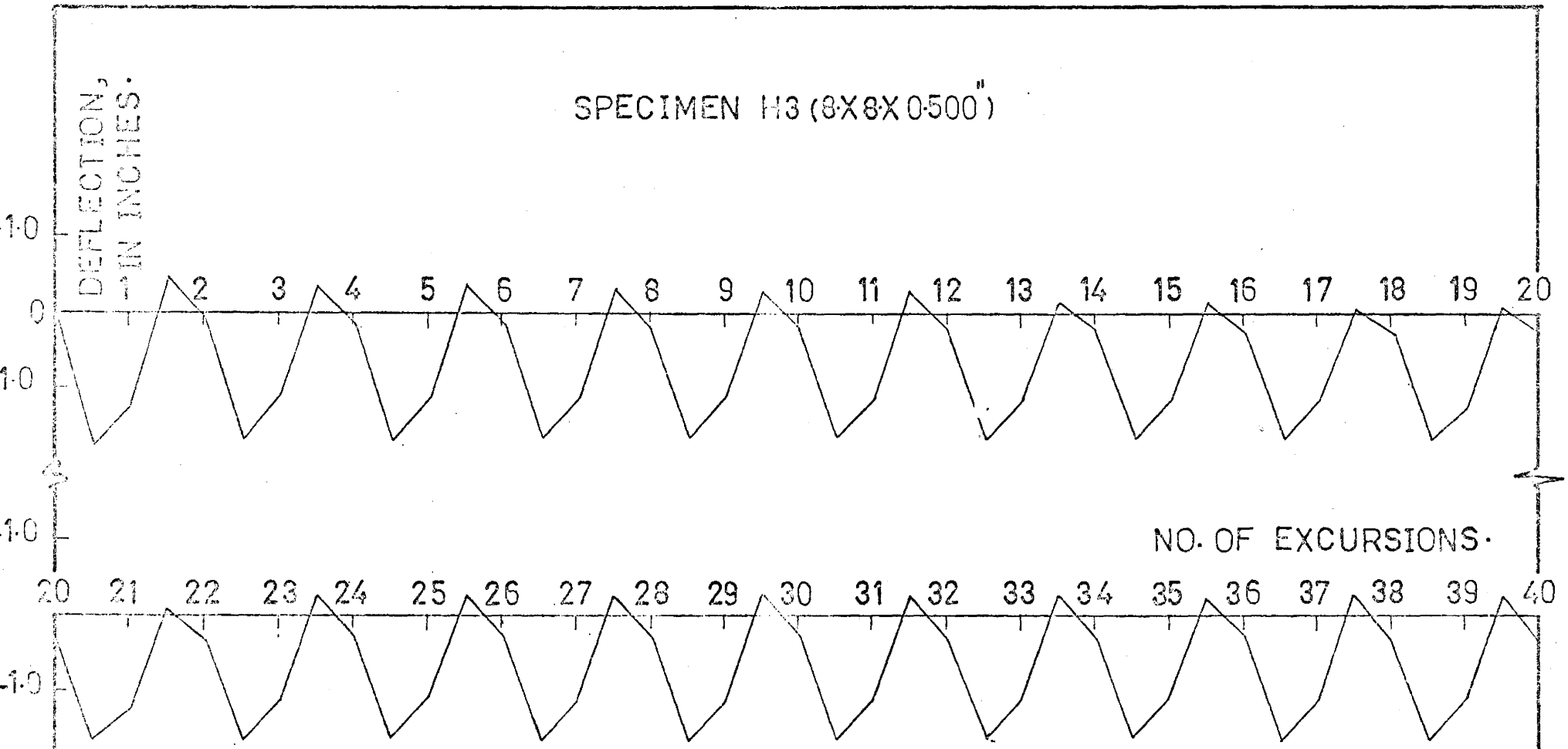

Fig·4·24- DEFLECTION VS· NO·OF EXCURSIONS

FOR (8·0 X 8·0) INCH MEMBERS·

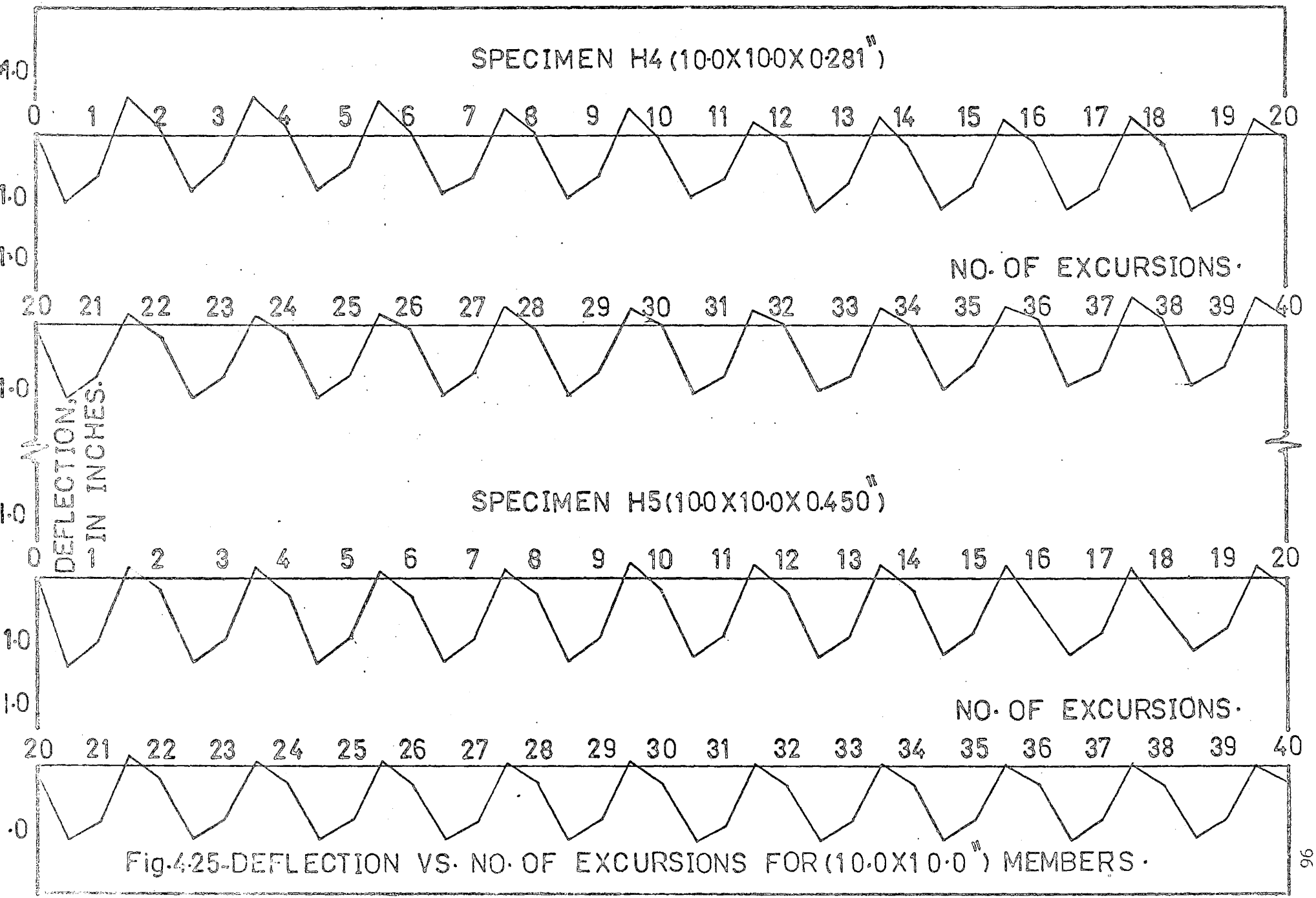

Fig.4.25-DEFLECTION VS. NO. OF EXCURSIONS FOR (10.0X10.0") MEMBERS.

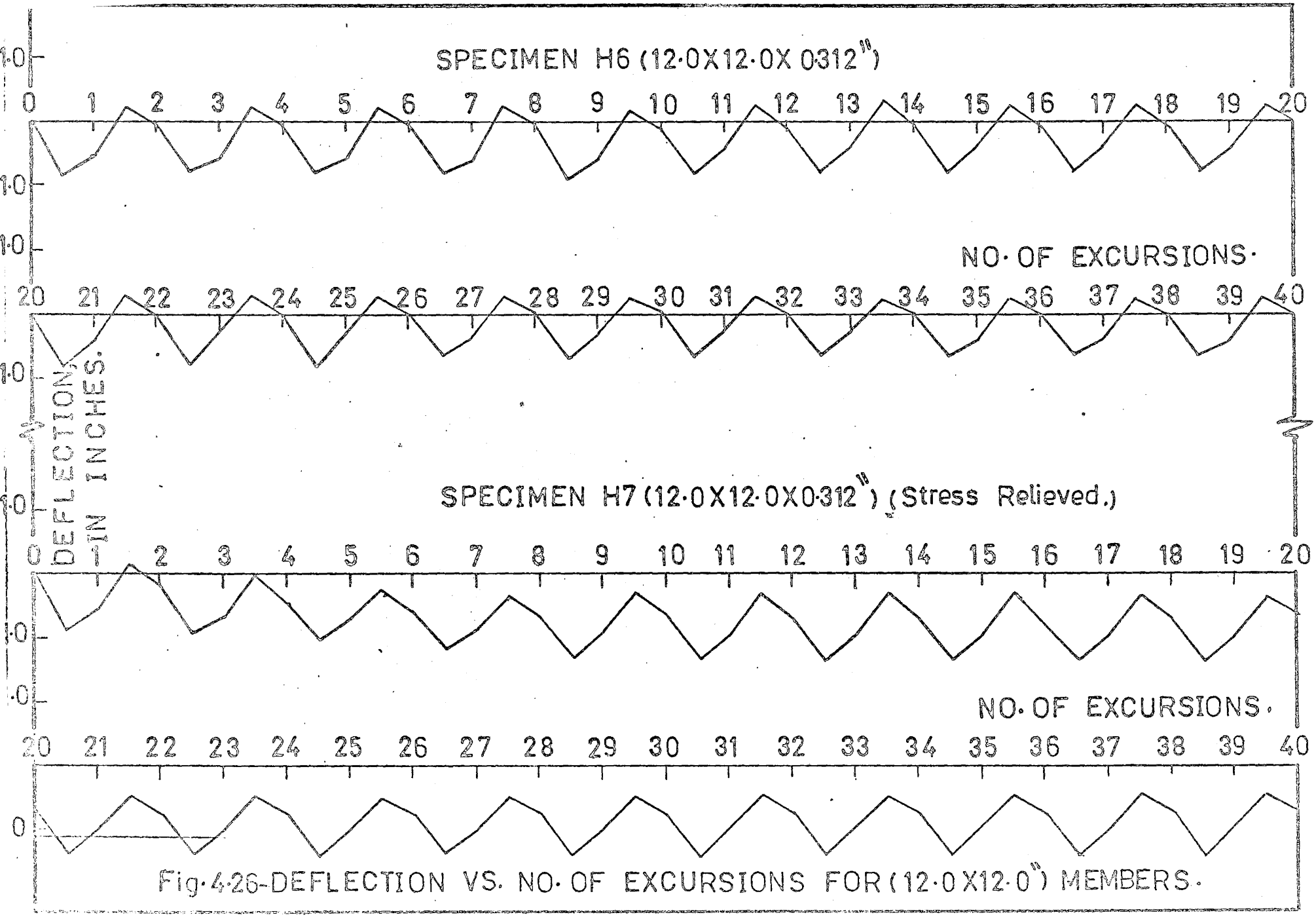

Fig·4·26-DEFLECTION VS. NO· OF EXCURSIONS FOR (12·0X12·0") MEMBERS·

Fig. 427- ΣT_d VS. NO. OF EXCURSIONS, FOR (8·0 X 8·0") SPECIMENS

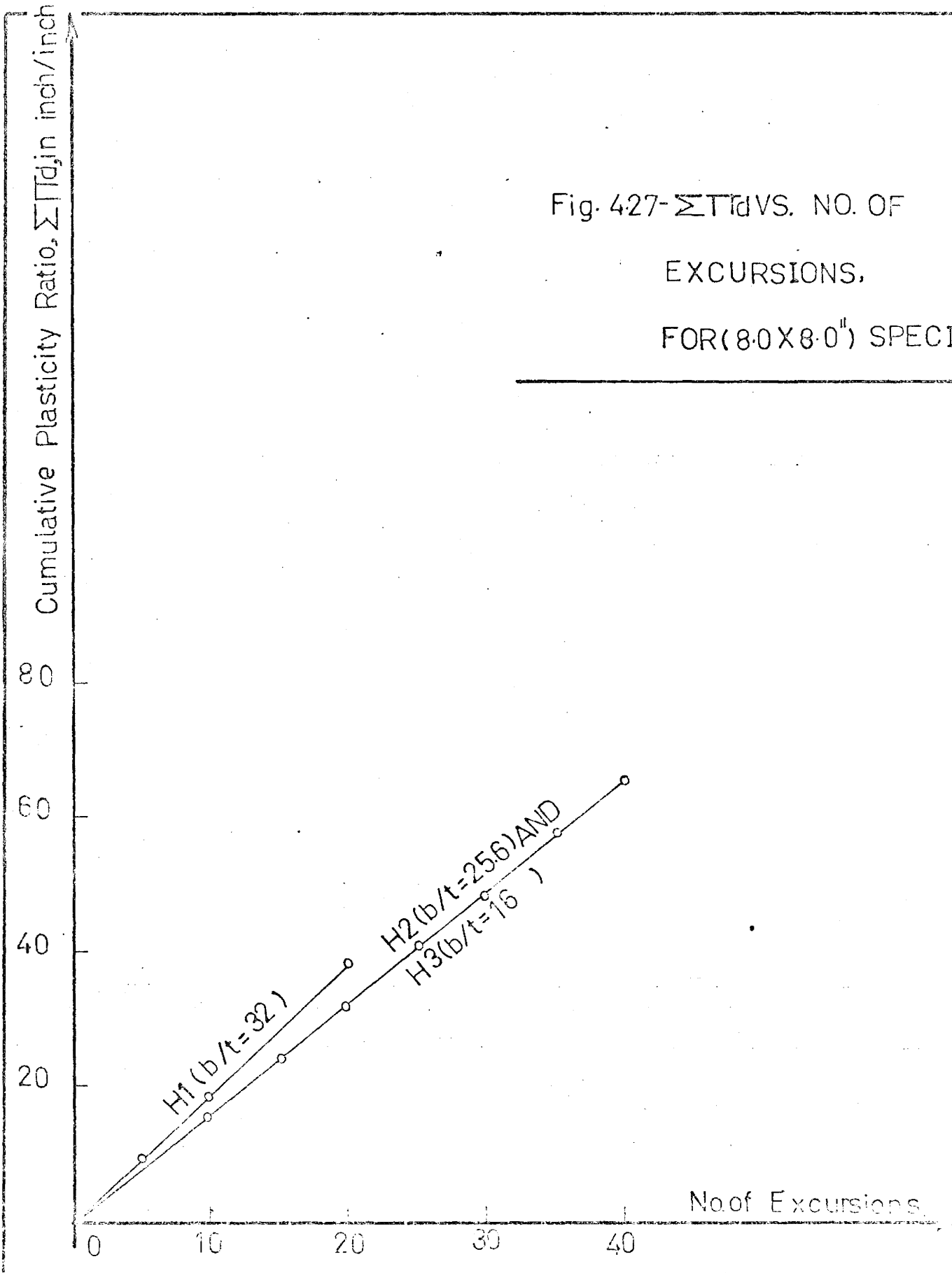

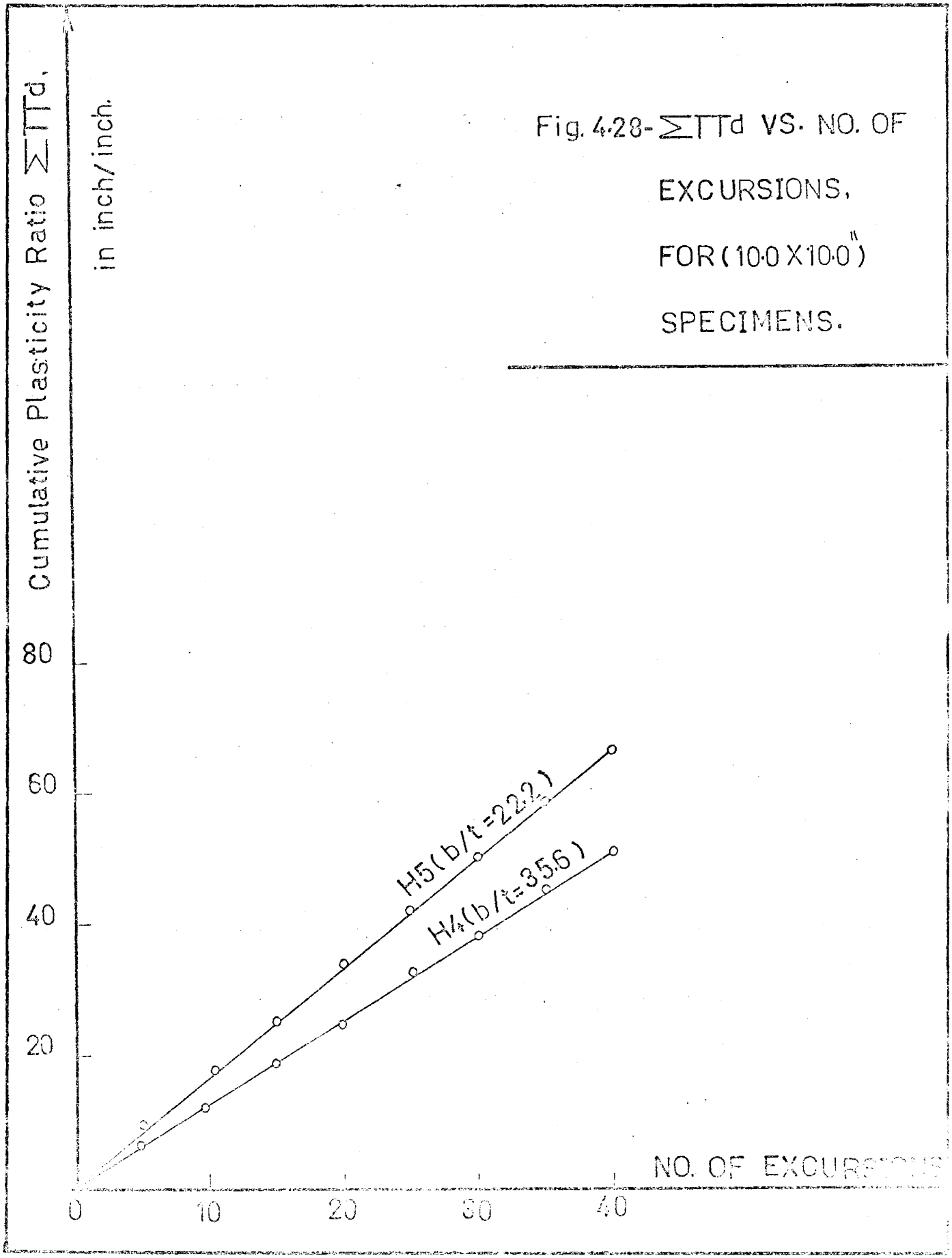

Fig. 4.28- ΣTTd VS. NO. OF EXCURSIONS, FOR (10.0 X 10.0") SPECIMENS.

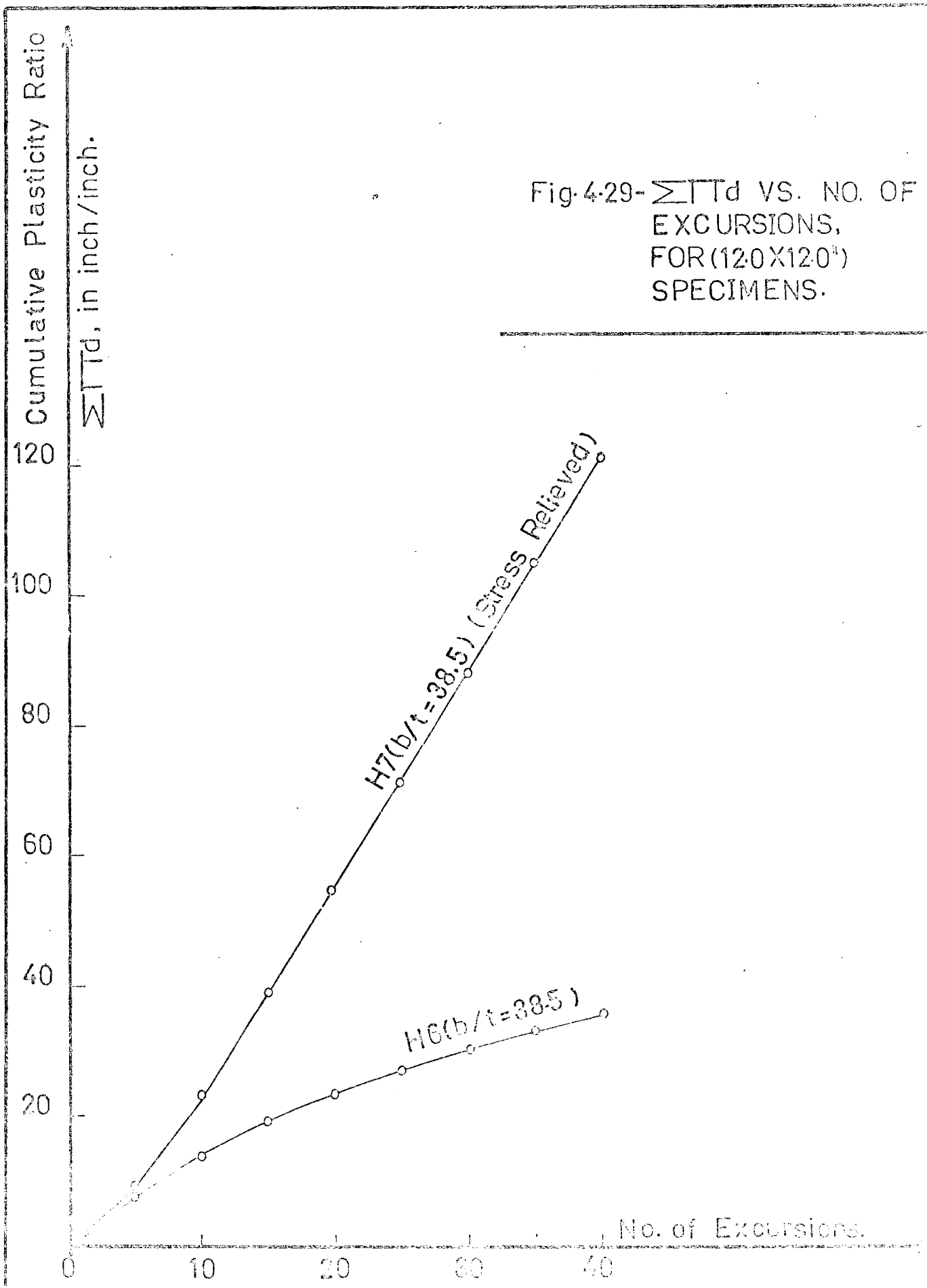

Fig. 4.29- $\sum \Pi d$ VS. NO. OF EXCURSIONS, FOR (12.0 X 12.0") SPECIMENS.

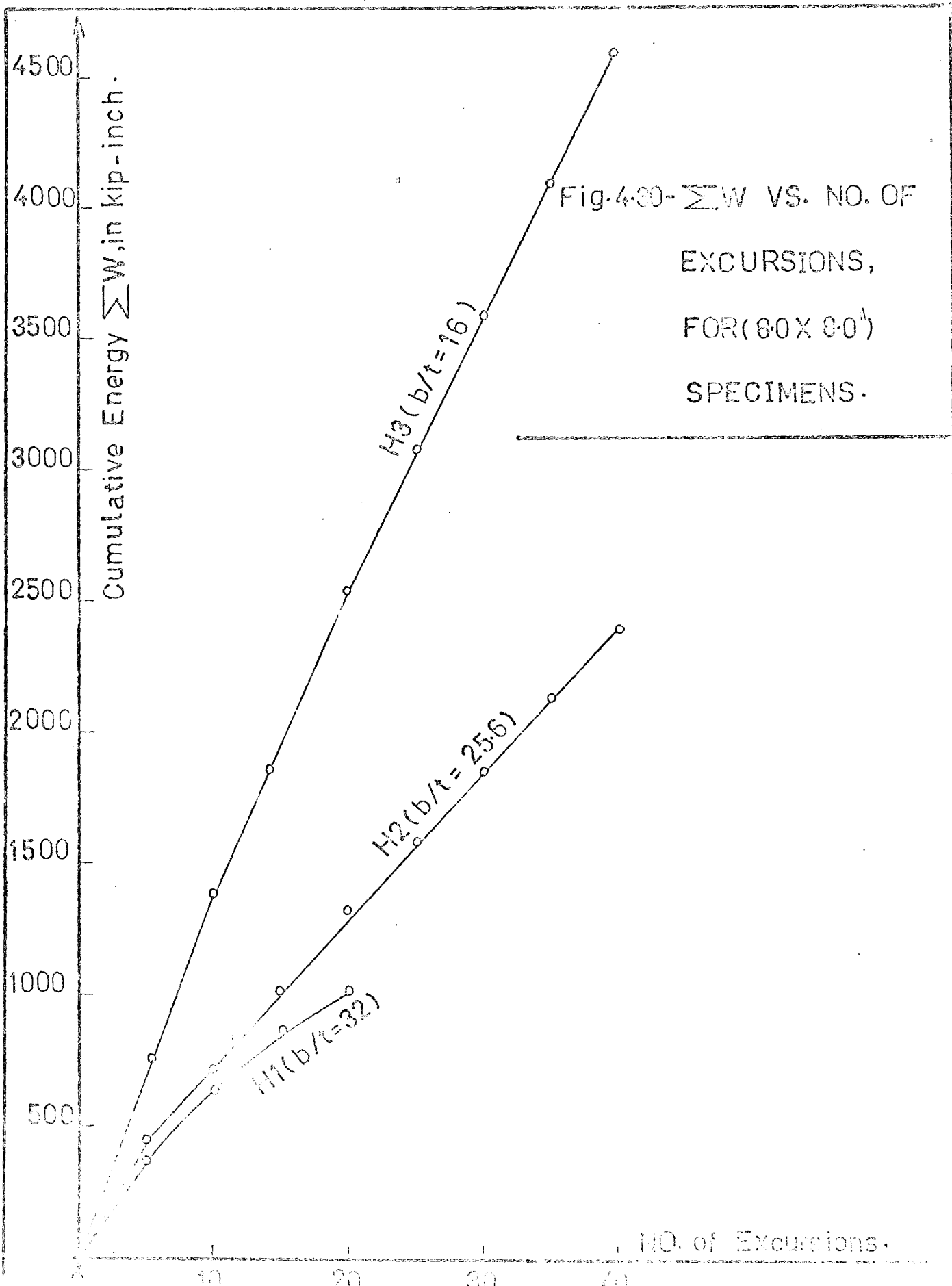

Fig. 4.30 - ΣW VS. NO. OF EXCURSIONS, FOR (8.0 X 8.0") SPECIMENS.

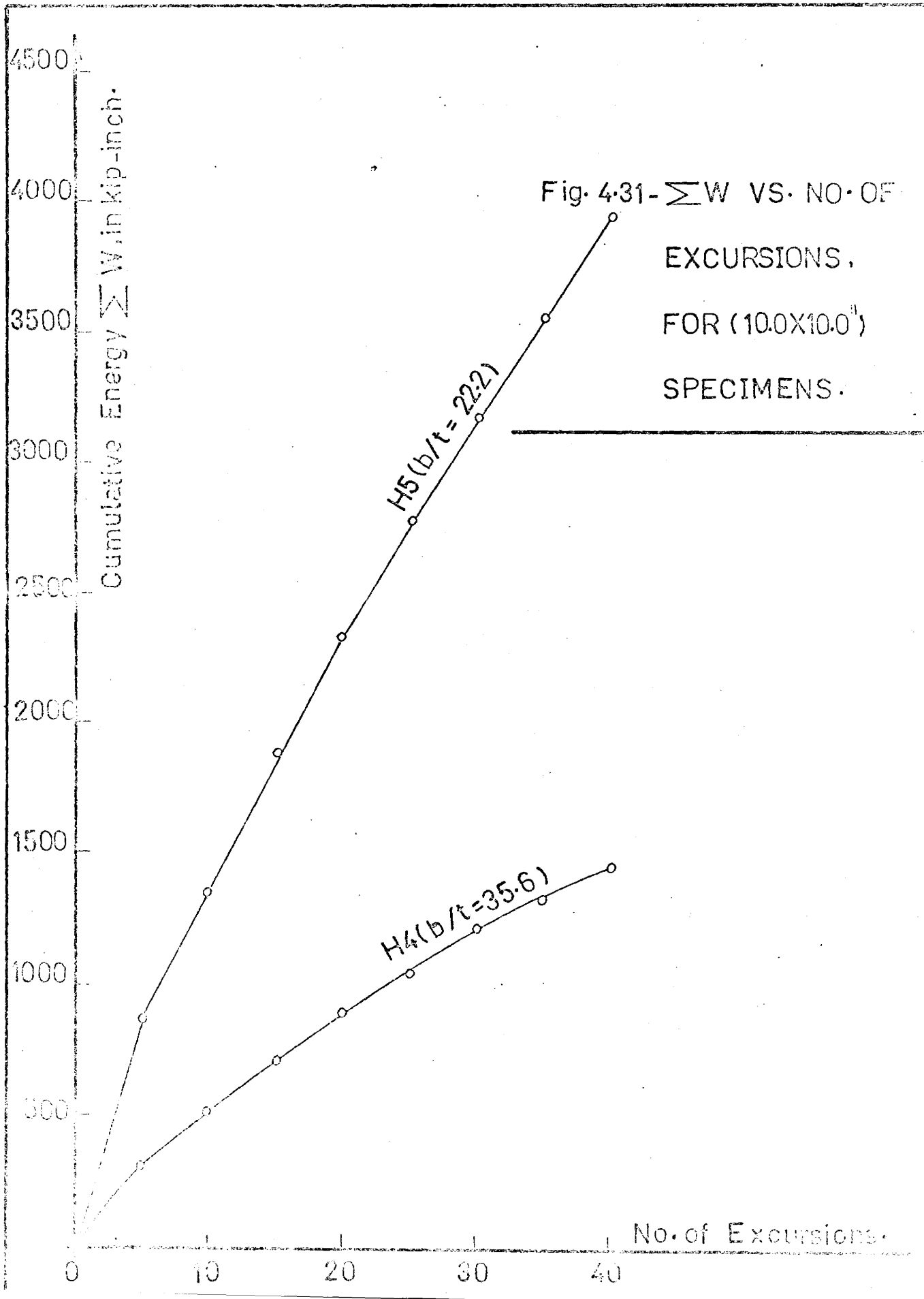

Fig. 4.31 - ∑W VS. NO. OF EXCURSIONS, FOR (10.0X10.0") SPECIMENS.

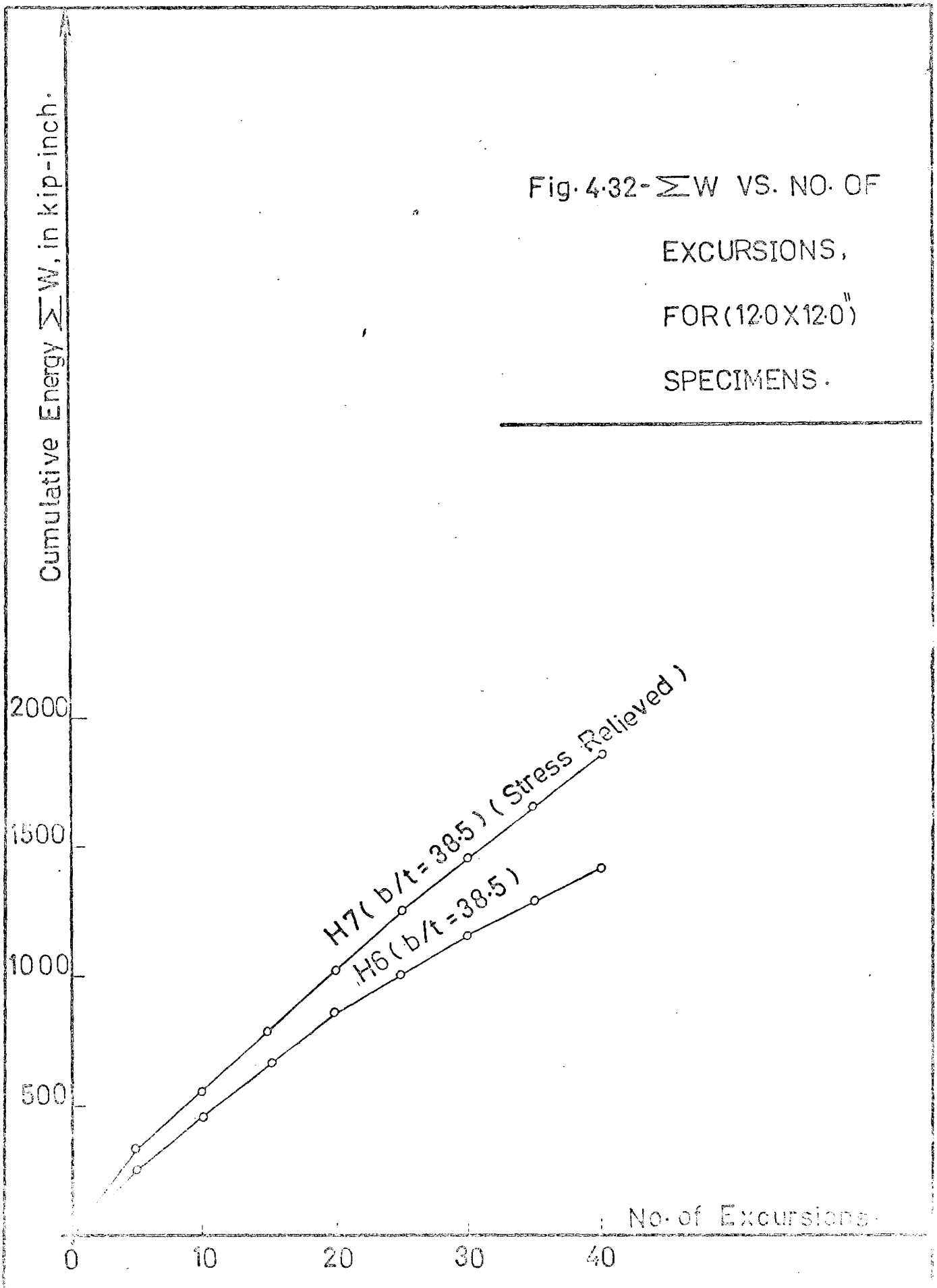

Fig. 4.32 - ΣW VS. NO. OF EXCURSIONS, FOR (12.0 X 12.0") SPECIMENS.

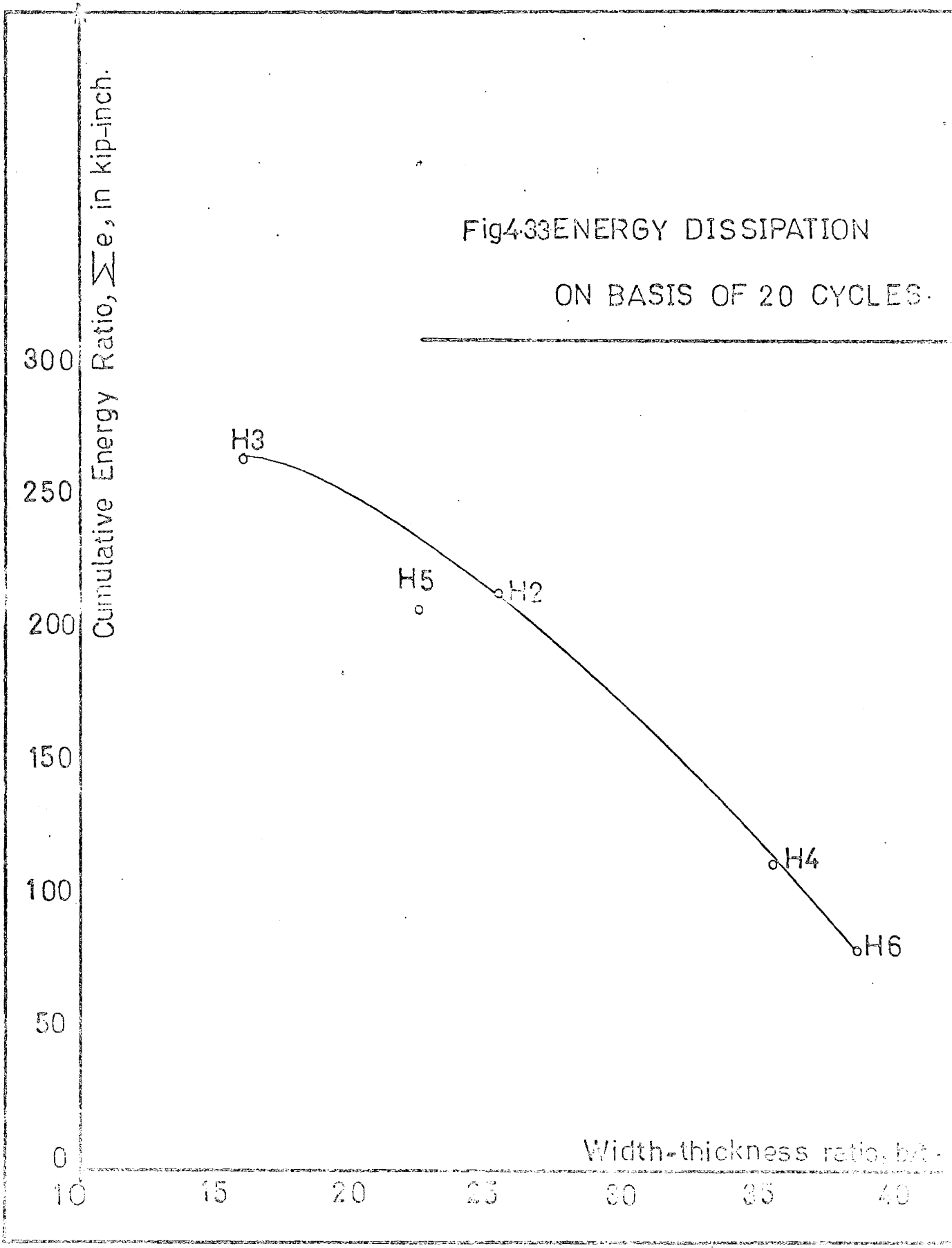

Fig4-33ENERGY DISSIPATION ON BASIS OF 20 CYCLES.

CHAPTER V

DISCUSSIONS AND CONCLUSIONS

5.1 Introduction

An attempt is made in this chapter to compare the slenderness ratio criteria recommended by the ASCE manuals, 1971[4], and those specified by the recent Canadian Building Code[16]. The previous research work[2,5,6] involved testing conventional rolled steel sections in inelastic strain reversals, while the present work tested HSS under similar conditions. The specifications referred to are concerned with general static loading aspects, while the ASCE manuals[4] are specifically concerned with the plastic capacities of rolled sections. Our purpose is to construct preliminary guidelines for HSS limitations in cyclic load aspects and to compare these guidelines with static load limitations. In addition, a comaprison with standard sections will be made from Popov's work to evaluate the relative resistance of square hollow sections to cyclic loads.

5.2 Review of Current Specifications

The ASCE manuals for 1971[4] summarized the current research concerning the geometrical requirements of conventional rolled sections, such that they acquire the necessary plastic moment capacity. In plastic design sections, this plastic moment value, as emphasized earlier, should not be impaired by local or lateral-torsional buckling until the required rotation has been achieved. Although local and lateral-torsional buckling are not always independent phenomena, they have been treated separately in the literature. This is mainly due to the complexity of the combined problem.

The problem of the flange buckling of rolled sections have been tackled assuming that the flange is strained uniformly to a strain equal to ε_{st}. It is also assumed that the material will strain harden with modulus E_{st} at strain ε_{st}.

Assuming the general case of beams under moment gradient and taking the effect of web restraint into consideration, for a value of Poisson's ratio, $\nu = 0.3$ and $E/G = 2.6$ where G is the modulus of elasticity in shear, the b/t ratio was specified by the ASCE manual[4] as follows:

$$\frac{b}{t} = \frac{3.56}{\sqrt{\frac{\sigma_y}{E}}} \sqrt{\frac{1}{\left(3 + \frac{\sigma_f}{\sigma_y}\right)\left(1 + \frac{E}{5.2E_{st}}\right)}} \qquad 5.1$$

where b = flange width

t = mean flange thickness

σy = yield stress level

E = Young's modulus of elasticity

σ_f = tensile strength of weld metal or bolt

E_{st} = strain hardening modulus.

Taking E_{st} = 800 ksi, the minimum b/t ratios would be as follows:

for A36 steel, σ_u = 58 b/t = 16.70

for A441(50) steel, σ_u = 70 b/t = 14.50 5.2

for A572(65) steel, σ_u = 80 b/t = 13.00

The minimum limiting web depth to web thickness ratio, h/w recommended by the previous reference, for conventional rolled sections is:

$$\frac{h}{w} = 43 \sqrt{36/\sigma y} \qquad 5.3$$

where h is the beam depth, and w is the web thickness.

Equation 5.3 allows high slenderness ratios for the web of wide flange sections in plastic design, which is expected as the flange loading is directly transferred to the web. Unlike the previous case, the web slenderness limitation for square hollow sections should be more conservative.

According to the Canadian Standards Association S-16, 1969[16], the requirements of slenderness ratio for compact sections with an axis of symmetry in the plane of bending are specified not to exceed the following limits:

(a) For projecting elements of the compression flange of rolled or built up sections:

$$\frac{b'}{t} \leq \frac{64}{\sqrt{\sigma y}} \qquad 5.4$$

where b', for rolled or built up sections, is one-half the full nominal flange width, or the distance from the free edge to the first row of bolts or welds. The thickness, t, is the mean flange section as defined earlier.

(b) For flange plates of rectangular or square hollow sections, between the rounded corners:

$$\frac{b}{t} \leq \frac{200}{\sqrt{\sigma y}} \qquad 5.5$$

where b is the full width of the section.

The plastic design requirements for square and rectangular hollow sections were investigated by Korol[17], and he proved that the b/t ratio

specified by equation 5.5 for both compact and plastic design purposes was inadequate for plastic design. The criterion used in the previous investigations to judge a section's adequacy for plastic design was that a minimum plastic rotation of four times that corresponding to M_p must be obtained prior to the moment dropping below M_p.

The previous investigation suggested the following criterion:

$$\frac{b}{t} \leq \frac{160}{\sqrt{\sigma y}} \qquad 5.6$$

Equation 5.6 takes into account that in practice, the load is applied on the straight width of the flange only rather than on the rounded corners as well, a factor which makes the section more susceptible to premature local buckling.

5.3 Summary of Experimental Work

The previous cyclic tests using standard rolled sections, conducted by Bertero and Popov[2,6], and by Popov and Pinkney[5] utilized wide flange rolled sections. The b/t ratio for these sections ranged between 10.4 and 21.2, and the beams tested were all in the form of a cantilever.

The maximum strain values applied on the 4X4 M13 section was 2.5%, causing failure of the specimen in the 16th cycle. For the 8WF20 sections, failure occurred after 22 1/2 cycles under a constant strain of 1.5%.

The 18WF50 and 24WF76 sections were subjected to four increasing deflection levels, for a number of two cycles at each level.

The current work includes a wide range of dimensions of square hollow sections tested cyclically at a strain level of 2%. A criterion of twenty cycles at the previous strain level was believed to be adequate to judge the capabilities of these sections for cyclic design. From the previous results it could be concluded that b/t ratio of about 22 guarantees a reasonable level of performance under the previous conditions. This adequate performance is proved by the stability of the P-Δ hysteresis loops and the stability of the energy dissipated through cycling. The static test after 20 cycles indicates a reasonable performance provided that no fracture occurred. The performance of beam H5 emphasizes the previous conclusion.

It should be noted that the chosen b/t ratio of 22 is confined to those sections with a specified yield stress of 50 ksi. In general, the relationship could be written in the form:

$$\frac{b}{t} \leq \frac{155}{\sqrt{\sigma_y}} \qquad 5.7$$

It is interesting to notice that the previous strain of 2% is equal to four times the elastic strain at yield from the definition of the yield stress. Therefore, it is meaningful to compare the b/t ratio requirement for cyclic loads at 2% strain level with the corresponding ratio specified for plastic design. Equations 5.6 and 5.7 show a close agreement bearing in mind that no minimum rotation requirements at the

level of plastic moment, M_p, are specified for the cyclic design sections.

Figure 5.1 shows the relationship between the number of cycles to failure versus the controlling cyclic strain based on the tests conducted by Bertero and Popov[2] and Popov and Pinkney[5] using 4X4 M13 and 8WF20 sections, respectively. The intermediate continuous line of Figure 5.1 is an interpolation between the aforementioned two sets of results to establish the b/t ratio of a fictitious section that resists 20 cycles at a controlling strain of 2%. The required ratio is shown to be in the range of 15 corresponding to a yield stress of 36 ksi. In general, the previous relationship could be written as follows:

$$\frac{b}{t} \leq \frac{90}{\sqrt{\sigma y}} \qquad 5.8$$

Table 5.1 shows the limiting requirements for both wide flange and square hollow sections. The static load requirements are quoted from the CSA-S16 Standard (1969[16] and the cyclic load requirements are the suggested values based on the current work and conclusions.

5.4 Suggestions for Further Research

It would be useful to study the behaviour of a variety of HSS under different peak strain levels of cyclic loading. This would help us to determine the effect of the inelastic strain levels on the number of

cycles that a member can survive. This would also enable us to estimate the critical slenderness ratio for different strain levels.

The current experiments aimed at simulating the case of columns in actual construction where there are necessary connections at floor levels that must be guarded against local buckling. Therefore, the collar provision was adopted at the midspan of tested beams in an attempt to prevent local buckling. It is suggested to study the case of sections without provisions against local buckling. The areas of possible stress concentration at the load application positions should also be studied along with their effects on the beam's structural capacity from the point of view of cyclic loading.

As mentioned earlier, connections in any framed structure are expected to be highly stressed and are possible regions for the formation of plastic hinges. Therefore, it is important to study the behaviour of a variety of connections involving various design and fabrication techniques, under the effect of cyclic loads.

TABLE 5.1

Comparison Between the Limiting b/t Requirements for WF sections versus HSS

Type of Section / Category	Limiting b/t Ratio			
	CSA-S16 (1969)			Suggested Values
	Non-Compact	Compact	Plastic Design	Cyclic Loading
Wide Flange	$\frac{255}{\sqrt{\sigma y}}$	$\frac{128}{\sqrt{\sigma y}}$	$\frac{108}{\sqrt{\sigma y}}$	$\frac{90}{\sqrt{\sigma y}}$
Square Hollow Section	$\frac{255}{\sqrt{\sigma y}}$	$\frac{200}{\sqrt{\sigma y}}$	$\frac{160}{\sqrt{\sigma y}}$	$\frac{155}{\sqrt{\sigma y}}$ *

*Based on the 2% strain limitation as described in Chapter III

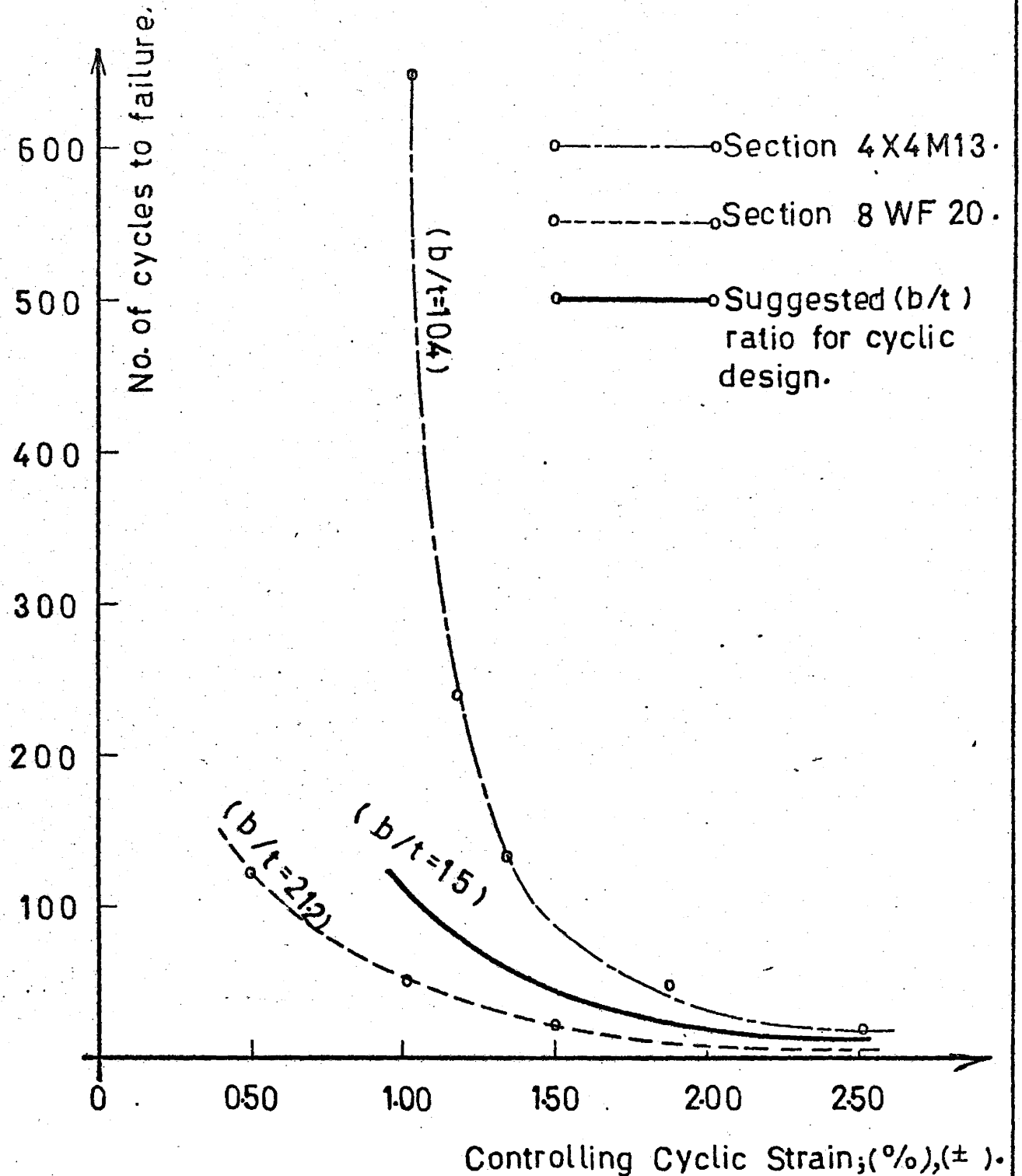

Fig·5·1 - NO· OF CYCLES TO FAILURE VS· CONTROLLING STRAIN·

APPENDIX I

EXPERIMENTAL RECORDS

This Appendix contains the detailed experimental records of the seven beams tested.

TABLE A.1

Experimental Record of Specimen H1

(8.0 x 8.0 x 0.25) inches

Half-Cycle	P kips	Δ inch	Δ' inch	W kip-inch	$P = \frac{P}{P_p}$	$\mu_l = \frac{\Delta}{\Delta_p}$	$\pi_d = \frac{\Delta'}{\Delta_p}$	$e = \frac{W}{1/2\ P_p \Delta_p}$
1	-46.25	-1.72	1.17	97.5	1.02	4.35	2.96	10.9
2	+45.20	+0.45	0.05	87.0	0.99	1.14	0.13	9.75
3	-43.00	-1.74	1.23	70.0	0.94	4.40	3.11	7.83
4	+42.60	+0.38	0.10	60.0	0.94	0.96	0.25	6.71
5	-38.00	-1.78	1.30	63.0	0.83	4.50	3.29	7.05
6	+40.30	+0.29	0.18	50.0	0.88	0.73	0.46	5.59
7	-35.00	-1.83	1.36	55.0	0.77	4.62	3.44	6.15
8	+38.30	+0.22	0.22	50.0	0.84	0.56	0.56	5.59
9	-33.80	-1.87	1.40	55.0	0.74	4.72	3.54	6.15
10	+36.80	+0.08	0.27	45.5	0.81	0.20	0.68	5.08
11	-32.60	-1.90	1.43	50.5	0.72	4.80	3.62	5.65
12	+35.20	+0.05	0.19	44.25	0.77	0.13	0.48	4.95
13	-31.70	-1.92	1.44	52.0	0.70	4.85	3.64	5.81
14	+31.90	+0.04	0.19	37.0	0.70	0.10	0.48	4.13
15	-30.30	-1.92	1.42	44.25	0.67	4.85	3.59	4.95
16	+28.50	+0.05	0.18	34.25	0.63	0.13	0.46	3.83
17	-28.00	-1.87	1.42	34.00	0.62	4.72	3.59	3.80
18	+26.50	+0.07	0.15	29.5	0.58	0.18	0.38	3.30
19	-26.00	-1.94	1.40	30.0	0.57	4.90	3.54	3.36
20	+24.30	+0.08	0.14	28.0	0.53	0.20	0.35	3.13

TABLE A.2

Experimental Record of Specimen H2

(8.0 x 8.0 x 0.312) inches

Half-Cycle	P kips	Δ inches	Δ' inches	W kip-inch	$P = \frac{P}{P_p}$	$\mu_l = \frac{\Delta}{\Delta_p}$	$\pi_d = \frac{\Delta'}{\Delta_p}$	$e = \frac{W}{1/2\ P_p \Delta_p}$
1	-69.00	-1.56	1.11	103.00	1.26	3.92	2.79	9.40
2	+67.20	+0.42	0.14	75.00	1.23	1.06	0.35	6.85
3	-68.80	-1.58	1.12	80.00	1.25	3.98	2.82	7.30
4	+65.00	+0.35	0.20	66.00	1.18	0.88	0.50	6.02
5	-67.00	-1.58	1.03	70.00	1.22	3.98	2.59	6.40
6	+63.50	+0.32	0.23	65.00	1.16	0.81	0.58	5.95
7	-65.50	-1.58	1.05	70.25	1.20	3.98	2.64	6.41
8	+62.00	+0.30	0.15	62.50	1.13	0.76	0.38	5.70
9	-64.30	-1.59	1.06	67.5	1.17	4.00	2.66	6.16
10	+60.80	+0.25	0.21	60.00	1.11	0.63	0.53	5.48
11	-63.90	-1.64	1.10	68.25	1.16	4.12	2.77	6.23
12	+60.10	+0.12	0.22	56.25	1.10	0.30	0.55	5.15
13	-62.65	-1.63	1.11	64.00	1.14	4.10	2.79	5.85
14	+59.50	+0.12	0.23	58.0	1.08	0.30	0.58	5.30
15	-61.70	-1.62	1.09	61.25	1.12	4.06	2.74	5.60
16	+58.60	+0.06	0.24	55.25	1.07	0.15	0.60	5.05
17	-61.50	-1.61	1.14	58.00	1.12	4.05	2.87	5.30
18	+58.10	+0.09	0.25	56.00	1.06	0.23	0.63	5.11
19	-60.50	-1.60	1.09	58.00	1.10	4.01	2.74	5.30
20	+57.50	+0.08	0.25	55.00	1.05	0.20	0.63	5.00
21	-60.30	-1.62	1.10	62.00	1.10	4.06	2.77	5.66
22	+57.15	+0.06	0.27	52.50	1.04	0.15	0.68	4.80
23	-59.80	-1.63	1.14	58.00	1.09	4.10	2.87	5.30
24	+57.25	+0.04	0.27	52.50	1.04	0.10	0.68	4.80
25	-58.90	-1.58	1.08	55.00	1.07	3.97	2.71	5.00
26	+57.00	+0.11	0.22	55.50	1.04	0.28	0.55	5.06
27	-58.00	-1.60	1.08	56.50	1.06	4.02	2.71	5.16
28	+56.50	+0.12	0.22	52.50	1.03	0.30	0.55	4.80
29	-57.80	-1.53	1.04	53.00	1.06	3.85	2.62	4.85
30	+56.30	+0.12	0.21	53.00	1.03	0.30	0.53	4.85
31	-57.80	-1.62	1.11	57.50	1.06	4.06	2.79	5.25
32	+55.75	+0.09	0.23	52.50	1.02	0.23	0.58	4.80
33	-57.55	-1.64	1.11	56.25	1.05	4.12	2.79	5.15
34	+55.40	+0.07	0.34	52.5	1.01	0.18	0.80	4.80
35	-57.15	-1.62	1.11	55.00	1.04	4.06	2.79	5.02
36	+55.00	+0.05	0.26	52.50	1.00	0.13	0.65	4.80
37	-56.90	-1.64	1.13	54.25	1.04	4.12	2.84	4.95
38	+54.65	+0.03	0.28	52.00	1.00	0.08	0.70	4.75
39	-56.70	-1.65	1.14	52.50	1.03	4.15	2.87	4.80
40	+54.30	+0.02	0.30	50.00	0.99	0.05	0.75	4.56

TABLE A.3

Experimental Record of Specimen H3

(8.0 x 8.0 x 0.50) inches

Half-Cycle	P kips	Δ inch	Δ' inch	W kip-inch	$\bar{P} = \frac{P}{P_p}$	$\mu_l = \frac{\Delta}{\Delta_p}$	$\pi_d = \frac{\Delta'}{\Delta_p}$	$e = \frac{W}{1/2\ P_p \Delta_p}$
1	-117.1	-1.74	1.22	197.5	1.43	4.20	2.94	11.50
2	+118.4	+0.44	0.07	142.5	1.44	1.06	0.07	8.30
3	-117.35	-1.67	1.11	152.5	1.431	4.02	2.68	8.85
4	+117.1	+0.36	0.12	125.0	1.43	0.87	0.29	7.26
5	-115.4	-1.66	1.14	145.0	1.41	4.00	2.75	8.43
6	+115.0	+0.34	0.16	125.0	1.41	0.82	0.39	7.26
7	-113.0	-1.66	1.15	138.25	1.38	4.00	2.77	8.05
8	+112.00	+0.29	0.19	119.0	1.36	0.70	0.46	6.92
9	-112.0	-1.65	1.15	131.0	1.36	3.98	2.77	7.60
10	+110.5	+0.26	0.21	117.0	1.35	0.63	0.51	6.80
11	-110.3	-1.65	1.15	125.0	1.35	3.98	2.77	7.26
12	+108.6	+0.13	0.23	112.5	1.32	0.32	0.55	6.55
13	-109.3	-1.64	1.15	123.5	1.33	3.96	2.77	7.18
14	+107.0	+0.12	0.24	110.0	1.30	0.29	0.58	6.40
15	-108.0	-1.64	1.14	119.0	1.31	3.96	2.75	6.92
16	+106.0	+0.11	0.25	107.0	1.29	0.27	0.60	6.22
17	-107.75	-1.64	1.15	120.0	1.31	3.96	2.77	6.97
18	+104.40	+0.07	0.27	109.0	1.27	0.17	0.65	6.35
19	-106.70	-1.63	1.25	116.5	1.30	3.93	3.01	6.76
20	+103.0	+0.06	0.28	106.25	1.25	0.15	0.68	6.18
21	-106.0	-1.63	12.4	115.0	1.29	3.93	2.99	6.68
22	+102.4	+0.06	0.28	105.25	1.25	0.15	0.68	6.13
23	-105.0	-1.63	1.11	112.50	1.28	3.93	2.68	6.55
24	+101.8	+0.28	0.27	101.25	1.24	0.68	0.65	5.90
25	-103.6	-1.62	1.11	106.0	1.26	3.90	2.68	6.16
26	+101.6	+0.27	0.28	104.0	1.24	0.65	0.68	6.05
27	-102.6	-1.62	1.12	106.0	1.25	3.90	2.70	6.15
28	+101.4	+0.28	0.28	102.0	1.24	0.68	0.68	5.93
29	-102.0	-1.62	1.11	102.5	1.24	3.90	2.68	5.96
30	+101.1	+0.28	0.28	105.0	1.23	0.68	0.68	6.10
31	-101.5	-1.60	1.11	105.0	1.24	3.86	2.68	6.10
32	+100.5	+0.24	0.28	98.0	1.22	0.58	0.68	5.70
33	-101.0	-1.60	1.11	99.25	1.23	3.86	2.68	5.76
34	+100.0	+0.23	0.29	99.50	1.22	0.55	0.70	5.80
35	-100.0	-1.60	1.10	100.0	1.22	3.86	2.66	5.80
36	+ 99.5	+0.22	0.29	96.25	1.21	0.53	0.70	5.60
37	- 99.5	-1.60	1.10	95.50	1.21	3.86	2.66	5.55
38	+ 99.3	+0.28	0.29	100.0	1.21	0.68	0.70	5.80
39	- 98.7	-1.60	1.10	98.0	1.20	3.86	2.66	5.70
40	+ 99.2	+0.28	0.29	96.50	1.21	0.68	0.70	5.60

TABLE A.4

Experimental Record of Specimen H4

(10 x 10 x 0.281) inches

Half-Cycle	P kips	Δ inch	Δ' inch	W kip-inch	$P = \frac{P}{P_p}$	$\mu_I = \frac{\Delta}{\Delta_p}$	$\pi_d = \frac{\Delta'}{\Delta_p}$	$e = \frac{W}{1/2\ P_p \Delta_p}$
1	-70.20	-1.03	-0.66	88.50	0.89	3.26	2.09	7.10
2	-71.10	+0.60	0.13	78.00	0.90	1.90	0.41	6.25
3	-63.40	-0.90	0.47	51.75	0.80	2.85	1.49	4.15
4	+65.85	+0.61	0.13	41.50	0.83	1.93	0.41	3.32
5	-61.30	-0.87	0.52	49.50	0.77	2.75	1.65	3.96
6	+62.30	+0.53	0.06	38.50	0.77	1.68	0.19	3.08
7	-58.50	-0.93	0.70	45.00	0.74	2.94	2.22	3.60
8	+59.50	+0.45	0.07	37.50	0.75	1.43	0.22	3.00
9	-57.00	-0.99	0.65	44.25	0.72	3.14	2.06	3.54
10	+57.65	+0.40	0.05	36.00	0.73	1.27	0.16	2.88
11	-55.15	-1.04	0.71	43.00	0.70	3.29	2.25	3.44
12	+56.05	+0.19	0.09	34.50	0.71	0.60	0.29	2.76
13	-53.75	-1.18	0.74	42.00	0.68	3.74	2.34	3.36
14	+54.35	+0.30	0.14	35.00	0.69	0.95	0.44	2.80
15	-52.65	-1.12	0.79	42.50	0.66	3.55	2.50	3.40
16	+54.35	+0.25	0.11	32.50	0.69	0.79	0.35	2.60
17	-51.55	-1.15	0.80	42.50	0.65	3.64	2.53	3.40
18	+52.45	+0.30	0.08	34.00	0.66	0.95	0.25	2.72
19	-50.30	-1.19	0.85	50.00	0.63	3.77	2.69	4.00
20	+49.75	+0.31	0.07	34.00	0.63	0.98	0.22	2.72
21	-48.35	-1.17	0.82	40.50	0.61	3.70	2.60	3.24
22	+48.50	+0.21	0.14	32.50	0.61	0.67	0.44	2.60
23	-46.00	-1.15	0.80	36.00	0.58	3.64	2.53	2.88
24	+46.80	+0.20	0.14	30.00	0.59	0.63	0.44	2.40
25	-44.70	-1.14	0.78	34.50	0.57	3.60	2.47	2.76
26	+45.80	+0.21	0.05	28.50	0.58	0.67	0.16	2.28
27	-43.45	-1.12	0.76	32.00	0.55	3.54	2.40	2.56
28	+44.65	+0.32	0.05	27.00	0.56	1.00	0.16	2.16
29	-42.25	-1.11	0.75	31.00	0.53	3.51	2.38	2.48
30	+42.50	+0.24	0.02	26.25	0.54	0.76	0.06	2.10
31	-40.35	-1.08	0.82	30.50	0.51	3.41	2.60	2.44
32	+40.60	+0.27	0.01	25.00	0.51	0.85	0.03	2.00
33	-38.35	-1.05	0.78	28.25	0.48	3.32	2.47	2.26
34	+39.55	+0.31	0.04	22.50	0.50	0.98	0.13	1.80
35	-36.00	-1.02	0.64	24.00	0.45	3.23	2.03	1.92
36	+38.35	+0.33	0.08	21.25	0.48	1.05	0.26	1.70
37	-33.75	-0.99	0.71	23.00	0.43	3.13	2.25	1.84
38	+37.30	+0.47	0.11	21.00	0.47	1.50	0.35	1.68
39	-31.40	-0.96	0.68	22.50	0.40	3.04	2.15	1.80
40	+35.80	+0.50	0.15	20.00	0.45	1.58	0.48	1.60

TABLE A.5

Experimental Record of Specimen H5

(10 x 10 x 0.45) inches

Half-Cycle	P kips	Δ inch	Δ' inch	W kip-inch	$P = \frac{P}{P_p}$	$\mu_l = \frac{\Delta}{\Delta_p}$	$\pi_d = \frac{\Delta'}{\Delta_p}$	$e = \frac{W}{1/2\ P_p \Delta_p}$
1	-142.80	-1.37	1.01	260.5	1.17	4.22	3.12	13.25
2	+138.60	+0.21	0.18	160.5	1.14	0.65	0.56	8.15
3	-136.30	-1.32	0.94	166.0	1.12	4.07	2.90	8.43
4	+134.50	+0.20	0.22	137.0	1.10	0.62	0.68	6.96
5	-131.00	-1.32	0.98	144.0	1.08	4.07	3.03	7.31
6	+130.00	+0.17	0.23	121.5	1.07	0.53	0.71	6.16
7	-126.20	-1.28	0.95	123.0	1.04	3.95	2.94	6.50
8	+126.60	+0.15	0.24	105.0	1.04	0.46	0.74	5.34
9	-124.00	-1.29	0.94	126.0	1.02	3.98	2.90	6.40
10	+126.50	+0.23	0.18	108.0	1.04	0.71	0.56	5.50
11	-121.00	-1.25	0.92	119.0	0.99	3.86	2.84	6.05
12	+123.50	+0.21	0.19	100.0	1.02	0.65	0.59	5.09
13	-119.00	-1.24	0.91	115.0	0.98	3.83	2.81	5.84
14	+121.90	+0.22	0.18	97.5	1.00	0.68	0.56	4.95
15	-117.00	-1.22	0.89	107.5	0.96	3.77	2.75	5.46
16	+120.00	+0.20	0.18	97.0	0.99	0.62	0.56	4.93
17	-115.35	-1.20	0.87	96.0	0.95	3.71	2.69	4.88
18	+118.75	+0.21	0.18	85.0	0.98	0.65	0.56	4.31
19	-113.60	-1.16	0.83	98.0	0.93	3.58	2.56	4.98
20	+118.00	+0.22	0.15	84.0	0.98	0.68	0.46	4.26
21	-112.70	-1.13	0.82	95.0	0.93	3.49	2.53	4.82
22	+117.30	+0.21	0.16	86.0	0.97	0.65	0.50	4.36
23	-111.70	-1.11	0.80	91.0	0.92	3.42	2.48	4.62
24	+114.50	+0.12	0.20	84.0	0.94	0.37	0.62	4.26
25	-110.60	-1.12	0.81	90.0	0.91	3.46	2.50	4.57
26	+112.75	+0.10	0.22	75.0	0.93	0.31	0.68	3.81
27	-110.40	-1.13	0.82	87.5	0.91	3.49	2.53	4.45
28	+111.90	+0.10	0.22	74.0	0.92	0.31	0.68	3.76
29	-109.50	-1.13	0.81	86.0	0.90	3.49	2.50	4.36
30	+112.00	+0.10	0.23	75.0	0.92	0.31	0.71	3.81
31	-109.16	-1.13	0.92	88.0	0.90	3.49	2.84	4.46
32	+110.60	+0.10	0.23	71.0	0.91	0.31	0.71	3.61
33	-108.85	-1.12	0.81	84.0	0.89	3.46	2.50	4.26
34	+110.30	+0.09	0.23	70.0	0.91	0.28	0.71	3.55
35	-108.20	-1.12	0.81	84.0	0.89	3.46	2.51	4.26
36	+109.70	+0.07	0.23	73.0	0.90	0.22	0.71	3.71
37	-107.75	-1.12	0.81	83.0	0.88	3.46	2.51	4.21
38	+108.90	+0.07	0.23	68.0	0.89	0.22	0.71	3.45
39	-107.30	-1.11	0.82	79.0	0.88	3.42	2.54	4.01
40	+107.65	+0.07	0.23	67.5	0.88	0.22	0.71	3.43

TABLE A.6

Experimental Record of Specimen H6

(12 x 12 x 0.312) inches

Half-Cycle	P kips	Δ inch	Δ' inch	W kip-inch	$P = \frac{P}{P_p}$	$\mu_I = \frac{\Delta}{\Delta_p}$	$\pi_d = \frac{\Delta'}{\Delta_p}$	$e = \frac{W}{1/2\ P_p \Delta_p}$
1	-121.30	-0.90	0.60	63.75	0.942	3.44	2.30	3.77
2	+121.25	+0.20	0.10	70.50	0.940	0.76	0.38	4.16
3	-117.20	-0.80	0.60	44.75	0.910	3.06	2.30	2.65
4	+119.20	+0.20	0.10	45.25	0.925	0.76	0.38	2.68
5	-114.60	-0.80	0.60	41.25	0.890	3.06	2.30	2.44
6	+116.65	+0.20	0.10	40.25	0.905	0.76	0.38	2.38
7	-113.00	-0.82	0.63	37.00	0.875	3.14	2.41	2.19
8	+114.80	+0.22	0.08	41.50	0.890	0.84	0.31	2.46
9	-113.45	-0.90	0.60	41.00	0.880	3.44	2.30	2.42
10	+116.00	+0.15	0.15	43.00	0.900	0.57	0.57	2.54
11	-107.50	-0.82	0.50	41.00	0.834	3.14	1.91	2.42
12	+114.00	+0.20	0.15	35.25	0.884	0.76	0.57	2.08
13	-107.10	-0.80	0.40	35.50	0.831	3.06	1.53	2.10
14	+112.60	+0.30	0.12	38.50	0.873	1.15	0.46	2.28
15	-106.60	-0.80	0.40	41.50	0.825	3.06	1.53	2.46
16	+111.40	+0.25	0.10	40.00	0.865	0.96	0.38	2.36
17	-105.70	-0.80	0.40	45.50	0.820	3.06	1.53	2.70
18	+110.50	+0.25	0.10	36.00	0.856	0.96	0.38	2.13
19	-105.00	-0.80	0.40	36.50	0.814	3.06	1.53	2.16
20	+109.60	+0.25	0.00	33.00	0.850	0.96	0.00	1.95
21	-104.55	-0.80	0.40	30.75	0.810	3.06	1.53	1.82
22	+109.40	+0.30	0.00	35.50	0.850	1.15	0.00	2.10
23	- 98.00	-0.80	0.35	28.50	0.760	3.06	1.34	1.69
24	+107.75	+0.30	0.00	27.75	0.835	1.15	0.00	1.64
25	- 98.15	-0.80	0.30	31.25	0.760	3.06	1.15	1.85
26	+107.05	+0.45	0.00	30.50	0.830	1.72	0.00	1.80
27	- 95.30	-0.65	0.40	26.00	0.738	2.48	1.53	1.54
28	+106.10	+0.30	0.00	28.00	0.824	1.15	0.00	1.66
29	- 95.60	-0.70	0.30	28.00	0.741	2.68	1.15	1.66
30	+105.25	+0.25	0.00	28.00	0.815	0.96	0.00	1.66
31	- 95.20	-0.65	0.25	28.00	0.737	2.48	0.96	1.66
32	+104.80	+0.25	0.00	29.00	0.811	0.96	0.00	1.72
33	- 95.40	-0.65	0.25	29.00	0.738	2.48	0.96	1.72
34	+101.75	+0.25	0.00	28.00	0.787	0.96	0.00	1.66
35	- 95.00	-0.65	0.40	27.00	0.736	2.48	1.53	1.60
36	+101.35	+0.25	0.00	27.00	0.785	0.96	0.00	1.60
37	- 94.60	-0.65	0.40	28.00	0.735	2.48	1.53	1.66
38	+101.50	+0.20	0.00	22.50	0.786	0.77	0.00	1.335
39	- 94.55	-0.70	0.40	23.50	0.734	2.68	1.53	1.39
40	+100.70	+0.25	0.00	25.00	0.780	0.96	0.00	1.48

TABLE A.7

Experimental Record of Specimen H7

(12 x 12 x 0.312) inches
(Stress Relieved)

Half-Cycle	P kips	Δ inch	Δ' inch	W kip-inch	$P = \frac{P}{P_p}$	$\mu_1 = \frac{\Delta}{\Delta_p}$	$\pi_d = \frac{\Delta'}{\Delta_p}$	$e = \frac{W}{1/2\ P_p \Delta_p}$
1	-152.80	-0.84	0.53	126.25	1.20	3.21	2.02	7.50
2	+133.30	+0.16	0.17	44.00	1.04	0.61	0.65	2.60
3	-151.50	-0.88	0.66	80.00	1.19	3.36	2.52	4.75
4	+111.30	+0.02	0.42	25.00	0.87	0.765	1.60	1.48
5	-147.50	-1.02	0.70	66.50	1.15	3.90	2.68	3.94
6	+103.50	-0.23	-0.59	24.00	0.81	0.88	2.26	1.42
7	-139.15	-1.15	-0.82	60.00	1.09	4.40	3.13	3.56
8	+105.80	-0.29	-0.65	31.00	0.83	1.10	2.48	1.84
9	-133.80	-1.31	-0.89	58.00	1.05	5.00	3.40	3.42
10	+111.10	-0.28	-0.66	40.00	0.87	1.07	2.52	2.37
11	-128.60	-1.33	-0.93	58.00	1.00	5.07	3.55	3.42
12	+109.90	-0.30	-0.71	35.50	0.86	1.15	2.71	2.10
13	-125.40	-1.34	-0.92	52.5	0.98	5.11	3.51	3.11
14	+110.35	-0.30	-0.70	38.00	0.86	1.15	2.67	2.25
15	-124.65	-1.35	-0.93	41.50	0.98	5.15	3.55	2.46
16	+110.30	-0.30	-0.85	53.00	0.86	1.15	3.24	3.56
17	-121.60	-1.35	-0.94	56.00	0.95	5.15	3.59	3.32
18	+108.20	-0.32	-0.70	37.00	0.85	1.22	2.68	2.19
19	-120.00	-1.37	-0.95	55.00	0.94	5.23	3.63	3.26
20	+107.15	-0.33	-0.62	39.00	0.84	1.26	2.36	2.31
21	-118.00	-1.37	0.97	49.00	0.93	5.23	3.70	2.90
22	+105.25	-0.45	-0.73	37.00	0.83	1.72	2.79	2.19
23	-117.0	-1.39	-0.98	48.50	0.92	5.30	3.74	2.88
24	+104.00	-0.46	-0.74	38.00	0.82	1.76	2.83	2.25
25	-115.90	-1.39	-1.01	47.50	0.91	5.30	3.86	2.81
26	+102.50	-0.48	-0.75	37.50	0.80	1.83	2.87	2.22
27	-114.55	-1.40	-1.01	48.00	0.90	5.35	3.86	2.84
28	+ 98.70	-0.48	-0.75	38.00	0.77	1.83	2.87	2.25
29	-113.85	-1.42	-1.01	48.00	0.89	5.42	3.86	2.84
30	+ 94.50	-0.47	-0.74	37.00	0.74	1.79	2.83	2.19
31	-111.50	-1.42	-1.01	47.00	0.87	5.42	3.86	2.78
32	+ 92.00	-0.47	-0.74	39.00	0.72	1.79	2.83	2.31
33	-109.30	-1.42	-1.01	46.25	0.85	5.42	3.86	2.74
34	+ 90.10	-0.47	-0.74	34.00	0.71	1.79	2.82	2.02
35	-107.50	-1.42	-1.01	39.00	0.84	5.42	3.86	2.31
36	+ 88.50	-0.47	-0.74	37.50	0.69	1.79	2.82	2.22
37	-104.35	-1.42	-1.01	40.50	0.82	5.42	3.86	2.40
38	+ 85.20	-0.44	-0.72	34.50	0.67	1.68	2.75	2.04
39	-102.80	-1.42	-1.00	36.00	0.80	5.42	3.81	2.13
40	+ 81.15	-0.43	-0.70	37.50	0.64	1.64	2.67	2.22

APPENDIX II

NOMENCLATURE

B	breadth of section
h	depth of section
t	flange thickness
w	web thickness
Δ	deflection of midspan of beam
Δ_p	fictitious elastic deflection corresponding to plastic load, P_p
Δ_i	deflection corresponding to the last load reversal
Δ_o	additional displacement incurred during yielding (see equation 2.35 and Figure 2.6)
$\lvert\Delta\rvert_{max}$	maximum absolute deflection
Δy	yield deflection
Δ_n	non-linear displacement: departure from the initial tangent at the force level of $\lvert\Delta\rvert_{max}$ (see Figure 2.6)
Δ_ℓ	linear displacement: displacement along the initial tangent at the load level of $\lvert\Delta\rvert_{max}$ (see Figure 2.6)
Δ'	residual plastic deflection after an excursion
P	concentrated load applied to midspan of beam
P_p	plastic load, computed from actual section and material properties

P_i	load value corresponding to the last load reversal
α	Ramberg-Osgood parameter
r	Ramberg-Osgood exponent
β	shape factor relating slope of unloading P-Δ curve to initial elastic slope
W	energy dissipated during a single excursion
e	energy ratio
ε, ε_{max}	strain
ε_y	yield strain
ε_{st}	strain at onset of strain hardening
σ, σ_{max}	stress
σ_y	yield stress
ϕ	curvature
ϕ_y	value of curvature at yield
M	moment
M_y	yield moment
π_d	plasticity ratio, subscript denoting deflection measure
K	stiffness for small displacements of the bilinear hysteresis system of Figure 2.6
K_2	stiffness for the second portion of the bilinear hysteresis system of Figure 2.6
μ_1, μ_2, μ_3	ductility factors defined by equations 2.39, 2.43 and 2.46, respectively
G	modulus of elasticity in shear

ν	Poisson's ratio
σ_f	tensile strength of weld metal or bolt
σ_{ym}	empirical yield stress level

APPENDIX III

LIST OF REFERENCES

1. Wiegel, Robert L., "Earthquake Engineering", Prentice-Hall Inc., Englewood Cliffs, N.J., 1970.
2. Bertero, V. V., and Popov, E. P., "Effect of Large Alternating Strains of Steel Beams", J. of the Structural Division, ASCE, Vol. 91, No. ST1, Proc. 4217, Feb. 1965, pp. 1-12.
3. Benham, P. P., and Ford, H., "Low Endurance Fatigue of a Mild Steel and Aluminum Alloy", J. of Mechanical Engineering Science, Vol. 3, No. 2, June, 1961, pp. 119-132.
4. "Commentary on Plastic Design in Steel", ASEC Manual, No. 41, 1971.
5. Popov, E. P., and Pinkney, R. B., "Behaviour of Steel Building Connections Subjected to Inelastic Strain Reversals", Univ. of California (Bulletin No. 13, American Iron and Steel Institute).
6. Popov, E. P., and Bertero, V. V., "Cyclic Loading of Steel Beams and Connections", J. of the Structural Division, ASCE, Vol. 99, No. ST6, Proc. Paper 9790, June, 1973, pp. 1189-1204.
7. Popov, E. P., and Franklin, H. A., "Steel Beam-to-Column Connections Subjected to Cyclically Reversed Loading", Proceedings, Structural Engineering Association of California, October, 1965.
8. Ramberg, W., and W. R. Osgood, "Description of Stress-Strain Curves by Three Parameters", Technical Note 902, NACA, July, 1943.

9. Jennings, Paul C., "Earthquake Response of a Yielding Structure", J. of the Engineering Mechanics Division, ASCE, Vol. 91, No. EM4, Proc. Paper 4435, August, 1965, pp. 41-68.

10. Kaldjian, M. J., "Moment-Curvature of Beams as Ramberg-Osgood Functions", J. of the Structural Division, ASCE, Vol. 93, No. ST5, Proc. Paper 5488, October, 1967, pp. 53-65.

11. Masing, G., "Eigenspannungen und Versfestigung beim Messing", Proceedings of the Second International Congress for Applied Mechanics, Zurich, September, 1926.

12. Hildebrand, F. B., "Introduction to Numerical Analysis", McGraw-Hill Book Co., Inc., New York, N.Y., 1956.

13. Melbourne, F. Giberson, "Two Non-linear Beams with Definitions of Ductility", J. of the Structural Division, ASCE, Vol. 95, No. ST2, Proc. Paper 6377, February, 1969, pp. 137-156.

14. Hudoba, J., "Plastic Design Capabilities of Hollow Structural Sections", M.Eng. Thesis, McMaster University, 1971.

15. ASTM "Physical and Mechanical Testing of Metals; Non-destructive Tests", Part 31, May, 1967.

16. "CSA Standard S16-1969, Steel Structures for Buildings", Canadian Structural Design Manual.

17. Korol, R. M., and Hudoba, J., "Plastic Behaviour of Hollow Structural Sections", J. of the Structural Division, ASCE, Vol. 98, No. ST5, Proc. Paper 8872, May, 1972, pp. 1007-1023.